

Diss. ETH N° 19969

**HYDROLOGICAL RESPONSE OF A GLACIER FOREFIELD  
TO METEOROLOGICAL FORCING ON DIURNAL,  
SEASONAL AND DECADAL TIME SCALES**

A dissertation submitted to

ETH ZURICH

for the degree of

Doctor of Sciences



**Jan Magnusson**

M.Sc. Aquatic and Environmental Engineering

2011



Diss. ETH N<sup>O</sup> 19969

**HYDROLOGICAL RESPONSE OF A GLACIER FOREFIELD  
TO METEOROLOGICAL FORCING ON DIURNAL,  
SEASONAL AND DECADAL TIME SCALES**

**DISSERTATION**

Submitted to

ETH ZURICH

for the degree of

**DOCTOR OF SCIENCES**

by

JAN OLOF MAGNUSSON

M.Sc. Aquatic and Environmental Engineering

born February 1, 1980

Sweden

accepted on the recommendation of

Prof. Dr. James Kirchner, examiner

Prof. Dr. Jan Seibert, co-examiner

Dr. Tobias Jonas, co-examiner

2011



# Table of contents

Summary.....	iii
Kurzzusammenfassung .....	iv
<b>1 Introduction.....</b>	<b>1</b>
1.1 The hydrology of glacierized watersheds .....	1
1.2 Study objectives.....	2
1.3 Field site .....	4
1.4 Outline of this thesis .....	6
<b>2 Quantitative evaluation of different hydrological modelling approaches in a partly glacierized Swiss watershed.....</b>	<b>9</b>
2.1 Introduction .....	10
2.2 Study site and data.....	10
2.3 Model descriptions .....	12
2.4 Extrapolation of meteorological measurements .....	15
2.5 Methods to distribute precipitation.....	18
2.6 Results of snow cover simulations .....	20
2.7 Results of runoff simulations.....	23
2.8 Conclusions .....	29
<b>3 Snow cover response to climate change in a high alpine and half-glacierized basin in Switzerland .....</b>	<b>31</b>
3.1 Introduction .....	32
3.2 Study area .....	33
3.3 Data and methods .....	33
3.4 Results .....	38
3.5 Discussion and conclusions .....	41
<b>4 Melt water driven stream and groundwater stage fluctuations on a glacier forefield (Damma gletscher, Switzerland).....</b>	<b>45</b>
4.1 Introduction .....	46
4.2 Study site and data.....	46
4.3 Observed water level fluctuations .....	49
4.4 Characterizing stream-groundwater interactions using estimates of residence times	51
4.5 Modelling groundwater fluctuations .....	53
4.6 Discussion.....	61
4.7 Conclusions .....	63
<b>5 The energy balance and temperature dynamics of a proglacial stream, and their implications for spatially integrated hydraulic geometry and riparian aquifer transmissivity.....</b>	<b>65</b>

5.1	Introduction .....	66
5.2	Field site and data.....	67
5.3	Observed thermal and hydrological conditions across the proglacial field .....	69
5.4	Temperature increase observed over individual stream reaches .....	71
5.5	Processes influencing stream temperature warming: Theory.....	72
5.6	Processes influencing stream temperature warming: Identifying dominant processes . .....	74
5.7	Inferring hydraulic geometry relationships from stream temperature measurements	78
5.8	Processes influencing stream warming: Analysing the stream energy balance .....	82
5.9	Inferring information about surface-groundwater interactions from stream temperature measurements .....	86
5.10	Summary and conclusions .....	90
<b>6</b>	<b>Conclusions and outlook.....</b>	<b>93</b>
<b>7</b>	<b>References .....</b>	<b>97</b>
<b>8</b>	<b>Acknowledgements .....</b>	<b>109</b>
<b>9</b>	<b>Curriculum vitae .....</b>	<b>110</b>

## **Summary**

In many mountain regions, large land areas have become ice-free with the ongoing glacier retreat. In these pristine landscapes, stream and groundwater flows influence biological, chemical and physical processes. Little is known about the hydrology of glacier forefields, typically characterized by large spatial and temporal variations in stream and groundwater flow. The large spatial variability arises due to the heterogeneous glacial till and complex topography. The strong diurnal and seasonal fluctuations in proglacial discharge are caused by variations in snow and ice melt rates in response to meteorological forcing. In the long-term, the local hydrological system on proglacial fields will adapt to a changing climate and variations in the glacier extent and snow cover on the watershed scale.

This thesis comprises four studies of separate hydrological aspects of the Damma glacier forefield (Switzerland). In a first study, the diurnal and seasonal variations in proglacial discharge were simulated using two different hydrological models. The simulations reproduced the observed discharges accurately, and provided estimates of the fractions of snow melt, ice melt and rainfall contributing to proglacial discharge. In a second study, the seasonal snow cover response to long-term variations in climate was investigated by simulations using an energy-balance snow cover model. The results suggest that the average snow water equivalent in the watershed will decrease by nearly one-third in future (2071-2100) compared to present conditions (1981-2007). In a third study, local stream-groundwater interactions were investigated by studying how stream stage fluctuations propagate into the riparian zone near the main stream channel. It was shown that a diffusion model forced by the stream stage variations could reproduce the groundwater level fluctuations in the riparian zone. In the final study, spatial patterns in stream temperature were used to draw inferences about the energy balance of the stream, the hydraulic geometry of the braided stream channels, and stream-groundwater interactions. The results illustrate that proglacial stream temperatures can yield spatially integrated information about thermal and hydrological processes.

## Kurzzusammenfassung

Mit dem Rückgang der Gletscher sind in vielen Gebirgsregionen grosse, eisfreie Landflächen entstanden, auf denen sich ober- und unterirdische Gewässersysteme entwickeln. Die Gewässer haben einen entscheidenden Einfluss auf die Vegetationsentwicklung und die Verwitterung und Erosion der noch jungen Landschaft. Die Hydrologie von Gletschervorfeldern unterliegt einer grossen zeitlichen und räumlichen Dynamik, die im Detail aber noch wenig verstanden wird. Die räumliche Heterogenität der Gewässerläufe ist dem komplexen Substrataufbau der Moränen und der bewegten Topographie geschuldet. Die grossen zeitlichen Abflussschwankungen werden durch tageszeitliche und saisonale Unterschiede der Schnee- und Eisschmelzraten verursacht. Auf lange Sicht wird sich die Hydrologie von Gletschervorfeldern an wärmeres Klima, weiteren Gletscherrückgang und einer veränderten Schneedecke anpassen.

Die vorliegende Arbeit besteht aus vier Studien über unterschiedliche hydrologische Aspekte eines Gletschervorfeldes, am Beispiel des Dammagletschers in der Schweiz. In der ersten Studie wurden die tages- und jahreszeitlichen Schwankungen des Abflusses mit zwei verschiedenen hydrologischen Modellen simuliert. Die Abflusssimulationen stimmten gut mit gemessenen Abflüssen überein und erlaubten eine Abschätzung der Schneeschmelz-, Eisschmelz- und Regenanteile am Gesamtabfluss. In der zweiten Studie wurden die Auswirkungen von Klimaänderungen auf die saisonale Schneedecke mit Hilfe eines Schneedeckenmodells untersucht. Die Ergebnisse deuten darauf hin, dass das durchschnittliche Schneewasseräquivalent für die Jahre 2071-2100 im Vergleich zu aktuellen Werten (1981-2007) um ein Drittel abnehmen wird. In der dritten Studie wurden lokale Wechselwirkungen zwischen Bach- und Grundwasser untersucht, etwa wie sich Schwankungen des Flusspegels auf das Grundwasser auswirken. Mittels eines Diffusionsmodells konnten die Fluktuationen im Grundwasserstand in der Uferzone simuliert werden. In der vierten Studie wurden Messungen der räumlichen Verteilung von Wassertemperaturen in den Bächen verwendet, um Rückschlüsse auf die Energiebilanz der Bäche zu ziehen. Die Ergebnisse zeigen, dass Variationen der Wassertemperaturen räumlich integrierte Informationen über thermische und hydrologische Prozesse in Gletschervorfeldern liefern können.

# Chapter 1

## 1 Introduction

### 1.1 The hydrology of glacierized watersheds

The ongoing glacier retreat influences the hydrological conditions in many alpine watersheds (Stahl et al., 2008). The water supply from snow and glacier melt is very sensitive to a warming climate (Barnett et al., 2005; Bradley et al. 2006). In glacierized watersheds, the water sources that contribute to discharge shift as temperatures increase. The currently negative glacier mass balance results in an increased discharge, with large contributions from ice melt, during a transitional phase. In future, after additional glacier loss, runoff will likely decline, however, with an increasing contribution from seasonal snow melt and rainfall rather than ice melt (Hannah et al., 2007; Huss et al. 2008b). Thus, in glacierized watersheds, the hydrological conditions have changed much during the past hundred years due to glacier retreat, and the water availability in the future is also likely to differ much from the conditions observed today. The ability to reconstruct and predict changes in hydrological conditions is among other reasons important because the water leaving those watersheds is often used for production of hydropower energy (Schaeefli et al., 2007). Therefore, future variations in discharge may have a large economic impact and proper management of this resource is necessary, in particular long-term planning of reservoir capacity. A sound understanding of the interaction between meteorological forcing, snow cover and glaciers on the scale of whole catchments is necessary for developing hydrological models yielding, for example, reliable discharge estimations. With such models, the hydrology of glacierized watersheds may be reconstructed using long-term meteorological recordings or can be predicted based on climate change scenarios.

Downstream of retreating glaciers, the interactions between hydrological conditions and both biotic and abiotic processes on the proglacial fields are of particular interest. Typically, glacier melt water is routed through braided streams down-valley on the proglacial zone, sometimes with large subsurface water flows through the glacial till in the nearby riparian zone (Malard et al., 2002). Both the surface and groundwater flow influence the chemical, physical and biological processes taking place on glacier forefields (Fairchild et al., 1999; Warburton, 1992; Ward et al., 1999). Water availability can affect the vegetation on young soils near the glacier snout, and studies have shown that the location of melt water channels influence the spatial distribution of plant species (Schwarz et al., 1992). Both ground and surface water flow transport nutrients and the products of chemical weathering downstream. In hilly terrain, such mechanisms may play an important role with slow vegetation growth rates in groundwater recharge areas and high growth rates in discharge areas (Giesler et al., 1998). Thus, the water flow also seems to be important for vegetation growth further away from the glacier and likely influences the turnover rates of organic matter, and consequently also the amount of carbon stored in the soil (Bernasconi et al., 2008). Hydrological conditions additionally affect chemical processes like weathering fluxes, and the products influence soil formation. However, the weathering rates measured in laboratory studies under controlled conditions typically differ from those obtained in field studies. This discrepancy partly arises because many of the site's hydrological conditions are unknown, and not fully reproducible in laboratory conditions (White and Brantley, 2003). Furthermore, physical processes can

# Chapter 1

influence the position and lifespan of the braided streams across the forefield resulting in spatially and temporally variable surface water flows. Formation of braided streams depends on the sediment load in the surface waters which depend on a variety of interactions such as the proglacial stream flow dynamics and the riparian vegetation (Gurnell et al., 1999). As pointed out above, many different chemical, physical and biological processes shape the landscapes developing downstream of melting glaciers, and those processes are often influenced by the prevailing hydrological conditions. Thus, for understanding how such pristine landmasses may develop, a sound knowledge of hydrological processes in such regions is necessary.

From a hydrological perspective, proglacial fields are particularly interesting because they display several fascinating and unusual characteristics. During days in summer with fair-weather, a large pulse of glacier melt water feeds the braided stream system, one characteristic making those watersheds different from many others (Hock, 2003). The timing and the amplitude of the stream level variations change during the season depending on whether snow or glacier ice is melting and on the nature of the glacier drainage system (Hodson et al., 1998; Jobard and Dzikowski, 2006). Because of the large temporal variations in water supply, the network of streams display a large diurnal and seasonal expansion/contraction cycle (Malard et al., 2000) and parts of the proglacial field may be flooded on a regular basis. The diurnal discharge pulse also influences the interaction between the surface water and groundwater. For example, the stage variations in streams driven by snow melt may propagate into the riparian zone in flat meadow aquifers (Loheide and Lundquist, 2009). The diurnal regime with strong and predictable discharge variations over short time scales allows many interesting experiments in glacierized watersheds. For example, stream-groundwater interactions can be studied over a wide range of stream flow regimes. Another interesting aspect is the aquifer material; namely, the heterogeneous glacial till typically covering the underlying bedrock in many watersheds which were glacierized in the past (Anderson, 2007). It is unclear whether the standard porous media approaches describing water flow apply to some unconsolidated sediments found in for example moraines (Roy and Hayashi, 2009). The storage capacity of the sediments found in alpine watersheds is also an open question, and stream flow may depend on the groundwater level in a non-linear manner (Clow et al., 2003; Hinton et al., 1993). Understanding how water flows through such sediments is of particular importance because steep mountainous terrain typically provides large hydraulic gradients driving the down-valley ground water flow. Thus, water may flow fast both in the streams and in the subsurface with large spatial and temporal variations because of the heterogeneous sediments and variable water sources. As a result, proglacial areas provide ideal conditions to investigate several special hydrological processes (e.g. expansion/contraction cycle of braided streams and groundwater flow through very heterogeneous sediments).

## 1.2 Study objectives

This thesis illuminates important open questions related to the hydrology of glacier forefields. The overall goal is to provide a scientific basis for an improved understanding and modelling of the flow and residence time of water across glacier forefields. To this end four major objectives have been pursued:

- In partly glacierized watersheds, rain along with snow and ice melt contributes to discharge. In this study, the overall objective was to provide a reliable method for quantifying the watershed discharge, and to estimate how much the individual sources

## Introduction

contributed to runoff during the course of the year. This was achieved by hydrological modelling which required the solution to two specific questions because the field site is mountainous, partly glacierized and remotely situated: (1) Most important, models predicting discharge from such watersheds need to handle both the melting of snow and ice. In such a situation, where both components play an important role in the runoff formation, it is still not known whether a physically based or a parametric approach to modelling snow and ice melt will give the most reliable discharge simulations. (2) Another important issue which often receives little attention is whether the models can be provided with representative input data of sufficient accuracy. Thus, the second open question addressed was whether the two different models could be supplied with sufficiently accurate input data despite the sparsely distributed weather stations and the highly variable meteorological conditions in the mountainous landscape. (Chapter 2)

- In high alpine regions, the snow cover typically influences the hydrological regime strongly, and even in watersheds with melting glaciers, the snow pack may still contribute significantly to stream discharge. Thus, prognostic simulations of how the snow cover may respond to a warming climate are valuable for the management of water resources in alpine regions. In this study, the main objective was to investigate how climate change may influence the snow cover conditions across the whole Damma glacier basin. The simulations for this study were conducted with a detailed snow cover model and two main research questions were formulated: (1) By how much may the seasonal snow cover duration reduce at the end of the 21<sup>st</sup> century compared to present conditions? (2) By how much may the average snow water equivalent in the basin decrease at the end of this century, again, compared to current conditions? (Chapter 3)
- In glacierized watersheds, the stream flow varies highly with time displaying large diurnal fluctuations. Another unusual characteristic of those catchments, also mentioned previously, is the heterogeneous sediments typically covering the bedrock. Thus, in such mountainous landscapes, stream-groundwater interactions may display very different behavior than what has been observed in flatter lowland regions with homogenous soils. Therefore, the overall objective was to increase our understanding of how stream and groundwater interact across a proglacial field. At the study site, both in the stream and in the groundwater, large diurnal fluctuations were monitored, and two specific questions were addressed related to the observed diurnal stage variations: (1) How may the groundwater fluctuations in the riparian zone (driven by stream stage variations) be modelled? (2) Do the large diurnal groundwater level fluctuations move a considerable amount of water back and forth between the stream and the groundwater reservoir? (Chapter 4)
- Both surface and groundwater flow on proglacial fields can display large spatial and temporal variations. Large spatial variations in stream-groundwater exchange rates likely occur because of the heterogeneous glacial till and the complex topography. The braided channels also display large variations in width and depth over short distances due to the mountainous terrain and large stones and boulders in the stream channels. In this study, the main objective was to examine whether longitudinal stream temperature changes may be valuable for inferring average information about thermal and hydrological processes along entire stream reaches. Two specific research questions were addressed: (1) What physical factors dominated the stream temperature

increase observed along individual stream reaches? (2) May the observed longitudinal temperature increase in the streams be used to characterize the hydraulic geometry of the stream and stream-groundwater interactions over individual reaches? (Chapter 5)

## 1.3 Field site

The data used in this thesis was collected within the framework of two projects: the BigLink project of the Competence Center for Environment and Sustainability (CCES) within the ETH Domain, and the project “Klimaänderung und Wasserkraftnutzung” financially supported by swisselectric research. The field site for both projects was the glacier forefield at the base/foot of the Damma glacier in central Switzerland ( $N46^{\circ}38.177'$   $E08^{\circ}27.677'$ ). The whole watershed covers a small area of roughly  $12 \text{ km}^2$  and a large altitude range between 1800 and 3630 m above sea level (Figure 1.1). The watershed displays highly mountainous terrain with very steep slopes. Today, the glacier covers about half the watershed and is located at high elevations, approximately between 2400 and 3300 m. Recordings show that the glacier front has receded at an average rate of about 10 m/year during the last century (Haemmerli et al., 2007). The glacier tongue was separated from the main ice-body recently, in the early 2000s, and a so called dead-ice body currently remains the most prominent feature on the upper parts (~2050 m) of the glacier forefield. The water from the catchment discharges completely into the hydropower reservoir Göschenenalpsee. The total catchment area draining to the reservoir is approximately  $92 \text{ km}^2$  large.



**Figure 1.1.** Landscape view of the study site with the proglacial field in the valley floor and the Damma glacier in the background underneath the mountain ridge.

The forefield in the valley floor is delineated by the small dead-ice body ( $\sim 0.15 \text{ km}^2$ ) and two large side moraines resulting from the last large advance of the glacier during the Little Ice Age which ended around 1850 (Figure 1.2). Two periods during which the glacier advanced ended 1927 and 1992, respectively, and are marked by two small terminal moraines. Most melt water, about two third of the total discharge, passes underneath the dead-ice body before reaching the glacier forefield. The remaining surface water flows into the field site in a stream cutting through the western side moraine. On the glacier forefield, the melt water flows through braided streams which display strong diurnal and seasonal variations in extent. The streams are braided because of the variable topography on the forefield and due to the large rocks and boulders covering the whole proglacial field.

## Introduction

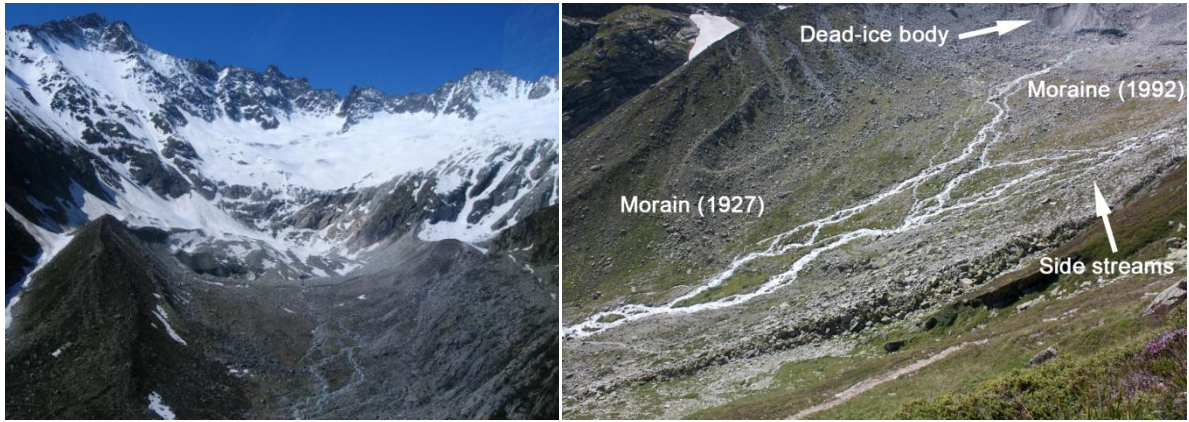


**Figure 1.2.** The Damma glacier forefield located downstream of the dead-ice body and between the two large side moraines dating back from the end of the Little Ice Age (left panel). The braided streams on the glacier forefield passing the two terminal moraines (right panel).

Since 2007, many different measurements have been performed across the watershed in order to study both large and small scale hydrological processes. However, the field site is remotely located and only accessible by foot. Thus, maintenance becomes laborious with consequently long service intervals, and during winter the steep, avalanche prone terrain makes field campaigns difficult. Therefore, at this field site, much effort was invested into conducting measurements in a robust and simple manner with low maintenance requirements. This approach provided measurement records even during winter and other harsh field conditions like high flows. Basic meteorological variables, such as air temperature, precipitation and radiation, were recorded in the center of the proglacial field (Figure 1.3). Runoff was continuously recorded at three sites capturing the water flowing into and out from the glacier forefield: (1) near the dead-ice body, (2) where the side stream cut the large western moraine and (3) downstream from the point where the streams from the dead-ice body and the side streams join. The meteorological measurements showed that the weather in the watershed was rather cold and wet; average annual temperature on the proglacial field is roughly 2 °C and the total annual precipitation is about 2200 to 2300 mm. Because the mass-balance of the glacier is currently negative, the total yearly runoff of approximately 2700 mm is larger than the annual precipitation amount (Kormann, 2009).



**Figure 1.3.** Basic hydrological and meteorological measurements on the proglacial field. Runoff was measured with a radar device (left panel) and snow depth among other variables was recorded at the weather station situated on the middle of the forefield (right panel).

In order to study stream-groundwater interactions, monitoring wells were installed on transects perpendicular to the stream (Figure 1.4). The simple measurement method provided information on how stream stage variations may propagate into the heterogeneous glacial till. In order to measure discharge and stream flow velocity, dilution gauging was used because of the turbulent water caused by the large rocks and stones in the channels. Measurements with fluorescent dyes were particularly practical because much lower tracer amounts were needed than when using salt dilution gauging. Many measurements which are easy to perform in most areas were not possible on the remote field site, and much effort was needed to find suitable alternatives.



**Figure 1.4.** Observations of groundwater level in monitoring wells in the riparian zone close to the stream (left panel) and measurements of stream discharge and velocity during low flow conditions using fluorescent tracers (right panel). The pictures also display the rough nature of the glacial till and the variable streambed topography.

## 1.4 Outline of this thesis

The thesis comprises four studies which are listed below.

The first manuscript is published under the reference: Magnusson J, Farinotti D, Jonas T, Bavay M. 2011. Quantitative evaluation of different hydrological modelling approaches in a partly glacierized Swiss watershed. *Hydrological Processes*, 25(13): 2071-2084. The article describes the hydrology on the watershed scale by simulating the proglacial discharge record using a physically based model and a parametric model. The results suggest that the physically based model describing snow and ice melt required accurate input data, in particular a representative snow distribution, to match the measured runoff. On the other hand, the calibration of the parametric model displayed compensating mechanisms, and the model was less sensitive to different input data sets than the physically based model. Only long-term measurements were used as input data to mimic the typical input data situation for hydrological simulation. Finally, the rain and melt water was routed through the watershed with a simple linear reservoir model, and this approach was shown to be sufficient to reproduce the discharge dynamics of the watershed.

The second manuscript is published under the reference: Magnusson J, Jonas T, Lopez-Moreno I, Lehning M. 2010. Snow cover response to climate change in a high alpine and half-glacierized basin in Switzerland. *Hydrology Research*. 41:230–240. The manuscript

## Introduction

describes how the snow storage in the Damma glacier basin may respond to a warming climate. The simulations were performed using a detailed snow cover model, and span a reference period (1981–2007) and one future period (2071–2100) for which two different emission scenarios of greenhouse gases were used. The results indicate that the duration of the seasonal snow cover may shorten by about two months in future compared to the reference period. The simulations also suggest that the yearly highest (basin-averaged) snow water equivalent will decrease by nearly one third in future compared to the results of the reference period.

The third manuscript is submitted under the reference: Magnusson J, Kobierska F, Huxol S, Jonas T, Kirchner JW. Melt water driven stream and groundwater stage fluctuations on a glacier forefield (Damma gletscher, Switzerland). *Hydrological Processes*. The article describes how diurnal stream stage fluctuations driven by glacier melt propagate into the nearby riparian zone along the channels. At three relatively flat sites, the measured groundwater stage fluctuations were well reproduced using a diffusion model when forcing the model with the measured stream stage fluctuations. The calibration procedure of the model yielded an estimate of the hydraulic diffusivity of the glacial till in the riparian zone. At a fourth and steep location, the observed groundwater stage variations were only reproduced with reasonable parameter values using an advection-diffusion model describing the propagation of stream stage fluctuations. However, the hydraulic diffusivity was not well-constrained by the calibration. Residence time measurements of the groundwater showed that only minimal mixing between the water in the riparian zone and the stream occurred on a diurnal basis, in spite of the large observed daily stage fluctuations.

The fourth manuscript is submitted under the reference: Magnusson J, Jonas T, Kirchner JW. The energy balance and temperature dynamics of a proglacial stream, and their implications for spatially integrated hydraulic geometry and riparian aquifer transmissivity. *Water Resources Research*. This manuscript describes how time-series stream temperature observations can be used to draw inferences about the stream's energy balance over entire reaches. An analysis based on a simple energy balance equation revealed that along three adjacent reaches radiative heating and frictional warming could largely explain the observed stream warming. Over a fourth reach, neither of these energy balance components explained the warming, but the analysis instead suggested that groundwater inflow caused the observed longitudinal temperature increase. The study shows that a reasonable relationship between stream width and discharge can be inferred from the observed longitudinal temperature increase. The study also suggests that rates of groundwater inflow and hydraulic properties of the riparian zone can be estimated from longitudinal stream temperature measurements, together with groundwater monitoring in the riparian zone.

Supplementary material to the thesis have been presented in three additional manuscripts:

Hindshaw RS, Tipper ET, Reynolds BC, Lemarchand E, Wiederhold JG, Magnusson J, Bernasconi S, Kretzschmar R, Bourdon B. 2011. Hydrological control of stream water chemistry in a glacial catchment (Damma Glacier, Switzerland). *Chemical Geology*. 285:215–230.

Farinotti D, Magnusson J, Huss M, Bauder A. 2010. Snow accumulation distribution inferred from time-lapse photography. *Hydrological Processes*. 24: 2087–2097.

## Chapter 1

Jonas T, Marty C, Magnusson J. 2009. Estimating the snow water equivalent from snow depth measurements in the Swiss Alps. *Journal of Hydrology*. 378(1–2): 161–167.

## CHAPTER 2

# 2 Quantitative evaluation of different hydrological modelling approaches in a partly glacierized Swiss watershed

Jan Magnusson, Tobias Jonas and Mathias Bavay

*WSL Institute for Snow and Avalanche Research SLF, Flüelastrasse 11, CH-7260 Davos Dorf, Switzerland*

Daniel Farinotti

*Laboratory of Hydraulics, Hydrology and Glaciology (VAW), ETH Zurich, CH-8092 Zurich, Switzerland*

Manuscript Published in Hydrological Processes, 25, 2071-2084, 2011.

### ABSTRACT

Mountain water resources management often requires hydrological models that need to handle both snow and ice melt. In this study, we compared two different model types for a partly glacierized watershed in central Switzerland: (1) an energy-balance model primarily designed for snow simulations; and (2) a temperature-index model developed for glacier simulations. The models were forced with data extrapolated from long-term measurement records to mimic the typical input data situation for climate change assessments. By using different methods to distribute precipitation, we also assessed how various snow cover patterns influenced the modelled runoff.

The energy-balance model provided accurate discharge estimations during periods dominated by snow melt, but dropped in performance during the glacier ablation season. The glacier melt rates were sensitive to the modelled snow cover patterns and to the parameterization of turbulent heat fluxes. In contrast, the temperature-index model poorly reproduced snow melt runoff, but provided accurate discharge estimations during the periods dominated by glacier ablation, almost independently of the method used to distribute precipitation. Apparently, the calibration of this model compensated for the inaccurate precipitation input with biased parameters.

Our results show that accurate estimates of snow cover patterns are needed either to correctly constrain the melt parameters of the temperature-index model or to ensure appropriate glacier surface albedos required by the energy-balance model. Thus, particularly when only distant meteorological stations are available, carefully selected input data and efficient extrapolation methods of meteorological variables improve the reliability of runoff simulations in high alpine watersheds.

## 2.1 Introduction

Hydrological models of glacio-nival watersheds need to cope with both the melting of snow and ice. At the same time, the melt processes have to be expressed in a distributed way, because the meteorological conditions and the snow and ice cover vary spatially. In previous studies of glacierized watersheds, melt rates have been simulated with either energy-balance or temperature-index models (e.g. Hock, 1999; Hock and Holmgren, 2005; Huss et al., 2008b; Michlmayr et al., 2008). The two model types show rather similar performance for snow-dominated regions (e.g. Zappa et al., 2003; Lehning et al., 2006). However, it is still unclear whether detailed energy-balance models or simpler temperature-index melt models developed for both snow and ice produce more reliable predictions of discharge dynamics in watersheds with a glacio-nival runoff regime. Addressing this topic is important for mountain water resources management in the Alps because here watersheds combining both glaciers and snow-dominated areas are rather the rule than the exception.

Hydrological models require meteorological input data often obtained by extrapolating measurements from coarsely distributed weather stations. In mountainous regions, meteorological conditions usually vary greatly over short distances. Therefore, extrapolated weather station data may not fully represent the spatial variations in meteorological driving forces that determine snow and ice melt. Thus, a second important question to address is whether the two melt model types mentioned above have different capabilities in coping with only partly representative input data. This topic gains additional importance when using such models for climate change studies, which typically have to rely on rare meteorological stations providing long-term data records.

In this study, we analysed different discharge modelling approaches in a Swiss glacio-nival watershed under input data constraints typical for long-term simulations, such as climate change assessments. We first assessed different extrapolation schemes of long-term meteorological measurement records using evaluation data from supplementary stations deployed at the study site. In particular, we examined four different methods to distribute solid precipitation. We then compared the performance of a detailed energy-balance and a temperature-index melt model forced with data obtained from the above mentioned extrapolations of long-term weather station data. The energy-balance model (ALPINE3D) was particularly designed to simulate snow cover dynamics (Lehning et al., 2006). The temperature-index melt model, on the other hand, was developed primarily for glacier mass balance modelling studies (Hock, 1999). The four methods to distribute solid precipitation were evaluated through the snow simulations using measured snow water equivalents and snow covered area. To generate a discharge hydrograph, we applied a simple linear reservoir approach for both melt models and evaluated the discharge simulations with measured runoff. Our results show that accurate estimates of snow distribution patterns (i.e. distribution of solid precipitation) are an important prerequisite for reliable prognostic runoff predictions by both models. They are needed either to constrain the melt parameters of the temperature-index model correctly or to ensure appropriate glacier surface albedos required by the physically based model.

## 2.2 Study site and data

The Damma glacier basin in the central Swiss Alps ( $N46^{\circ}38.177' E08^{\circ}27.677'$ ) covers an area of  $9.9 \text{ km}^2$  and an elevation range from 1940 to 3630 m a.s.l (Figure 2.1). The hydrological regime of the study area is dominated by runoff generation from the seasonal snow cover and

## Comparison of two melt models

the glacier. The runoff from the basin discharges entirely to a hydropower dam (Göscheneralpsee). The topography of the watershed is characterized by high alpine terrain with steep slopes facing towards the glacier. On the forefield downstream the glacier, a debris-covered dead-ice body constitutes the most prominent feature. The glacier front has receded at an average rate of about 10 m/year since 1921 (Haemmerli et al., 2007). A last temporary advance of the glacier front was recorded between 1972 and 1991. The catchment was 50% glacier-covered in 2007. The catchment is underlain by granite bedrock and glacial tills are found on the recently deglaciated parts. The topography of the watershed is known from a high-accuracy digital elevation model obtained by airborne photogrammetry in 2007. For this study, the digital elevation model was resampled to a 50 m grid.

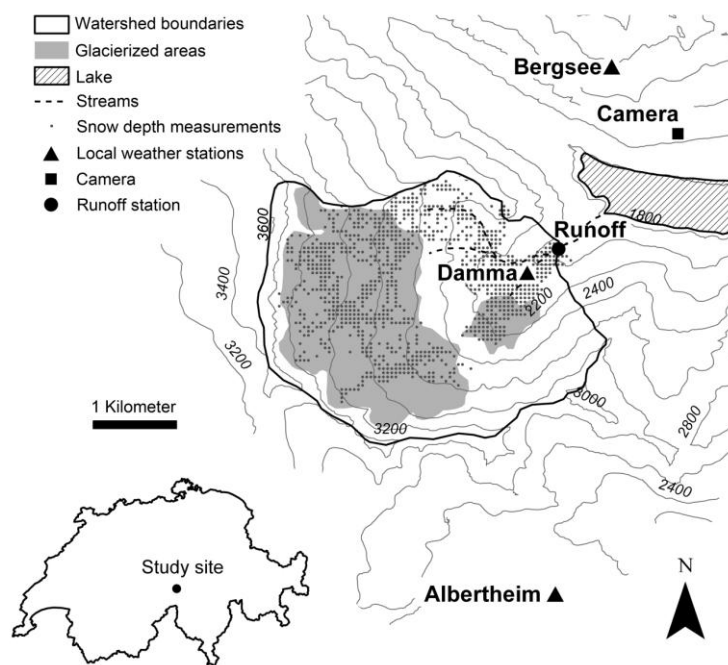


**Figure 2.1.** Overview map of the Dammagletscher watershed showing ice-covered regions (grey shaded regions), the local automatic weather stations (triangles), the runoff station (filled circle), the camera (filled rectangle) and the locations of the snow depth measurements averaged to the grid cells of the digital elevation model (dots). Terrain elevation is indicated by 200 m contour lines.

Meteorological measurements from three different station networks were used (Table 2.1): (1) three local weather stations (Figure 2.1) provided short-term records (up to two hydrological years) of hourly averages of air temperature, relative humidity, wind speed, wind direction, liquid precipitation, snow depth, snow surface temperature, incoming and reflected short-wave radiation as well as incoming long-wave radiation; (2) two meteorological stations of the ANETZ network of the Federal Office of Meteorology and Climatology in Switzerland (MeteoSwiss) provided long-term measurements (i.e. 30 hydrological years) of air temperature, relative humidity, wind speed, wind direction, incoming short-wave radiation as well as liquid and solid precipitation; (3) one station of the MeteoSwiss NIME-network provided long-term daily liquid and solid precipitation measurements. No meteorological measurements were recorded on the glacier surface directly. Runoff was measured at a gaging station at the outlet of the watershed (Figure 2.1).

**Table 2.1.** Meteorological variables recorded at the stations used in this study.

Station	Elevation (m a.s.l.)	Distance to basin (km)	Measurement period	Parameters
Local stations:				
Damma	2025	-	9.2007 – 10.2009	TA, RH, VW, DW, $P_{\text{rain}}$ , ISWR, RSWR, TSS, HS
Albertheim	2341	3.9	10.2008 – 10.2009	TA, RH, VW, DW, $P_{\text{rain}}$ , ISWR, RSWR, TSS, ILWR, HS
Bergsee	2586	2.6	10.2008 – 10.2009	TA, RH, VW, DW, $P_{\text{rain}}$ , ISWR, RSWR, TSS, HS
Regional stations:				
Gütsch (ANETZ)	2283	12.0	1981 – 2009	TA, RH, VW, DW, P, ISWR
Grimsel (ANETZ)	1977	12.3	1989 – 2009	TA, RH, VW, DW, P, ISWR
Göscheneralp (NIME)	1740	3.2	1969 – 2009	P

TA: air temperature; RH: relative humidity; VW: wind velocity; DW: wind direction;  $P_{\text{rain}}$ : liquid precipitation; P: solid and liquid precipitation; ISWR: incoming short-wave radiation; RSWR: reflected short-wave radiation; TSS: snow surface temperature; ILWR: incoming long-wave radiation; HS: snow depth.

Snow depths and densities were measured on the accessible parts of the drainage basin on four different survey dates (5 May 2008, 15 May 2008, 17 January 2009 and 4 May 2009). Altogether, 2309 snow depth measurements and 7 snow density profiles were collected. For the individual surveys, the point snow depth measurements were averaged to one value for each grid cell of the digital elevation model with 50 m resolution. This procedure resulted in 1317 point snow depth measurements available for evaluation. Snow water equivalents were estimated from the snow depth measurements, in combination with a statistical model for snow density that accounts for snow depth, season and elevation (Jonas et al., 2009). The model allows a site-specific snow density offset, which was evaluated from the observed snow densities. The evolution of the snow cover distribution during the spring, summer and autumn months was tracked with photography. Snow covered areas were extracted from the photographs with a method developed by Farinotti et al. (2010), where examples of the snow distribution images for the Dammagletscher basin are available. The camera was located about 2 km east from the catchment outlet and the field of view covered 62% of the drainage basin (Figure 2.1). The ice-thickness distribution for the Dammagletscher presented by Farinotti et al. (2009) was adopted in this study.

## 2.3 Model descriptions

### *Energy-balance model*

The energy-balance model (ALPINE3D) is a deterministic and distributed model, designed for high-resolution simulations of snow processes in mountainous terrain (Lehning et al., 2006). Initially ALPINE3D was not developed for simulations of glacierized basins, but

## Comparison of two melt models

can reproduce glacier melt and accumulation dynamics (Michlmayr et al., 2008; Mott et al., 2008). It is based on the one-dimensional SNOWPACK model described in detail by Lehning and Fierz (2008) and references therein. The SNOWPACK model simulates the snow pack development by solving the heat and mass transfer equations of the snow cover. The snow micro-structure in individual layers of the snow pack determines the thermal conductivity and viscosity. Phase changes and snow compaction are accounted for in the model. Many validation studies of the model have been published and in our context the simulations by Obleitner and Lehning (2004) of snow and ice development on a glacier is likely the most important. Their study suggests that SNOWPACK should be able to reproduce accumulation areas of glaciers, where aging snow transforms to ice.

The energy-balance at the surface is divided into radiation and turbulent heat flux terms. The radiation distribution in the basin is handled by a radiosity model, which includes arbitrary multiple terrain reflections, solar shadowing, and long-wave irradiance by surrounding terrain (Helbig et al., 2009, 2010). Furthermore, the model also distributes incoming radiation over the uppermost snow layers with a density dependent extinction coefficient (Lehning et al., 2002b). This allows for a more realistic simulation of the surface energy-balance and subsurface melting. It may be important to note that for an energy- and mass-balance model, ice melt is not different from snow melt, although ice has a lower albedo, which needs to be estimated. The albedo formulation for snow is based on a statistical model developed for seasonal snow in alpine terrain (Lehning et al., 2002b). The albedo of glacier ice was set to 0.3 (slightly dirty ice) after Paterson (1994). The assumption of a constant albedo of glacier ice has been shown to have minor effects on runoff formation (Hock and Holmgren, 2005). The albedo of snow was limited to values between 0.95 (newly fallen snow) and 0.53 (average firn albedo) following Paterson (1994).

The turbulent heat fluxes of the energy-balance are described by the Monin-Obukhov similarity theory (Lehning et al., 2002b). The surface fluxes include the latent heat transfer, and therefore surface evaporation and sublimation are modelled. A variety of stability correction functions are now implemented, but can be switched off, which is often a good choice to avoid unrealistic dampening of the turbulent transfer in rough terrain (Stoessel et al., 2010). How the stability corrections are handled in this study is described in detail below.

For our investigation area, the Dammagletscher, initial simulations showed that the glacier melt rates were largely affected by the formulation of atmospheric stability, especially after melt-out of seasonal snow, that is, for the exposed ice surface. Heuristically, we achieved reasonable glacier melt rates by: (1) assuming neutral stability outside the glacier which means that no stability correction was performed; (2) assuming neutral stability over the glacier if air temperatures were below 5 °C; and (3) applying the implemented stability-correction scheme of Stearns and Weidner (1993) over the glacier if the air temperatures exceeded 5 °C. This choice is reasonable because it has been shown that very often over snow in complex terrain, stability correction functions dampen the turbulent fluxes in an unreasonable way (Martin and Lejeune, 1998) and the assumption of neutral stability shows better results (Stoessel et al., 2010). At the same time, a strong stable stratification often develops over the rather smooth ice surface of a melting glacier (Paterson, 1994).

The model is initialized with a digital elevation model (here with 50 m grid resolution), a description of the soil properties, and the ice-thickness distribution of the glacier. The model is driven by hourly measurements of air temperature, relative humidity, wind speed, precipitation and incoming short- and long-wave radiation. In this study, the model separates

## Chapter 2

between snow and rain by a threshold temperature of 1.2 °C. Furthermore, we did not use an ALPINE3D module describing the small scale transport of snow (Lehning et al., 2008).

### *Temperature-index model*

The temperature-index model adopted in this study is based on a distributed temperature-index approach proposed by Hock (1999). Hourly snow- and ice-melt rates  $M_i$  occurring at any location  $i$  are computed according to:

$$M_i = \begin{cases} (f_M + r_{\text{snow,ice}} \cdot I_{\text{pot},i}) \cdot T_i & \text{if } T_i > 0^\circ\text{C} \\ 0 & \text{if } T_i \leq 0^\circ\text{C} \end{cases} \quad (2.1)$$

where  $f_M$  is a melt factor,  $r_{\text{snow,ice}}$  are two distinct radiation factors for snow and ice, respectively,  $I_{\text{pot},i}$  is the potential solar radiation at the location  $i$  and  $T_i$  is the mean hourly air temperature at the same location.  $I_{\text{pot},i}$  is a function of the considered location  $i$ , accounting for effects of slope, aspect and shading, and of the day of the year, accounting for the seasonality of incident solar radiation. Values of  $I_{\text{pot},i}$  are calculated in hourly time-steps.

Accumulation is calculated from the given precipitation fields by distinguishing solid and liquid precipitation through a threshold temperature of 1.2 °C. Once on the ground, solid precipitation is not further redistributed, as such effects are integrated in the precipitation fields.

The temperature-index model was calibrated exploring the parameter space given by  $f_M$ ,  $r_{\text{ice}}$  and  $r_{\text{snow}}$  through Monte Carlo simulation. On the basis of the assumptions that the residence time of the water in the catchment is shorter than 2 weeks and that evaporation and sub-surface runoff are negligible, the objective function was defined as the sum of squares of the residuals given as the difference between measured and modelled runoff aggregated over 2 weeks. The match between the observed and modelled melt-out patterns – quantified by the average percentage of catchment area for which the snow cover is reproduced correctly – was used as an additional criterion to judge the model performance.

### *Runoff routing scheme*

In order to assess how the two different melt models and the different methods to distribute precipitation affected the simulated discharges, we examined several simple runoff routing schemes based on the concept of linear storages. In the following, we present results from a model using two reservoirs, one representing the glacierized areas and one representing the non-glacierized regions of the watershed. More complicated constellations of reservoirs (e.g. linear storage models as presented by Schaeefli et al. (2005) and Huss et al. (2008b)) did not significantly improve the simulation results. Note that the runoff routing schemes were intentionally not calibrated to match the total observed discharge volume. This approach was used to inhibit the calibration procedure compensating for systematic overestimation of modelled melt rates.

The two recession coefficients were initially calibrated by exploring the parameter space through Monte Carlo simulations. The obtained best parameter set was then locally refined using an unconstrained nonlinear optimization algorithm (Lagarias et al., 1998). The squared correlation coefficient between simulated and measured discharge was used as the objective function. If instead the sum of squared errors were used, which is a common choice of

objective function, the calibration minimized the objective function by increasing the recession coefficients to unreasonable values whenever the models overestimated discharge during the calibration period.

In this study, the runoff routing scheme was decoupled from the melt models. This is the typical approach for energy-balance models, in which the parameters of the runoff model are calibrated after the melt simulations. The usual method for temperature-index models would be to couple the melt model with the runoff routing scheme and then calibrate the parameters together. We are convinced that our approach is the fairest test for comparing the two melt models. However, the temperature-index model would perhaps show higher performance measures if the complete system, melt model and runoff routing scheme coupled, was calibrated at once.

## 2.4 Extrapolation of meteorological measurements

We extrapolated data from weather stations of the ANETZ and NIME networks with long-term records to imitate the typical input data situation for hydrometeorological assessments of alpine watersheds. We used data from three stations within the networks, here termed ‘regional stations’ or ‘regional observations’ (Table 2.1). The Dammagletscher and the three regional stations were located in the same climatic region defined by Laternser (2002). The measurements at the regional stations were extrapolated to the watershed using different schemes. The performance of the extrapolation schemes was assessed by comparison against the Damma, Bergsee and Albertheim stations (Figure 2.1), here termed ‘local stations’ or ‘local observations’, using the complete available data records (Table 2.1). Note that the stations only cover altitudes below the main glacierized part of the basin and that the reliability of the methods is unknown for the highest regions of the watershed. The temperature-index model requires measurements of precipitation and air temperature. The energy-balance model also requires measurements of relative humidity, wind speed and short- as well as long-wave radiation in addition to these data. As precipitation is an important input variable but at the same time difficult to extrapolate, we tested different distribution schemes. This is why respective methods are presented in a separate section (Section on ‘Methods to distribute precipitation’).

### *Air temperature*

Hourly air temperatures were distributed to the model grid by shifting the measurements from the station Grimsel to the given altitudes using monthly lapse rates. The measurements at Grimsel showed the highest correlation ( $r^2 = 0.97$ ) with the local station on the glacier forefield. We determined the monthly temperature lapse rates using the two stations Grimsel and Gütsch because they showed much higher correlation with our local measurements ( $r^2 = 0.95 - 0.97$ , depending on the considered local stations) than the remaining regional stations ( $r^2 \leq 0.88$ ). Note also that the two stations Grimsel and Gütsch have a much longer time-series (20 years of data) than the local stations (1 year). The determined lapse rates varied between 0.24 (January) and 0.64 (May) °C/100 m. They showed good agreement with lapse rates determined from the local stations (RMSE = 0.07 °C/100 m).

The extrapolated air temperatures showed a nearly linear relation to the local observations, and the deviations between the records were small (Table 2.2). The statistical performance was similar to that found by Liston and Elder (2006b), who examined a meteorological model for a study area located in North America characterized by moderate topographic relief. Thus,

## Chapter 2

we consider that the extrapolated air temperatures represent the local conditions well. However, note that the local measurements may not be representative for air temperatures on the glacier.

**Table 2.2.** Performance measures of extrapolated meteorological variables for different time resolutions.

Parameter	Unit	Time resolution	$r^2$	Mean error	RMSE
Air temperature	°C	Hour	0.95 – 0.97	- 0.3 to 0.9	1.2 – 1.9
		Day	0.97 – 0.99	–	0.8 – 1.4
Relative humidity	%	Hour	0.67 – 0.77	- 1.2 to 3.4	11.1 – 11.3
		Day	0.85 – 0.88	–	5.8 – 7.7
Wind speed	m/s	Hour	0.01 – 0.18	- 0.5 to 0.8	1.8 – 3.6
		Day	0.07 – 0.29	–	1.2 – 2.7
Long-wave radiation	W/m <sup>2</sup>	Hour	0.58	- 11.2	34.0
		Day	0.71	–	25.8
Short-wave radiation	W/m <sup>2</sup>	Hour	0.87	- 9.8	104.2
		Day	0.80	–	47.9
Acc. precipitation	mm	Day	0.42 – 0.48	- 0.50 to - 0.16	7.9 – 9.0
		Three Day	0.57 – 0.59	- 1.50 to - 0.48	13.9 – 15.6

$r^2$ : squared correlation coefficient; Mean error: mean error defined as the average difference between extrapolated and observed record; RMSE: root mean squared error. If several measurements were available for comparison, the range of the performance measures is listed. The performance measures were determined for the complete available data records at the local stations (Table 2.1).

### *Relative humidity*

Relative humidity was distributed using extrapolated air and dewpoint temperatures from the Grimsel station which showed the highest correlation ( $r^2 = 0.77$ ) for relative humidity with the local measurements on the glacier forefield. Monthly varying lapse rates were assumed for both air and dewpoint temperature, and determined from measurements recorded at Grimsel and Gütsch (Section on ‘Air temperature’). The dewpoint was calculated using the inverted saturation pressure function presented by Buck (1981) and showed lapse rates between 0.29 (August) and 0.57 (November) °C/100 m. The root mean squared error between these monthly lapse rates and lapse rates determined using the local stations was 0.17 °C/100 m and decreased to 0.07 °C/100 m when omitting the values computed for June and July. The extrapolated air- and dewpoint temperatures were converted back to relative humidities using the function for saturation pressure of Buck (1981).

The extrapolated relative humidities were highly correlated to the local measurements with relatively small errors (Table 2.2). As for air temperature, the statistical performance was similar to that found by Liston and Elder (2006b). However, we again have to restrain the finding to non-glacierized regions because the local measurements may not be representative for the actual conditions on the glacier.

### *Wind speed*

Wind speed is difficult to predict in mountain regions (Ryan, 1977), and wind direction and speed vary greatly over short distances (Ha et al., 2009). To extrapolate wind speeds, we

## Comparison of two melt models

simplified the approach presented by Winstral and Marks (2002) and Winstral et al. (2009). The method is based on the terrain parameter  $Sx$  which indicates whether a grid cell of a digital elevation model is sheltered or exposed towards a specified wind direction. The parameter  $Sx$  is given by the maximum slope between the grid cell of interest and the grid cells along a 300 m long line pointing towards a specified wind direction from this grid cell (Winstral and Marks, 2002):

$$Sx(x_i, y_i) = \max \left( \tan^{-1} \left\{ \frac{ELEV(x_v, y_v) - ELEV(x_i, y_i)}{[(x_v - x_i)^2 + (y_v - y_i)^2]^{0.5}} \right\} \right) \quad (2.2)$$

where  $ELEV(x_i, y_i)$  is the altitude of the grid cell of interest with coordinates  $(x_i, y_i)$ , and  $ELEV(x_v, y_v)$  are the elevations of the grid cells with coordinates  $(x_v, y_v)$  along the 300 m long line pointing towards the wind direction from the grid cell of interest.

We used the following procedure to extrapolate wind speeds from the reference station Güttsch which showed the highest correlation coefficient ( $r^2 = 0.14$ ) with the station on the glacier forefield: (1) the terrain parameter was determined for the reference station  $Sx_{ref}$ , the local stations  $Sx_{local}$  and the model grid  $Sx_{grid}$ . We averaged the terrain parameters for all wind directions determined with  $5^\circ$  increments. The averaging was performed because the terrain modified the observed wind directions greatly; (2) the terrain parameters of the model grid  $Sx_{grid}$  were linked to wind speeds at the reference station with a so-called wind factor  $wf$ . The dependent wind factor was determined by a linear function with two parameters  $a$  and  $b$ :

$$wf = a + b \cdot (Sx_{grid} - Sx_{ref}) \quad (2.3)$$

and the difference between the terrain parameters of the model grid and the reference station ( $Sx_{grid} - Sx_{ref}$ ) as independent variables; (3) the two parameters of the linear function were determined by regression using the measurements of the local stations and the reference station. The dependent wind factors, here defined as the ratio of the averaged wind speed at the local stations and the reference station ( $VW_{local}/VW_{ref}$ ), were plotted against the independent variables, the difference between the terrain parameter of the local stations and the reference station ( $Sx_{local} - Sx_{ref}$ ). We used 5 months of data captured during winter for the regression because then the snow covered ground at the different measurement sites had similar surface roughnesses; (4) with the two parameters  $a$  and  $b$  defined, the wind factors for the model grid could be determined using equation (2.3). The wind speeds measured at the reference station were simply multiplied by the wind factors. To avoid unreasonable extrapolated wind speeds, a lower limit of 0.3 and an upper limit of 1.5 were used for the wind factors.

The extrapolated wind speeds correlated poorly with the observations, but the mean errors were, on the other hand, relatively low (Table 2.2). The scatter between the extrapolated and observed wind speeds was larger than in previous studies (Liston and Elder, 2006b; Winstral et al., 2009). This may be due to the larger study site and the rougher terrain which considerably modified the observed wind directions. Prior applications of the  $Sx$  parameter in smoother terrain were able to sufficiently resolve wind directions and isolate upwind terrain. The inability to resolve local wind direction in this basin goes against the designed usage of the  $Sx$  parameter and most likely compromised the results. Thus, our work points to the need for high elevation data from mountain basins and efficient methods for determining wind directions in highly complex terrains. Furthermore, catabatic winds may also affect the model

## Chapter 2

performance on the glacier. These effects were not examined because measurements on the glacier were unavailable.

### *Incoming short-wave radiation*

The local cloud cover affects the incident solar radiation, an effect difficult to predict from the available ground observations. Therefore, we uniformly extrapolated the measurements from the station Gütsch. The measurements at Gütsch are unaffected by shading from surrounding terrain. The small short-wave radiation dependence on elevation was neglected (Marty et al., 2002).

On average, the extrapolated radiation records agreed rather well with the observations at the Bergsee station (Table 2.2). The statistical performance between the extrapolated and observed short-wave radiation was in similar range to that found by Liston and Elder (2006b).

### *Incoming long-wave radiation*

Incoming long-wave radiation was not measured at the regional stations. Instead we predicted long-wave radiation using a parameterization with the extrapolated air temperatures, relative humidities and short-wave radiation as input. The different algorithms summarized and tested for several sites in China and North America by Flerchinger et al. (2009) were examined and compared against the observations at the station Bergsee. The clear-sky algorithm of Dilley and O'Brien (1998) combined with the cloud-correction algorithm of Unsworth and Monteith (1975) performed best in reproducing the measurements at Bergsee. The cloud-correction algorithm relies on an estimate of the cloud cover which we obtained by comparing the incoming short-wave radiation with the clear-sky solar radiation following Campbell (1985). See Flerchinger et al. (2009) for all the details of the methods used including the procedure to estimate clear-sky solar radiation.

The extrapolated incoming long-wave radiation reproduced the local observations well (Table 2.2). The statistical performance between the extrapolations and observations were similar to that found by Liston and Elder (2006b) and Flerchinger et al. (2009). Note that in the study by Flerchinger et al. (2009) local data was used as input for parameterizing long-wave radiation whereas we used extrapolated meteorological variables.

## 2.5 Methods to distribute precipitation

By using four different methods to distribute solid precipitation, we examined how various snow cover patterns influenced the runoff simulated by the two melt models. The precipitation fields were generated with hourly measurements from the station Grimsel and scaled on a monthly basis to match the monthly precipitation sums observed at the station Göschenenalp. This scaling was performed because the daily measurements at Göschenenalp showed the highest correlation with the station on the glacier forefield and the smallest errors (Farinotti et al., 2010).

In this study, we attempted to examine how various snow cover patterns influenced the simulated runoff. Therefore, we normalized the precipitation fields against each other to keep the precipitation amounts constant between the four methods. Without this normalization, the different precipitation amounts obtained by the four distribution methods would likely influence the runoff more than the variations in simulated snow cover patterns.

The three first methods represent interpolation schemes typically used when modelling the discharge of glacierized watersheds (Klok et al., 2001; Verbunt et al., 2003; Koboltschnig et al., 2008; Bavay et al., 2009). The fourth scheme includes the effect of snow redistribution and was first presented by Jackson (1994).

**P<sub>unif</sub>** – Precipitation was distributed uniformly. The hourly precipitation  $P_{\text{unif},i}$  at any location  $i$  of the model grid was set equal to the measured precipitation at the station Grimsel. The obtained hourly precipitations were normalized by a factor  $\Sigma P_{\text{grad},i} / \Sigma P_{\text{unif},i}$  so that the precipitation amounts equalled the results of the second method  $P_{\text{grad}}$ .

**P<sub>grad</sub>** – Precipitation increased linearly with altitude (Peck and Brown, 1962). The hourly precipitation  $P_{\text{grad},i}$  was determined by shifting the measured precipitation  $P_{\text{grimsel}}$  on elevation  $z_{\text{grimsel}}$  to any altitude  $z_i$  in the watershed using a constant lapse rate  $dP/dz$ :

$$P_{\text{grad},i} = P_{\text{grimsel}} + P_{\text{grimsel}} \cdot (z_i - z_{\text{grimsel}}) \cdot dP/dz \quad (2.4)$$

For solid precipitation, we used a lapse rate of 5%/100 m determined from regional measurements and local observations inferred from time-lapse photography (Farinotti et al., 2010).

**P<sub>prism</sub>** – Large-scale horizontal precipitation field combined with the gradient precipitation field. The hourly precipitation  $P_{\text{prism},i}$  was obtained by multiplying the results from the method  $P_{\text{grad}}$  by a location-dependent factor  $D_{\text{prism},i}$ :

$$P_{\text{prism},i} = P_{\text{grad},i} \cdot D_{\text{prism},i} \quad (2.5)$$

The factor  $D_{\text{prism},i}$  was determined by interpolating the gridded PRISM dataset, which describes the mean precipitation distribution throughout the European Alps for the period 1961–1990 (Schwab et al., 2001), to our model grid. With this method, more precipitation falls in the western parts of the watershed than in the eastern regions. The hourly precipitations were normalized by a factor  $\Sigma P_{\text{grad},i} / \Sigma P_{\text{prism},i}$ .

**P<sub>distr</sub>** – Snow redistribution was accounted for with a parametric approach (Huss et al., 2008a). The hourly precipitation  $P_{\text{distr},i}$  was determined by multiplying the precipitation obtained by the method  $P_{\text{grad}}$  with a location-dependent factor  $D_{\text{distr},i}$ :

$$P_{\text{distr},i} = P_{\text{grad},i} \cdot D_{\text{distr},i} \quad (2.6)$$

The location-dependent factor  $D_{\text{distr},i}$  was calculated in two steps following Huss et al. (2008a). In the first step, we linearly increased the factor between 0.5 (most convex-shaped terrain features) to 1.5 (most concave-shaped terrain features) on the basis of curvatures determined from the digital elevation model describing the watershed. In the second step, we linearly decreased the obtained factors from 100% to 0% for surface slope angles between 40° and 60°. Thus, solid precipitation is transferred from the steeper to the flatter regions of the watershed with more deposition in valleys than on ridges. We again multiplied the precipitations by a factor  $\Sigma P_{\text{grad},i} / \Sigma P_{\text{distr},i}$  to keep the total precipitation constant between the methods.

Liquid precipitation was distributed uniformly with the measurements from Grimsel again scaled on a monthly basis to match the precipitation sums observed at Göschenenalp. We neglected the influence of horizontal variations in liquid precipitation. The regional stations also showed no increase in liquid precipitation with altitude during summer.

The mean error between the daily precipitation sums obtained by the method  $P_{\text{grad}}$  and the local measurements ranged from -0.5 to -0.16 mm/day at the Damma and Albertheim stations (Table 2.2). This corresponds to an underestimation of the yearly precipitation sums of between 3% and 10%. The yearly precipitation records at the two local stations were determined by combining: (1) the liquid precipitation measurements of the unheated rain gauge; and (2) an estimate of solid precipitation using the model SNOWPACK (see energy-balance model description) forced with continuous measurements of snow depth, air temperature, relative humidity, wind speed, reflected short-wave radiation and snow surface temperature. Note that manual snow depth measurements showed no indications of snow redistribution around the stations. Further, the mean errors between the extrapolated and local precipitation records were below the uncertainties of the precipitation estimates from the SNOWPACK model (Egli et al., 2009). Therefore, we consider that the  $P_{\text{grad}}$  method reproduces the precipitation sums for the two local stations well. However, we recognize that the yearly precipitation falling within the watershed may deviate from those obtained by our precipitation fields.

The extrapolated hourly precipitation records of the  $P_{\text{grad}}$  method correlated poorly with the local observations ( $r^2 \leq 0.21$ ). Thus, large runoff events driven by short precipitation events might not be captured adequately by hydrological models forced with the precipitation fields. The daily and three-daily precipitation sums showed significantly higher correlations with the observations than the hourly records.

## 2.6 Results of snow cover simulations

The model results showed that the precipitation distribution method including snow redistribution ( $P_{\text{distr}}$ ) most accurately reproduced the measured snow covered area and snow water equivalents. With these precipitation fields the simulated snow cover area matched the observations best (Table 2.3) and adequately reproduced the accumulation area of the glacier late in summer (Figure 2.3). These simulations also captured the variability of observed snow water equivalents decently (Figure 2.2) with a relatively low mean error between the observations and simulations (0.15 m w.e.). This indicates that the total winter precipitation was accurately modelled. However, the last comparison is rather uncertain partly because the observed snow water equivalents were determined using a statistical model of snow densities which was accurate within 17 % from the observed snow densities. The comparison between point measurements and gridded model outputs also introduces further uncertainties.

For the simulations driven by the precipitation distributions not accounting for snow redistribution ( $P_{\text{unif}}$ ,  $P_{\text{grad}}$  and  $P_{\text{prism}}$ ), the steep slopes in the western part of the watershed remained snow covered during the summer and the accumulation area of the glacier was not reproduced correctly (Figure 2.3). These simulations also displayed much lower variability of snow water equivalents than what was observed in field (Figure 2.2). We conclude that the parametric approach to distribute precipitation improves the snow cover simulations significantly.

## Comparison of two melt models

**Table 2.3.** Evaluation of observed and modelled snow covered area. The simulations driven by the precipitation distribution method accounting for snow redistribution ( $P_{\text{distr}}$ ) matched the observed snow cover patterns more accurately than the remaining simulations.

Prec. Method	Period	Energy-balance model			Temperature-index model		
		Match %	Overestimate %	$\Delta\text{Glacier}$ %	Match %	Overestimate %	$\Delta\text{Glacier}$ %
$P_{\text{unif}}$	Calibration	76	18	-11	70	27	-1
	Evaluation	75	18	-6	72	23	6
$P_{\text{grad}}$	Calibration	76	18	-6	73	18	-8
	Evaluation	76	16	-3	73	13	-10
$P_{\text{prism}}$	Calibration	76	18	-5	72	17	-1
	Evaluation	76	16	-3	73	11	0
$P_{\text{distr}}$	Calibration	80	13	5	81	11	-2
	Evaluation	81	9	3	80	6	-7

Match: the percentage of matching grid cells between the observation and simulation ( $\text{Sim}_{\text{snow}} \cap \text{Obs}_{\text{snow}}$ ) U ( $\text{Sim}_{\text{snowfree}} \cap \text{Obs}_{\text{snowfree}}$ ) averaged over the observation period; Overestimate: the overestimation of snow covered area by the simulation compared to the observation ( $\text{Sim}_{\text{snow}} \cap \text{Obs}_{\text{snowfree}}$ ) – ( $\text{Sim}_{\text{snowfree}} \cap \text{Obs}_{\text{snow}}$ ) averaged over the observation period;  $\Delta\text{Glacier}$ : difference between simulated and observed snow cover area on the glacier at the end of the summer (in percentage of glacierized area). For the calibration period, 10 photos were available taken on regular intervals during the period from 23 May 2008 to 21 August 2008. For the evaluation period, six photos were available taken on regular intervals during the period from 30 May 2009 to 1 August 2009.

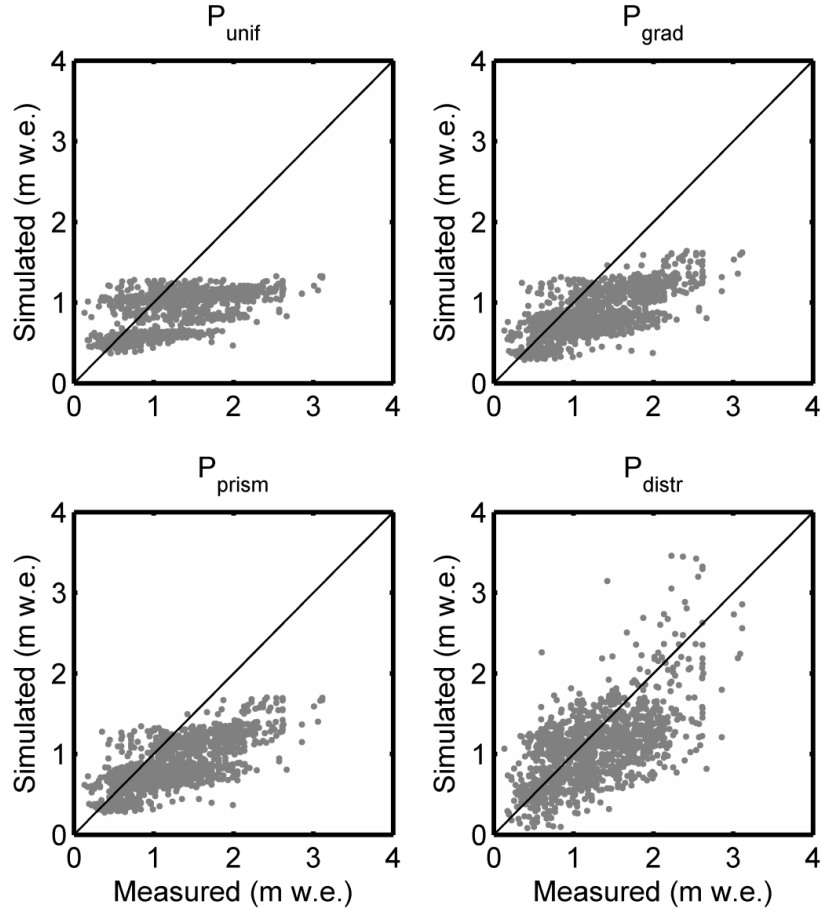


**Figure 2.2.** Scatter plots with measured and simulated snow water equivalents (in meters water equivalent) for the four precipitation distribution methods ( $P_{\text{unif}}$ ,  $P_{\text{grad}}$ ,  $P_{\text{prism}}$  and  $P_{\text{distr}}$ ). The plots show the energy-balance model results. The temperature-index model results were similar. The simulations driven by the precipitation distribution method including snow redistribution ( $P_{\text{distr}}$ ) reproduced the observed snow water equivalents roughly, whereas the other simulations showed no relationship between model results and observations.

## Comparison of two melt models

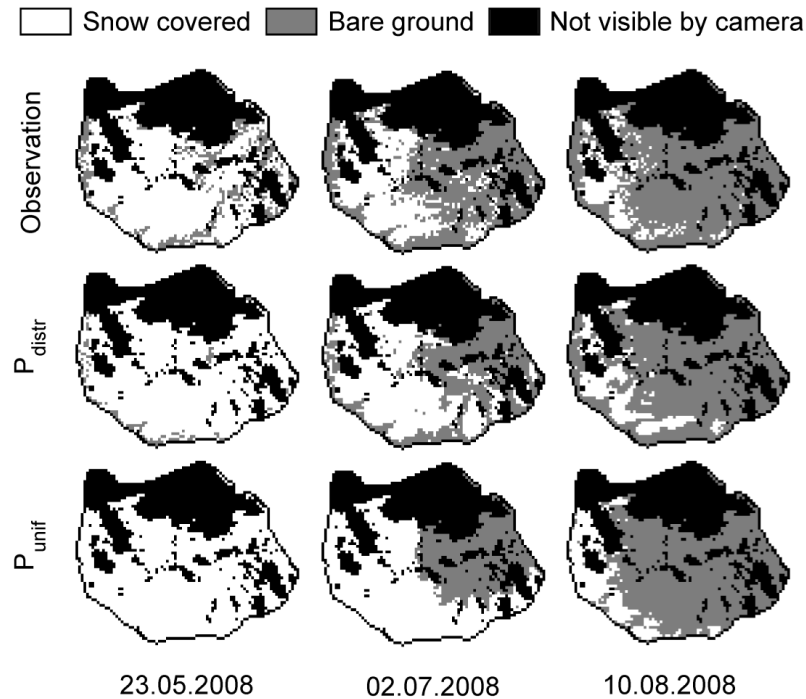


**Figure 2.3.** Observed snow covered area and simulated based on the  $P_{\text{distr}}$  and  $P_{\text{unif}}$  precipitation fields. The images show the energy-balance model results, which did not differ significantly from the temperature-index model results. Results of the  $P_{\text{grad}}$  and  $P_{\text{prism}}$  precipitation distribution methods are similar to the simulations driven by the  $P_{\text{unif}}$  precipitation fields. White regions are covered by snow. Grey regions are snow free. The black regions were not visible by the camera. The simulations forced by the precipitation distribution method accounting for snow redistribution ( $P_{\text{distr}}$ ) reproduced the accumulation areas of the glacier correctly. The steep slopes in the western part of the watershed remained snow covered during the summer for the remaining simulations instead.

## 2.7 Results of runoff simulations

In the following, we present results where we used the discharge measurements from 2008 for calibration and the measurements from 2009 for evaluation. The results of switching the calibration and evaluation periods are not shown, but are similar to the results reported here. In 2008, data from June to December were available (178 days). In 2009, data from March to October were available (214 days).

### *Influence of precipitation distribution on simulated runoff by the energy-balance model*

The runoff simulations by the energy-balance model were sensitive to the different precipitation distributions (Table 2.4). The simulations driven by the precipitation fields accounting for snow redistribution ( $P_{\text{distr}}$ ) reasonably captured the observed runoff. The total simulated discharge was close to the observations, deviating by only 11 mm ( $\leq 1\%$ ) during the calibration period and 79 mm (3%) during the evaluation period. The simulations forced by the precipitation fields not including snow redistribution deviated largely from the observations. The total simulated discharge differed up to 228 mm (10%) during the calibration period and 349 mm (15%) during the evaluation period from the observations. The simulations driven by uniformly distributed precipitation ( $P_{\text{unif}}$ ) performed worse than the simulations forced by the fields including elevation and horizontal gradients in precipitation ( $P_{\text{grad}}$  and  $P_{\text{prism}}$ ).

## Chapter 2

**Table 2.4.** Performance measures of runoff simulations by the energy-balance model and the temperature-index model. The statistical performance of the simulations by the energy-balance model increased (lower  $\Delta Q$  and higher NS-efficiency) when more realistic precipitation fields were used ( $P_{\text{distr}}$ ), whereas no such improvement was observed for the simulations by the temperature-index model.

Prec. Method	Period	Energy-balance model				Temperature-index model			
		$\Delta Q$	NS	Slope	Intercept	$\Delta Q$	NS	Slope	Intercept
$P_{\text{unif}}$	Calibration	228	0.76	1.06	0.023	18	0.84	0.83	0.100
	Evaluation	349	0.49	1.18	-0.021	145	0.70	0.81	0.170
$P_{\text{grad}}$	Calibration	149	0.76	1.03	0.019	47	0.85	0.85	0.094
	Evaluation	277	0.54	1.14	-0.018	208	0.66	0.82	0.187
$P_{\text{prism}}$	Calibration	128	0.76	1.02	0.019	-53	0.85	0.81	0.091
	Evaluation	256	0.55	1.13	-0.015	78	0.70	0.78	0.173
$P_{\text{distr}}$	Calibration	11	0.79	0.96	0.026	47	0.85	0.82	0.107
	Evaluation	79	0.64	1.04	-0.003	195	0.66	0.78	0.208

$\Delta Q$ : difference between the simulated and observed total discharge covering the calibration period (June 2008 to December 2008) and evaluation period (March 2009 to October 2009) in mm; NS: Nash–Sutcliffe efficiency; Slope: slope of linear regression curve between simulated and observed discharge; Intercept: intercept of linear regression curve between simulated and observed discharge (mm/h).

The  $P_{\text{distr}}$  method displayed lower streamflows than the other precipitation distribution methods (Figures 2.4 and 2.5) particularly during periods dominated by ice melt. The comparison between simulated and measured snow covered area in late summer showed that larger regions of the glacier were snow covered for the simulations forced by the  $P_{\text{distr}}$  method than the remaining precipitation distribution methods (Table 2.3). Thus, the snow cover patterns on the glacier largely affected the simulated discharge due to albedo effects.

## Comparison of two melt models

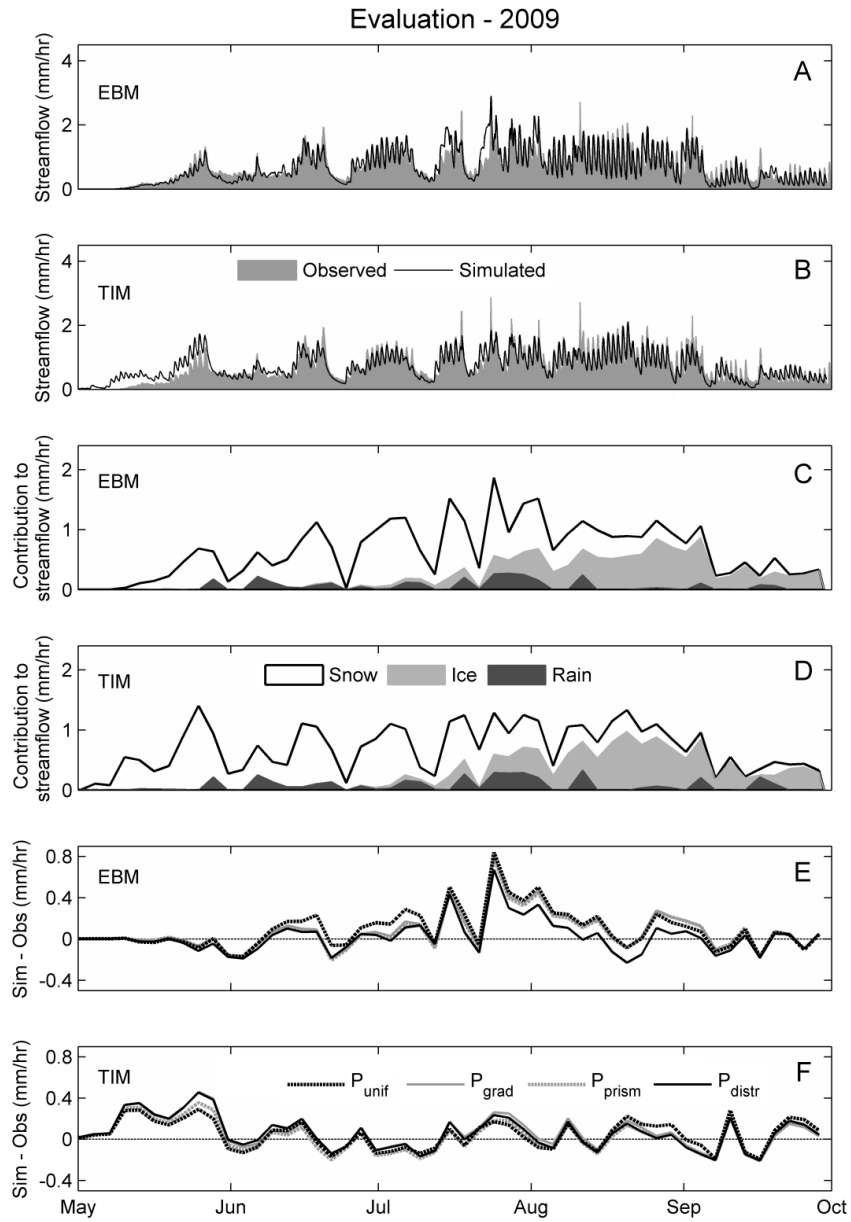


**Figure 2.4.** Simulated hourly runoff using the  $P_{distr}$  precipitation fields compared with the observed discharge (A and B) for the evaluation period (2009). Three-day averages of simulated water contributing to discharge of liquid precipitation, snow melt and glacier melt based on the  $P_{distr}$  precipitation distribution method (C and D). Three-day aggregated residuals, the difference between simulated and observed runoff (E and F). The temperature-index model simulated higher streamflows than the energy-balance model during snow melt, whereas the opposite during glacier melt.

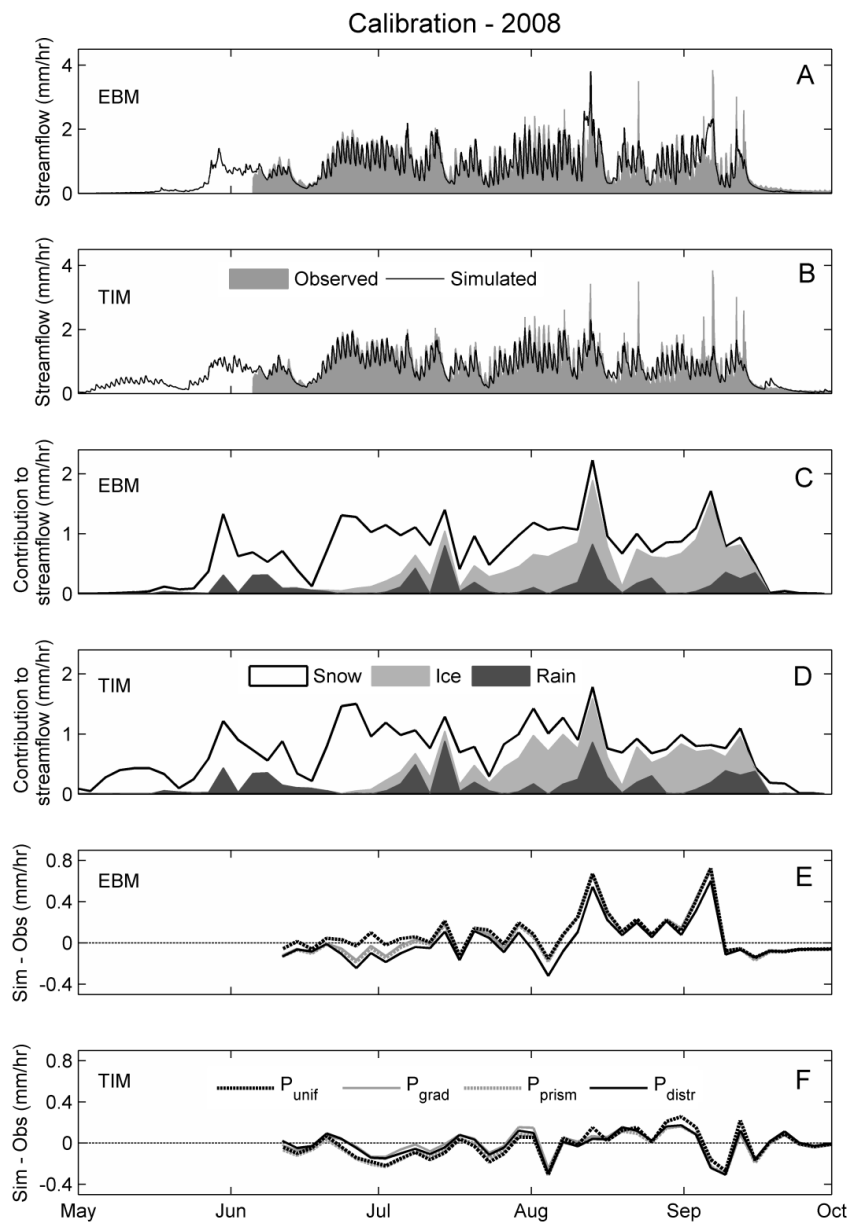


**Figure 2.5.** Simulated hourly runoff using the  $P_{distr}$  precipitation fields compared with the observed discharge (A and B) for the calibration period (2008). Three-day averages of simulated water contributing to discharge of liquid precipitation, snow melt and glacier melt based on the  $P_{distr}$  precipitation distribution method (C and D). Three-day aggregated residuals, the difference between simulated and observed runoff (E and F). The temperature-index model simulated higher streamflows than the energy-balance model during snow melt, whereas the opposite during glacier melt.

In this study, the total discharge varied by  $\leq 12\%$  when comparing the four simulations driven by the different precipitation fields. This result is similar to the findings by Dadic et al. (2008), where the discharge of the catchment decreased by 22% if gravitational snow transport was modelled. Furthermore, as found in earlier studies, we observed that the results of physically based snow cover models yield reasonable results provided that they are forced with accurate meteorological data (Winstral and Marks, 2002; Liston and Elder, 2006a).

## Comparison of two melt models

### *Influence of precipitation distribution on simulated runoff by the temperature-index model*

The runoff simulations by the temperature-index model were rather insensitive to the differently accurate precipitation inputs (Table 2.4). During the calibration period, the total simulated discharge was close to the observations deviating from the measurements by between -53 (-2%) and 47 mm (2%) depending on precipitation distribution. The deviation increased for the evaluation period to between 78 (3%) and 208 mm (9%), again depending on the method to distribute precipitation. The increasing deviation between simulated and observed total discharge from the calibration to evaluation period might indicate that the calibration parameters of the temperature-index model were non-stationary between the periods. The precipitation distribution method including snow redistribution did not improve the simulation results.

Figures 2.4 and 2.5 show that the simulations driven by the four methods to distribute precipitation behaved similarly during the complete calibration and evaluation period. The differences between simulated and observed runoff for the three-day average values varied slightly between the four simulations.

We conclude that the calibrated melt parameters were able to compensate for inaccuracies in the precipitation fields. Similar compensating mechanisms have been shown in parametric runoff models, and can be considered as a flexible feature of the model to nowcast discharge in spite of inaccurate inputs (Thorne and Woo, 2006). On the other hand, this study also implies that it is difficult to identify whether inappropriate input data may have caused biased parameters through calibration. We therefore suggest that both the simulated discharge and the model input data are validated against measurements. It is also important to note that the parameter values, which were obtained by calibration using short data records, may not be valid over longer periods as they might change with time. To increase the reliability of long-term simulations with temperature-index models (particularly climate change assessments), we would recommend to at least include estimates of the parameter uncertainty following, for example, the methods proposed by Beven (2009).

### *Runoff simulations reproducing snow melt*

The energy-balance model reproduced the snow melt dominated runoff period more accurately than the temperature-index model during the evaluation period (Figure 2.4). In May, during the first phase of snow melt the temperature-index model produced considerably higher streamflows than the energy-balance model and the observations. The differences between runoffs simulated by the temperature-index model and the observations were up to 0.45 mm/h averaged over three-day intervals during this period. In 2008, runoff measurements were not available during the same period for comparison. However, the temperature-index model produced higher streamflows than the energy-balance model in this period too (Figure 2.5). There are at least two possible reasons why the model shows this behaviour. First, the processes of refreezing and percolation of melt water within the snow pack are not included in the temperature-index model, and therefore snow melt may be released too early instead of being retained in the snow pack. Second, the calibration period does not include the complete snow melt period, which may decrease the temperature-index model performance and shows the importance of using an appropriate runoff record for calibration.

## Chapter 2

### *Runoff simulations reproducing glacier melt*

The temperature-index model reproduced the glacier melt dominated runoff period more precisely than the energy-balance model (Figures 2.4 and 2.5). During the period from July to October the temperature-index model displayed smaller deviations from the observations than the energy-balance model for the three-day average values. The largest discrepancies (about 0.84 mm/h) occurred when the sensible heat fluxes on the glacier simulated by energy-balance model exceeded 200 W/m<sup>2</sup>. Observations of sensible heat fluxes over alpine glaciers rarely reach these high values (Oerlemans and Grisogono, 2002).

It was impossible to distinguish whether the formulation of the turbulent heat fluxes was inappropriate or if air temperature, relative humidity or wind speed were wrongly extrapolated to the glacier, as direct measurements on the glacier were unavailable. However, the melt rates simulated by energy-balance model were highly sensitive to the assumption of atmospheric stability for the turbulent heat fluxes.

In order to examine the sensitivity of the applied atmospheric stability, two model simulations were performed with the  $P_{\text{distr}}$  precipitation fields. First, we used a neutral atmosphere over the complete watershed. This resulted in an overestimation of the discharge by 820 mm (35%) for the calibration period covering 178 days and 891 mm (38%) for the evaluation period covering 214 days. Second, we applied a stability correction scheme following Stearns and Weidner (1993). This resulted in an underestimation of discharge by -434 mm (-18%) for the calibration period and -350 mm (-15%) for the evaluation period. Thus, the variable stability correction scheme (see the description of the energy-balance model) was motivated by the following considerations: (1) that the atmospheric stability is mostly neutral over melting snow (Lehning et al., 2002b); and (2) that the atmospheric stability is often stable over a melting glacier surface (Paterson, 1994).

### *Statistical performance of runoff simulations*

The models displayed similar statistical performances (Table 2.4) provided that they were forced with the precipitation distribution method including snow redistribution ( $P_{\text{distr}}$ ). Then the Nash–Sutcliffe efficiencies and squared correlation coefficients were comparable between the models. During both the calibration and evaluation period, both models reproduced the total observed runoff within 8%. Thus, both models reproduced the observed discharge with similar statistical performance as found in studies where the input data was measured in the watershed itself (Zappa et al., 2003; Hock and Holmgren, 2005; Michlmayr et al., 2008).

The slope and intercept of the linear regression between simulated and observed discharge differed between the both models (Table 2.4). The temperature-index model displayed a flatter slope with a higher intercept than the energy-balance model. This indicates that fast discharge fluctuations were underestimated which suggest that over short time scales the melt rates might be influenced by single energy-balance terms not included in the model. Indeed, this is a known weakness of this model type (Huss et al., 2008a). However, fast discharge fluctuations are also largely influenced by the parameters of the runoff routing scheme. The decoupling of the runoff routing model from the melt model during calibration might also influence the performance of the temperature-index model.

## 2.8 Conclusions

We evaluated an energy-balance model with focus on snow processes and a temperature-index model designed for glacier mass balance studies in a watershed with glacio-nival runoff regime. The models were forced with data extrapolated from long-term measurement records to mimic the typical input data situation for climate change assessments. In general, the extrapolation schemes of the necessary model input variables accurately reproduced the local observations covering the lower elevation ranges at the study site. In particular, the method to distribute precipitation including snow redistribution effects ( $P_{\text{dist}}$ ) improved the snow cover simulations. However, hourly variations in precipitation and wind speed were not captured correctly by the applied extrapolation schemes. This may be an explanation why the models forced with these data occasionally failed to capture short-term runoff events. This study shows the importance of distributed meteorological measurements at higher elevations, which are needed to improve extrapolation schemes providing input data to hydrological models of alpine basins.

The runoff simulations by the detailed energy-balance model were accurate during the snow melt dominated period of the year, but dropped in performance during the glacier ablation season. For more reliable prediction of glacier melt, further studies with direct measurements on the glacier are needed in order to validate the input data and the contributions of single energy-balance terms to melting (i.e. turbulent heat fluxes and radiation budget). The snow distribution largely influenced the runoff simulations, mainly by affecting the glacier albedo. The results indicate that the simple method to distribute precipitation including snow redistribution effects may be an efficient method to ensure more accurate simulations of the average glacier albedo.

The temperature-index model properly reproduced the observed runoff during the glacier ablation season. However, during the snow melt dominated period of the year the runoff was considerably overestimated. The reason for this behaviour may be that the model neglects refreezing and percolation of melt water in the snow pack or that the runoff record used for calibration did not include the snow melt period. If the second explanation is correct, our results show the importance of using an appropriate runoff record for calibration. The model performance was independent of the precipitation distribution, showing that the calibration of the model compensated for inaccurate forcing fields.

We conclude that thorough input data pre-processing facilitates accurate runoff estimations in alpine watershed, especially if model input data need to be extrapolated from distant meteorological stations. Both model types tested reproduced observed discharge with similarly good statistical performance. However, with individual strengths and weaknesses, the models may be differently suited for specific applications.

## Acknowledgements

Financial support for this study was provided by the BigLink project of the Competence Center for Environment and Sustainability (CCES) of the ETH Domain. Many students and staff, particularly B. Fritschi and K. Steinier, helped with the field work and deserve gratitude. Many thanks to M. Lehning, who helped with the modelling. Finally, we acknowledge two reviewers for their helpful remarks.



## Chapter 3

### 3 Snow cover response to climate change in a high alpine and half-glacierized basin in Switzerland

Jan Magnusson, Tobias Jonas and Michael Lehning

*WSL Institute for Snow and Avalanche Research SLF, Flüelastrasse 11, CH-7260 Davos Dorf, Switzerland*

Ignacio López-Moreno

*Instituto Pirenaico de Ecología, CSIC, Campus de Aula Dei, P.O. Box 202, Zaragoza, Spain*

Manuscript Published in Hydrology Research, 41:230–240, 2010.

#### ABSTRACT

In alpine areas, the accumulation and melting of snow controls the hydrological regime. Even in watersheds where glacier melt dominates, the snow pack strongly influences the streamflow dynamics. Prognostic simulations of the response of the snow pack to climate change were conducted in a high alpine and half-glacierized basin in central Switzerland. The snow cover and glacier were simulated using a high-resolution alpine surface model. The simulations cover a reference period (1981–2007) and two predictions (2071–2100) where the measured records of temperature, precipitation and longwave radiation were modified using six regional climate model projections for two different emission scenarios of greenhouse gases. The results show that the snow season shortens by one month at the beginning of the winter and by one and a half months at the end of the season, compared to today. The maximum snow water equivalent decreases by 27% on average. The difference in the response of the snow pack to a change in climate between the emission scenarios is rather small. The most pronounced effects of a warming climate are simulated for the highest altitudes, where all snow completely melts during summer and no snow remains for glacier accumulation.

### 3.1 Introduction

Snow dominates the hydrological cycle in many alpine watersheds. The influence of the snow cover on the seasonal patterns of stream-flow increases with altitude. In mountain regions, the spring snowmelt is often the largest contribution to runoff throughout the year (Swift et al., 2005). On the other hand, discharge levels remain low during winter in snowmelt-dominated regions. On higher altitudes, the snow never melts and instead contributes to glacier regeneration. Even in watersheds where ice melt dominates the stream-flow dynamics, snowfalls on the glacier during summer increase the surface albedo. This leads to reduced melt rates with a significant effect on the temporary discharge dynamics. The meltwater from snow and ice provides water for drinking and irrigation in spring and summer. The water is often managed in reservoirs for later production of hydropower during times of increased energy demand (Schaeefli et al., 2007). In case of global warming, the accumulation and melt of snow are expected to change and affect the hydrological regime in large parts of the world (Barnett et al., 2005). From the hydrological point of view, prognostic simulations of the impacts of climate change on the snow are necessary.

The depth and duration of the snow cover in the Alps depends on elevation and typical weather conditions prevailing during individual winters, and is sensitive to changes in climate (Beniston et al., 2003a; Laternser and Schneebeli, 2003; Scherrer et al., 2004; Scherrer and Appenzeller, 2006). The most marked changes of the snow pack have been observed at sites on lower elevations, where relative changes are greater because of the shallow snow cover compared to the thicker snow packs at higher altitudes (Beniston, 1997; Marty, 2008). By combining trend analyses of historic snow measurements with predicted changes in temperature and precipitation, the duration of the seasonal snow cover is expected to shorten by about two months at the end of the 21<sup>st</sup> century in the Swiss Alps (Beniston et al., 2003a; Wielke et al., 2004). The abovementioned findings are based on measurements on lower elevations, while conclusions regarding higher mountain ranges are more uncertain.

Model studies of the snow cover response to changes in future climate in the European Alps are mainly included in assessments of the hydrological regime shift following glacier retreat. The results are consistent and show earlier snow cover depletion, enhanced glacier retreat and that the amount and timing of basin runoff will change (Bultot et al., 1994; Middelkoop et al., 2001; Shabalova et al., 2003; Jasper et al., 2004; Huss et al., 2008b). However, the representation of the snow cover in the models used in these studies is based on the temperature index method. This approach relies on the assumption of stationary calibration parameters, which may not be valid in the case of an increase in temperature outside of the calibration range. In this respect, energy balance models may be more reliable. However, crucial to all snow models is that they are driven with consistent input data representative of the study area, which may be a main challenge in complex alpine topography.

Simulations using energy balance models show similar trends in snow cover depletion and a shift in discharge regime for the European Alps due to global warming (Gellens et al., 2000; Etchevers et al., 2002; Beniston et al., 2003b; Keller et al., 2005; Bavay et al., 2009). These studies focus on large watersheds mainly without glaciers where temperatures are relatively warm compared to the higher regions in the Alps. For cold regions climate change may even lead to faster snow accumulation because of an expected increase in precipitation during winter, contradicting the above-mentioned findings (Hosaka et al., 2005; Raisanen, 2008). The energy balance models used in previous studies often have a limited representation of the effect of the mountainous terrain on snowmelt. Snow cover is represented on a single-layer

basis, and therefore with a rather simple representation of the energy budget. In spite of the existing studies dealing with the snow cover response to climate change in the Alps, many important regions have not yet been investigated with appropriate model simulations.

This paper examines the snow cover response to climate change in a high alpine and half-glacierized watershed where the hydrological regime is dominated by the accumulation and melting of snow and the glacier itself. The snow cover, in combination with the underlying glacier ice, was simulated with the physically based and spatially distributed model ALPINE3D (Lehning et al., 2006). The simulation covers almost 30 years with meteorological measurements from 1981 to 2007. Measurements of temperature, precipitation and radiation were modified using a statistical downscaling method to simulate the snow cover characteristics expected by the end of the 21<sup>st</sup> century, according to projections by six different regional climate models (RCMs).

### 3.2 Study area

The Damma glacier basin, northerly of the main Alp ridge in central Switzerland ( $N\ 46^{\circ}38.177'\ E\ 08^{\circ}27.677'$ ) has an area of  $12\ km^2$  and elevations from 1844 to 3621 m a.s.l. (Figure 3.1). The weather is mainly influenced from the north as the main ridge of the Alps in the south acts as a climate barrier. The runoff from the basin discharges entirely to a hydropower dam (Göscheneralpsee). Measurements of the glacier extension started in 1921 and since then the glacier front has retreated by about 10 m per year (Hammerli et al., 2007). An advance of the glacier front was recorded between 1972 and 1991. Today, the glacier occupies about  $5\ km^2$  of the total basin area. The catchment is underlain by granite bedrock and glacier tills are to be found on the land, which until recently was covered by the glacier.

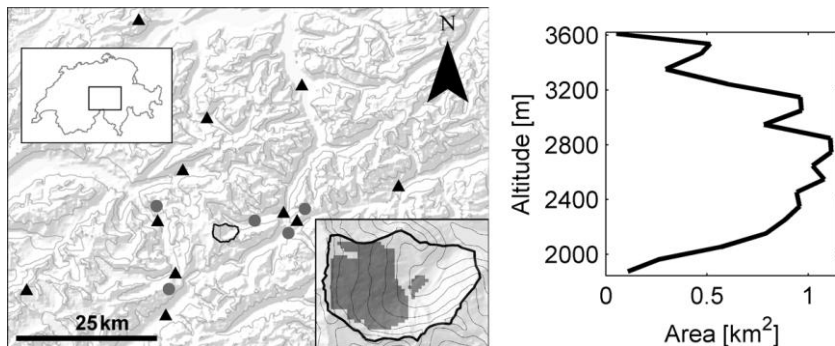


**Figure 3.1.** Left panel: Map of Damma glacier watershed (polygon in center of image) and surrounding area, location of weather stations (black triangles) and snow stations (grey circles). Right panel: Distribution of elevation within the watershed.

### 3.3 Data and methods

#### *Model description*

ALPINE3D is a spatially distributed model based on the physical behaviour of snow and is designed for high-resolution simulations of mountain surface processes in alpine terrain (Lehning et al., 2006). The snowpack is modelled by solving the heat and mass transfer equations of the snow cover. Simulations of the snow microstructure development within each layer of the snow pack determine the thermal conductivity and viscosity (Lehning et al., 2002a). As a stand-alone application, the snow module (SNOWPACK) has previously been

## Chapter 3

used for climate change impacts research (Rasmus et al., 2004) and is also capable of representing phase changes and densification from snow to ice. It can therefore be used for simulating glacier development and the transformation between snow and ice (Obleitner and Lehning 2004; Michlmayr et al., 2008). The radiation distribution in the basin is described by a view factor approach while solar shadowing, reflections and long-wave irradiance by surrounding terrain are included in the energy balance (Fierz et al., 2003).

ALPINE3D is initialized with a grid-based digital elevation model (100 m resolution) and a description of the soil properties on the same lattice. The simulations are driven by hourly meteorological measurements or predictions of air temperature, relative humidity, wind speed, precipitation and incoming long- and shortwave radiation. Data are provided by several surrounding automatic weather stations (details below). Precipitation is measured by heated gauges where, for each grid cell, the model determines whether precipitation falls as rain or snow by means of the local air temperature.

### *Description of the model simulations*

Three model simulations were completed for this study. In a first simulation, the present snow cover was modelled. The model was initialized with the glacier extent of the year 2000. The change in glacier extent within the simulation period was considered negligible because it only affected a few grid cells around the glacier tongue. In two further simulations, the snow cover at the end of the 21<sup>st</sup> century was modelled. These simulations were initialized without the glacier as studies predict that glaciers of similar size and at similar altitude ranges are expected to have completely melted due to global warming by then (Horton et al., 2006; Zemp et al., 2006). The focus of this study is on the dynamics of the seasonal snow cover. Ice and firn underlying the snow profiles were therefore removed in a post-processing step (firn was defined as snow older than one year).

In the first simulation, the present conditions were modelled using unmodified regional meteorological measurements from 1981 to 2007. In the two prediction simulations of the future, the snow cover conditions were modelled for the period 2071–2100 for two different emission scenarios of greenhouse gases. The two different emission scenarios were the Special Report on Emission Scenarios (SRES) A2 and B2 scenarios defined by the Intergovernmental Panel on Climate Change (IPCC) (Nakicenovic et al., 1998). Scenario A2 predicts a strong increase of carbon dioxide in the atmosphere, whereas scenario B2 predicts a moderate increase of greenhouse gases. For both prediction simulations, the observed regional meteorological measurements from 1981 to 2007 were modified to be representative of the future period based on the differences between the control and scenario runs of an ensemble of RCM simulations (for details see section ‘Model input: Modifying regional measurements to future conditions’).

Finally, as input for the three simulations, the observed and the modified measurement series were distributed to the model grid either by interpolation as a pre-processing step or by the radiation module of ALPINE3D (see following section for details).

### *Model input: Distributing regional measurements to the watershed*

Hourly measurements (observed or modified to future conditions) from eleven stations surrounding the basin were used to drive the model. These stations are located at a distance of 10–41 km away from the study area, and represent an altitude range 451–3580 m a.s.l.

(Figure 3.1). Temperature, humidity, wind speed and precipitation input data were distributed to the model grid using the interpolation methods of Zappa et al. (2005) for meteorological data. For these parameters, inverse distance weighting was selected as an interpolation method (Shepard, 1968) in combination with elevation-dependent detrending. However, radiation measurements were distributed within the watershed by the complex-terrain radiation module of ALPINE3D (Fierz et al., 2003). Hourly measurements of incoming shortwave radiation were acquired at a station 12 km away from the basin. Longwave radiation has not been measured in the vicinity, but was modelled from temperature, relative humidity and sunshine duration data (from the same station that provided shortwave radiation data) using methods given by Pirazzini et al., (2000). Pirazzini derived the incoming longwave radiation by applying the Stefan-Boltzmann equation using measured air temperature and an estimate of the atmospheric emissivity. The clear sky emissivity was described as a function of air temperature and water vapour pressure, the latter estimated from measurements of relative humidity and air temperature. Pirazzini included a correction factor to adjust for the increase in emissivity of a clouded sky.

### *Model input: Modifying regional measurements to future conditions*

To generate meteorological conditions representative of possible future climate characteristics, changes in temperature, precipitation and incoming longwave radiation were taken into account. These parameters were expected to have the greatest influence on the seasonal snow pack development. To estimate possible future climate conditions, RCM simulations were used (Christensen et al., 2007) of daily minimum and maximum temperatures, daily accumulated precipitation and daily averages of incoming longwave radiation. These simulations were available for a control period (1961–1990) and for a future period (2071–2100) with a spatial resolution of 50 km on the public PRUDENCE data archive (<http://prudence.dmi.dk>).

Data were downloaded for (1) the nearest grid cell to the study site, (2) the two IPCC scenarios of greenhouse gas emission A2 and B2 and (3) simulated by the five following models: HIRHAM (two different model runs available from the Danish as well as the Norwegian Meteorological institutes), PROMES (Universidad Complutense de Madrid), RCAO (Swedish Meteorological and Hydrological Institute), HadRM3P (Hadley Centre for Climate Prediction and Research) and RegCM (Abdus Salam International Centre for Theoretical Physics of Weather and Climate Section). Information about the different models is available in the final report of the PRUDENCE project, where further references are also given (Christensen, 2005).

The observed data series of precipitation, incoming longwave radiation and temperature were modified to represent climatic conditions towards the end of the 21<sup>st</sup> century, largely by following the methods described in Lopez-Moreno et al., (2008) and Bavay et al., (2009). An outline of the methodology is given below.

First, the daily precipitations simulated for each of the six different RCM runs were pooled into  $12 \times 3$  classes according to 12 months and 3 projections (current conditions, scenarios A2 and B2) (Figure 3.2, step 1). Second, within each of these 216 classes the values were subdivided into decile ranges (i.e. the lowest, second-lowest, ..., highest 10% of data) and the mean of all values within each decile (decile mean range or DMR) was derived (Figure 3.2, step 2). Third, the separate DRM values were averaged over the six RCM runs (Figure 3.2, step 3). Fourth, the difference between the two future scenarios and the current conditions was

## Chapter 3

described by dividing the DRM values for each scenario by the respective values of the reference simulations. This procedure finally results in 10 DRM quotients per 12 months per 2 scenarios (Figure 3.2, last step).

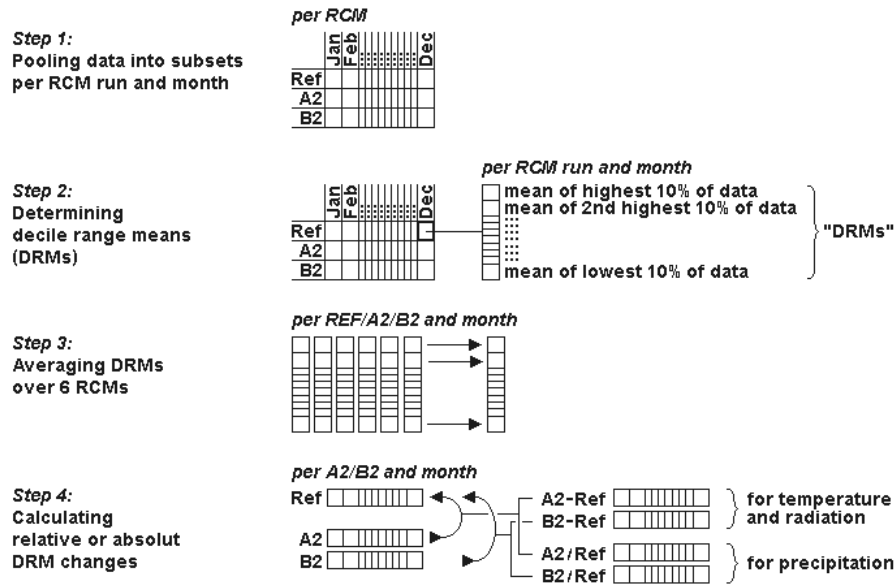


**Figure 3.2.** Flowchart illustrating the statistical downscaling procedure adopted from Bavay et al., (2009).

To generate model input data for the two scenarios, the measured data were manipulated using these DRM quotients. The measured precipitation data were pooled into monthly classes. For each of these 12 classes, the DRM values were calculated and each measured value was also assigned to its specific decile range. This allowed each measured precipitation value to be manipulated by multiplying it with its month-, deciles range- and scenario specific DRM quotient (Figure 3.3, left panel). To modify the incoming longwave radiation measurements, the same method was applied as for precipitation but with two exceptions. First, the DRM values of daily averages were determined instead of daily sums. Second, the effect of climate change was described with differences instead of quotients between the two future scenarios and the current conditions (Figure 3.3, right panel).

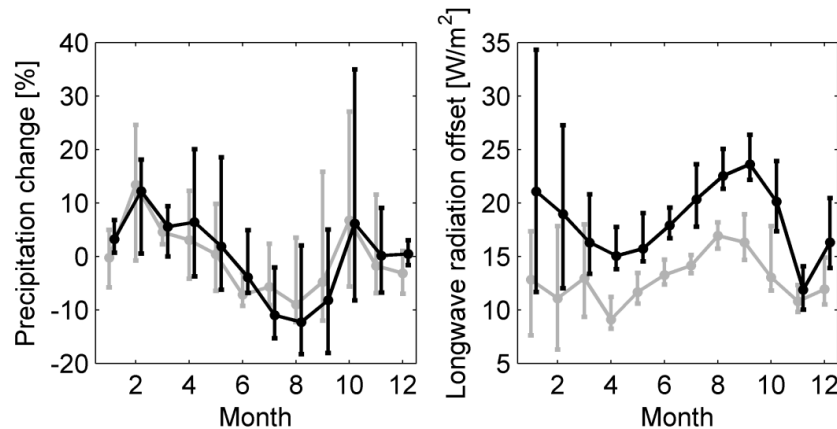


**Figure 3.3.** Change in precipitation (left panel) and incoming longwave radiation (right panel) due to climate warming for scenario A2 (black line) and scenario B2 (grey line). The line shows the change between the control period and the two emission scenarios for the fifth decile for each month in the year. The bars show the corresponding change for the first and the tenth deciles.

## Snow cover response to climate change

As temperature exhibits a daily cycle, the above described methodology was extended to account for the change in daily temperature range also. Therefore, the highest and lowest daily temperatures were modified separately (Figure 3.4). Finally, the hourly temperatures between the modified daily maximum and minimum values were determined in two steps. First, for both the originally observed as well as the already changed daily extreme values, a linear change was assumed for the temperatures lying between observations. Second, the differences between these two curves were added to the observed record of hourly temperatures. Note that this modification does not deform the altitudinal gradients as observed for the present conditions.

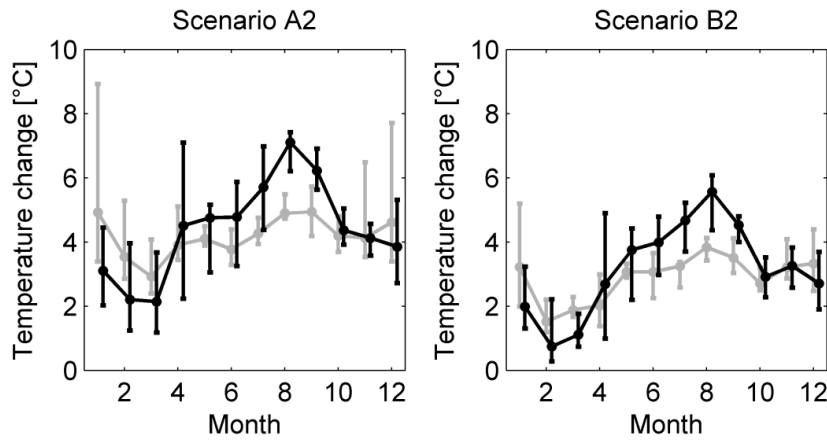


**Figure 3.4.** Change in maximum (black line) and minimum (grey line) temperatures for scenario A2 (left panel) and B2 (right panel). The line shows the change between the control period and the two emission scenarios for the fifth decile for each month in the year, and the bars shows the corresponding change for the first and the tenth deciles.

## 3.4 Results

### *Validation of reference simulation*

The modelled snow depths for the reference simulation were compared against independent measurements of snow depth (Figure 3.5). Measurements were only available from outside the basin. The five measurement stations were located on flat fields 5–15 km away from the basin, ranging in elevation from 1440 to 2430 m a.s.l. and only available after 1998. The measured snow depths were interpolated to the same grid (100 m resolution) as used for the ALPINE3D simulations applying the interpolation methods from Zappa et al. (2005). The average snow depth for all grid cells of flat pixels (slope angle less than 15°) between 2000 m and 2500 m elevation were compared because the interpolation is only able to reproduce snow depths in regions of similar terrain (i.e. flat fields) and of similar altitudes as the stations. The comparison shows good agreement between modelled and interpolated snow depths. The simulation represents dynamic changes well, but underestimates the peak snow depths for the first winter and overestimates the snow depths of the 2004/05 and 2005/06 winters.

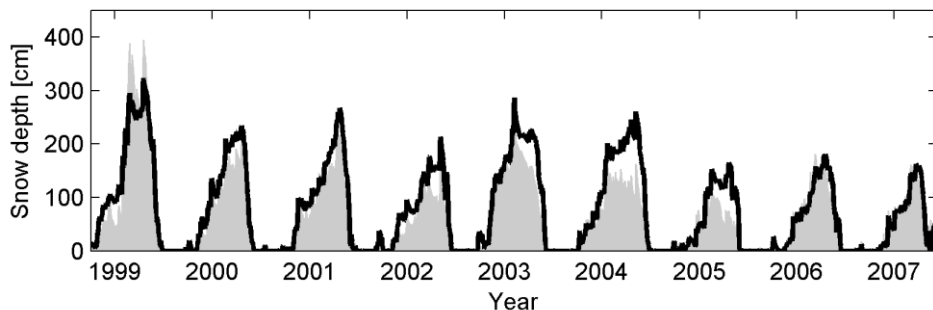


**Figure 3.5.** Modelled snow depths (filled line) and interpolated snow depths (grey area) averaged over the flatter regions of the basin (slope angle less than 15°) between 2000 and 2500 m elevation.

### *Climate change characteristics*

Predicted changes in precipitation show a strong seasonal pattern (Figure 3.3, left panel). Winter precipitation is expected to increase by up to 14% in February. In summer, however, the climate models simulate a reduction in precipitation by around 12% in July and August. Both emission scenarios provide similar precipitation estimates. For longwave radiation, on the other hand, an increase throughout the whole year is predicted with significant differences between the scenarios (Figure 3.3, right panel). The offsets lie between 11 and 24 W/m<sup>2</sup> for scenario A2 and between 9 and 17 W/m<sup>2</sup> for scenario B2. As expected, they correlate to the temperature increase which varies differently throughout the year for the daily highest and lowest temperatures (Figure 3.4). In August, the increase in the maximum temperatures (7 °C for scenario A2 and 5 °C according to scenario B2) are greater than for the lowest temperatures. In winter, on the contrary, the increase in minimum temperatures (5 °C for scenario A2 and 3 °C for scenario B2) is higher than for maximum temperatures. The monthly spread in temperature therefore increases for the summer, whereas it decreases during winter.

### *Snow-covered area and average water equivalent of snow*

Today, the whole basin is snow covered from the end of November until the end of May (Figure 3.6). Even in summer, 14% of the catchment remains snow covered and contributes to glacier accumulation. The peak in average snow water equivalent of 630 mm occurs during the first part of May. The accumulation period starts at the beginning of October and the

## Snow cover response to climate change

ablation period ends in late August. For scenario A2, the catchment is completely snow covered from the end of December until mid-April. The predicted snow season therefore begins almost one month later and ends at least one month earlier than today. For scenario B2, the corresponding snow-covered season lasts from mid-December until the beginning of May.

In summer, the basin will be snow free under both emission scenarios. For scenario A2, the predicted highest snow water equivalent occurs in the latter half of April and is 27% lower than today. The timing of the highest snow water equivalent is similar for scenario B2, which decreases by 18% compared to present conditions. The accumulation period starts at the beginning of October and the ablation period ends at the beginning of July for both emission scenarios. The predicted accumulation of snow seems to accelerate slightly while, according to these results, the predicted melting rate will be slower than under current climatic conditions.

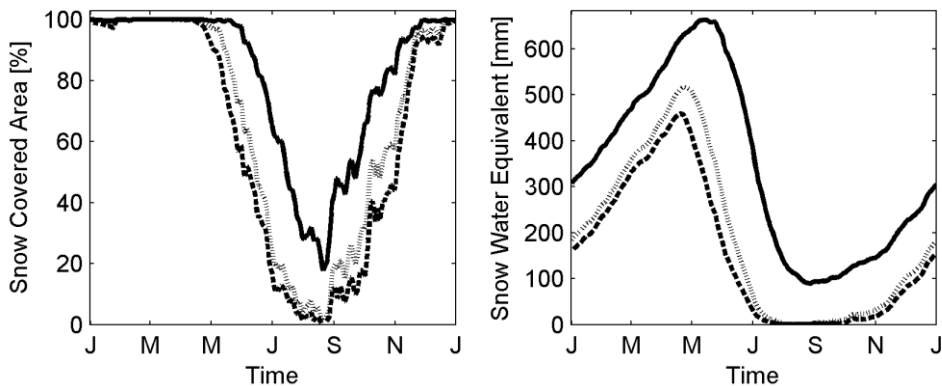


**Figure 3.6.** The effect of climate change on snow covered area (left panel) and on the average snow water equivalent (right panel). Current conditions (filled line), scenario A2 (dashed line) and scenario B2 (dotted line).

### *Variation of snow distribution with altitudes*

The peak snow water equivalents throughout the year increase with altitude because lower temperatures at the uppermost part of the basin allow a longer snow accumulation period (Figure 3.7). Under present climatic conditions, the highest snow water equivalent varies from 640 to 1925 mm depending on altitude. Almost no snow melts above elevations of 3300 m, resulting in peak snow water equivalents near the total yearly precipitation. For scenario A2, the highest snow water equivalents vary from 365 to 670 mm depending on altitude. For the less pronounced scenario B2, the values are slightly higher (from 460 to 720 mm). The changes in volume water stored as snow depend on the area distribution over the altitudes in the watershed and the peak snow water equivalents. Today, most water is stored as snow on the central and highest elevations with volumes between 0.84 and 0.94 million m<sup>3</sup> of water. Here, the greatest decreases are also simulated in the case of a warming climate. The volumes decrease on the middle altitudes with 0.18 million m<sup>3</sup> of water and on the higher elevations with 0.51 million m<sup>3</sup> of water.

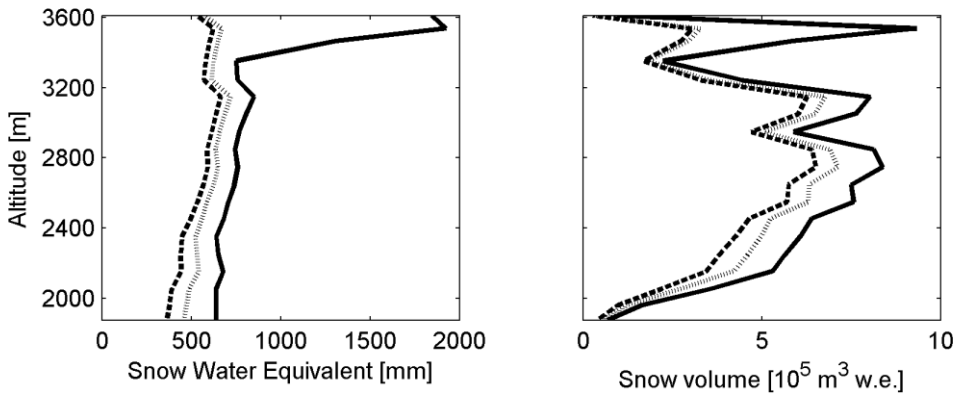


**Figure 3.7.** The effect of climate change on maximal snow water equivalent (left panel) and total volume of water equivalent (right panel) against altitude. Current conditions (filled line), scenario A2 (dashed line) and scenario B2 (dotted line).

#### *Duration of a seasonal snow cover for different altitudes*

As expected, the duration of seasonal snow cover is longer at higher altitudes because of the negative temperature gradient with elevation (Figure 3.8). Today, the snow season starts at altitudes just below 2800 m early in October and on the lowest elevations of the basin at the beginning of November. The snow season ends in mid-July just below 2800 m and at the beginning of June for the lowest parts. Above 2800 m, the snow pack lasts the whole summer during some of the years within the simulation period. There is therefore no well-defined period with a seasonal snow cover.

On the high elevations, the snow contributes to glacier accumulation. For scenario A2, the snow season is expected to start in late November at low elevations and in mid-October for the highest areas of the basin. The snow season starts about one month later than today. The snow season also ends earlier in the future according to these simulations, between the beginning of May and the end of July; this is around one and a half months earlier than today. The predicted changes are not as drastic for scenario B2, where the snow season starts between mid-November and the beginning of October. For both future scenarios, the snow cover in the basin is simulated to complete melt-out leaving no zones for glacier accumulation. The highest snow accumulation, which occurs as the snow water equivalent reaches its maximum, is simulated to occur one month earlier than the reference simulation.

## Snow cover response to climate change

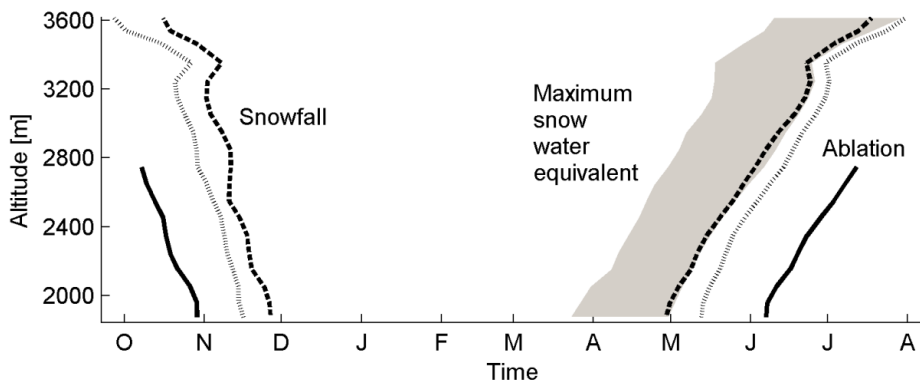


**Figure 3.8.** The elevation dependence of the first snowfall that builds a continuous snow cover until ablation and the shift in timing of highest snow water equivalent towards winter from spring. Current conditions (filled line), scenario A2 (dashed line), scenario B2 (dotted line) and shift in maximum snow water equivalent from current conditions to scenario A2 (shaded area).

### 3.5 Discussion and conclusions

Simulations of the snow-cover response to changes in climate have been presented. The study site represents a typical watershed on higher altitudes, and is covered by a glacier to half its extent. The glacier is evidence of cold temperatures and high precipitation rates over the past. The reference and the prognostic simulations cover time periods providing estimates of the conditions of today and at the end of the 21<sup>st</sup> century.

Snow-cover models using a degree-day factor approach can efficiently simulate the spatial and temporal distribution of a snow cover when carefully calibrated (Zappa et al., 2003). However, such methods may not be appropriate for climate change studies. The assumption of stationary calibration parameters may not be valid if entering new climatic conditions outside of the calibration range. This is likely to be the case as climate model projections predict an acceleration of global warming in the 21<sup>st</sup> century (IPCC, 2007). In contrast, models describing internal snow processes and simulating the surface albedo according to snow grain types seem more capable of representing the energy budget of the snow pack under varying meteorological conditions (Etchevers et al., 2004). This makes them more suitable for estimating trends in the snowpack response to climate change. ALPINE3D resolves these processes, the snow grain development within each layer of the snow pack and its influence on the surface albedo, as well as the interactions of the surrounding terrain on the radiation budget. The heat fluxes at the lower boundary between the snow pack and the ground are also taken into account. The effect of a glacier beneath the seasonal snow cover is therefore modelled well.

However, even with an appropriate snow model considerable limitations remain. Part of the uncertainty in the model results may arise from inconsistencies between the RCM projections and the observed meteorological records. Single RCM simulations were shown to reproduce observed temperatures with a bias of less than 2 °C and simulated precipitation amounts to compare to observations within 10–20% for the Alps (Giorgi et al., 2004). Deque et al. (2005) concluded that trust in RCM estimates of precipitation can only be achieved by an ensemble of model runs, as was the case with the PRUDENCE project.

Indeed, a follow-up study stated that the simulated climate change signal from the PRUDENCE ensemble is significant compared to the uncertainties between the models (Deque et al., 2007). In this study, the PRUDENCE model simulations were applied by

## Chapter 3

evaluating the differences between control and scenario runs. This delta-change approach is less sensitive to problems that may arise if the control run is not perfectly representative of local observations (Raisanen, 2008).

The interpolation of the meteorological measurements to gridded model input data may also introduce uncertainties in the results. Interpolating techniques cannot represent small-scale processes and local phenomena, such as catabatic winds from glaciers or effects due to persistent cloud patterns, with certainty. However, such techniques project the main pattern of spatial and temporal variability (such as temperature lapse rates) at a level of complexity that allows reasonable seasonal snow distribution model results. Using interpolated meteorological fields as input to snow models has previously been shown to give accurate estimates of snow-cover distributions and discharges in mountainous terrain (Lehning et al., 2006; Michlmayr et al., 2008; Bavay et al., 2009; Hirashima et al., 2008).

Also in this study, the reference simulation reproduces the snow cover reasonably well within the watershed (Figure 3.5). A further shortcoming relates to the parameterization of longwave radiation, which is typically site-specific. Here, transferability problems may introduce inaccuracies of the modelled snowmelt rates. However, the method used here was shown to accurately reproduce longwave radiation for different sites (Pirazzini et al., 2000; Michlmayr et al., 2008) and, in this study, the snowmelt rates simulated for the current conditions compared well with the observations. Finally, the redistribution of snow from wind and avalanches is important and influences the amount of snow on some grid points. The effects over those regions that have been averaged in this study are assumed to be minor.

The simulations show drastic changes in both the temporal and spatial patterns of the snow cover in the basin. The snow season shortens by one month at the beginning of the winter and by between one to two months at the end of the winter, compared to the conditions of today. Similar decreases in snow season duration in Switzerland have been modelled in previous studies (Beniston et al., 2003b; Jasper et al., 2004). The predicted decrease in days with snow cover is not as severe as on lower altitudes, where the average winter temperatures oscillate around zero (Hantel and Hirtl-Wielke, 2007). The combined effect of higher temperatures and longer snow free periods induces higher evaporation rates during summer and lower accumulated sublimation during winter (Dankers and Christensen, 2005). A shift in timing and a decrease in runoff can therefore be expected.

Further, in the studied basin the most marked impacts of climate warming on the snow pack will occur in the uppermost parts of the basin. At these locations, a predicted increase in temperature would lead to a total ablation of snow; consequently, the present accumulation area of the glacier would no longer exist. However, the predicted winter temperatures will still fall below zero at these high altitudes, allowing a significant snow accumulation. The predicted increases in precipitation during the first winter months seem to accelerate the snow accumulation rates compared to the reference simulation.

On the other hand, the melt rate of the snow pack seems to decelerate according to the prognostic simulations compared to the conditions of today. This could arise because the incident solar radiation is lower during the ablation period that occurs about one month earlier than today. As a simple validation of the simulations, the elevation profiles for the highest snow water equivalent are to be shifted upwards by about 500 m to match the current conditions. This corresponds to an increase in temperature of about 3.5 °C assuming a vertical

temperature lapse rate of 0.7 °C, which is between the mean annual temperature increase expected towards the end of the 21<sup>st</sup> century for scenarios A2 and B2 (Figure 3.4).

This study extends the earlier findings of a decline in snow cover due to climate change to the higher regions of the Alps in Switzerland. With a reduced snow cover, further glacier retreat and soil development, the hydrological response of the type of watershed studied may change. Further studies are therefore important.

## Acknowledgements

The research for this paper was carried out with the financial support of the ETH Centre of Competence for Environment and Sustainability CCES. The regional climate models were provided through the PRUDENCE data archive, funded by the EU through contract EVK2-CT2001-00132. MeteoSwiss provided the meteorological measurements. Henning Löwe, Gernot Michlmayr and Matthias Bavay deserve gratitude for all help. We also thank the two reviewers for their helpful comments.



# **Chapter 4**

## **4 Melt water driven stream and groundwater stage fluctuations on a glacier forefield (Damma gletscher, Switzerland)**

Jan Magnusson, Florian Kobierska and Tobias Jonas

*WSL Institute for Snow and Avalanche Research SLF, Flüelastrasse 11, CH-7260 Davos Dorf, Switzerland*

Stephan Huxol

*Swiss Federal Institute of Aquatic Science & Technology, Eawag, CH-8600 Dübendorf, Switzerland*

James Kirchner

*Swiss Federal Institute for Forest, Snow, and Landscape Research (WSL), CH-8903 Birmensdorf, Switzerland*

*Department of Environmental Sciences, Swiss Federal Institute of Technology (ETH), CH-8092 Zürich, Switzerland*

Manuscript Submitted to Hydrological Processes.

### **ABSTRACT**

In many mountain regions, large land areas with heterogeneous soils have become ice-free with the ongoing glacier retreat. On these recently formed proglacial fields, the melt of the remaining glaciers typically drives pronounced diurnal stream level fluctuations that propagate into the riparian zone. This behaviour was measured on the Damma glacier forefield in central Switzerland with stage recorders in the stream and groundwater monitoring wells along four transects. In spite of the large groundwater stage variations, radon measurements in the near-stream riparian zone indicate that there is little mixing between stream water and groundwater on daily time scales. At all four transects, including both losing and gaining reaches, the groundwater level fluctuations lagged the stream stage variations and were often damped with distance from the stream. Similar behaviours have been modelled using the diffusion equation in coastal regions influenced by tidal sea level variations. We thus tested the ability of such a model to predict groundwater level fluctuations in proglacial fields. The simulations reproduced the observed fluctuations accurately despite heterogeneous soils and irregular topography in most locations. Calibration of the model for individual transects yielded estimates of hydraulic diffusivities between the stream and groundwater monitoring wells, which are useful for modelling larger-scale groundwater flows in these environments. We conclude that studying diurnal groundwater fluctuations can yield important information about the subsurface hydrology of alpine watersheds dominated by glacier melt.

## 4.1 Introduction

Downstream of glaciers, melt water typically flows through braided streams on a glacial floodplain, with potentially large subsurface water fluxes through conductive till (Ward et al., 1999). This groundwater water flow may carry solutes from weathering processes, affecting the formation of soil and influencing the colonisation of ecosystems. The characteristics of groundwater flow in these heterogeneous environments with irregular topography and moraine-like soils are still poorly understood (Roy and Hayashi, 2009). In this study, we analysed how periodic stream level variations caused by glacier melt propagate into the riparian zone of the Damma glacier forefield in the central Swiss Alps.

Simple analytical models have adequately predicted tidal water table fluctuations in coastal aquifers (Montalto et al., 2007; Raubenheimer et al.; 1999 and Nielsen, 1990). They reproduce the basic properties of diffusive wave propagation, namely a nearly linear increase in time-lag and an exponential damping of the wave's amplitude with distance. The damping also increases with the frequency of the signal. For decades, the wave propagation method has been a fundamental part of hydrological studies in coastal areas where the modelling approximations hold: a homogenous aquifer with a flat base, and small water-table fluctuations relative to the aquifer thickness. In a sub-alpine riparian zone, Loheide and Lundquist (2009) showed that the diffusion models can also predict diurnal snowmelt-induced groundwater fluctuations. Their study site was a flat meadow with relatively homogeneous soil. However, glacier forefields usually have highly heterogeneous soils and irregular topography. Thus, the question remains whether these analytical models are also useful for simulating water table variations in these glacier forefields and whether they can be used to estimate hydraulic parameters of the aquifer.

In this paper, we show that stream stage fluctuations caused by melting ice and snow propagate into the aquifer of a glacier forefield. The measured groundwater fluctuations partly display an amplitude-damping and an increased time-shift away from the stream similar to the observations seen in tidally influenced coastal regions. Therefore, we test a diffusion model for the propagation of groundwater waves driven by water level fluctuations in the stream. Fitting the diffusion model to the field data yields a bulk hydraulic diffusivity value which summarizes important characteristics of the local aquifer. By extending the model for sloping terrain, we examine how the advection term representing the slope of the aquifer may influence the hydraulic parameters determined with the diffusion model. Finally, we use groundwater radon data to determine whether the large diurnal groundwater fluctuations cause a flushing of water in and out of the riparian zone.

## 4.2 Study site and data

The Damma glacier forefield in the central Swiss Alps ( $N46^{\circ}38.177' E08^{\circ}27.677'$ ) covers an area of about half a square kilometre and an elevation range from 1950 to 2050 m a.s.l. (Figure 4.1). The proglacial field is bounded upstream by a debris-covered dead-ice body (separated from the glacier, which has retreated further up the valley headwall) and laterally by two large side moraines dating from about 1850 (the end of the Little Ice Age). The topography of the watershed is characterized by high alpine terrain with steep slopes (up to nearly  $80^{\circ}$ ). The main stream exits the dead ice body and follows a braided path through the forefield. A side stream originating from the northern part of the glacier joins the main stream from the north-west. The hydrological regime of the study area is dominated by runoff

generation from the seasonal snow cover and the glacier (Magnusson et al., 2011). The average annual precipitation at the site is approximately 2200 to 2300 mm (Kormann, 2009).

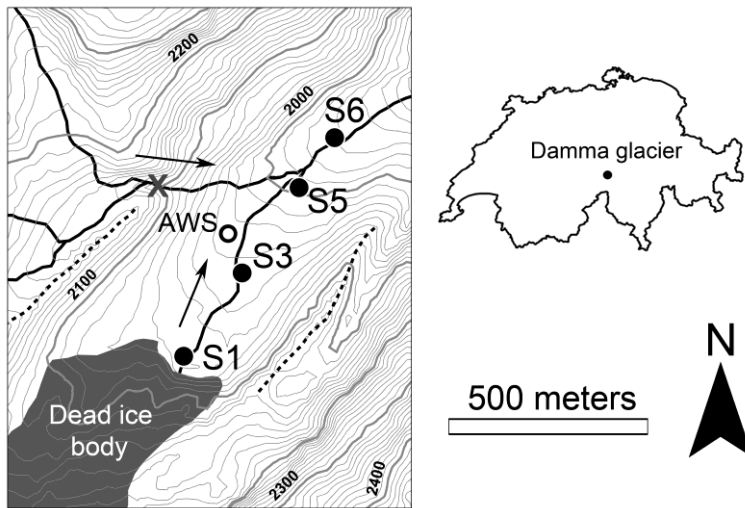


**Figure 4.1.** The Damma glacier forefield in central Switzerland. The forefield is bounded by a dead ice body and two large side moraines from the Little Ice Age (indicated with dotted black lines). The four sampling sites (numbered S1 for the most upstream to S6 for the most downstream site) are located along the main stream (black lines, with arrows showing the flow direction). In the channel draining the north-western part of the watershed, we monitored only the stream stage variations (grey cross). The automatic weather station (AWS) is located in the middle of the forefield. Terrain elevation is shown by 10 m contour intervals.

Glacial tills and debris of unknown depth cover the granite bedrock. Though there are large moraine boulders, the soils are mainly constituted of cobbles and sand with some silt and minor amounts of clay. To estimate hydraulic conductivity of the glacial till and soil, we conducted slug tests on groundwater monitoring wells (which we describe below) following the standard procedure (e.g. Butler, 1997). The hydraulic conductivities, varying between around 1 and 45 m/day, were determined by analyzing the slug tests following the methods of Bouwer and Rice (1976). These data only give rough estimates, due to the technical and analytical constraints of the method. However, the results yield values similar to those measured in glacial tills elsewhere (Boulton and Zatsepin, 2006; Hinton, 1993).

We measured water levels at four transects along the main stream channel, each consisting of one stream stage recorder and two groundwater tubes situated perpendicular to the stream (Figure 4.1). In these transects, the stream stages were monitored in perforated tubes whereas the groundwater levels were measured in monitoring wells. The wells consisted of fully-screened plastic tubes 6 cm in diameter, extending to depths between 60 and 130 cm. The well spacing varied between 2 and 5 m. The other stream channels draining the north-western part of the watershed were only monitored for stream stage. All water levels were recorded using non-vented pressure sensors (Hobo U20 Water Level Logger with 0.14 cm resolution and 0.3 cm accuracy according to the manufacturer's specification). The stream stages were measured with 2-minute sampling interval, and the groundwater stages were measured with 5-minute sampling interval. The measurements were averaged to 10 minute values. The absolute pressure readings were adjusted for atmospheric pressure variations (measured with the same type of pressure sensor on the forefield near site S6). The four transects are denoted S1, S3, S5 and S6 in increasing order downstream (see Figure 4.1). The site names are consistent with another study of the glacier forefield (Magnusson et al., Submitted, see Chapter 5), and as no groundwater measurements were performed at site S2 and S4 they were

## Chapter 4

omitted in this study. The in-stream water level recorders are denoted S1<sub>stream</sub> - S6<sub>stream</sub>, and the near-stream and more distant groundwater recorders are denoted S1<sub>near</sub> - S6<sub>near</sub> and S1<sub>far</sub> - S6<sub>far</sub>, respectively (see Figure 4.2). None of the sites were flooded during fair-weather periods.

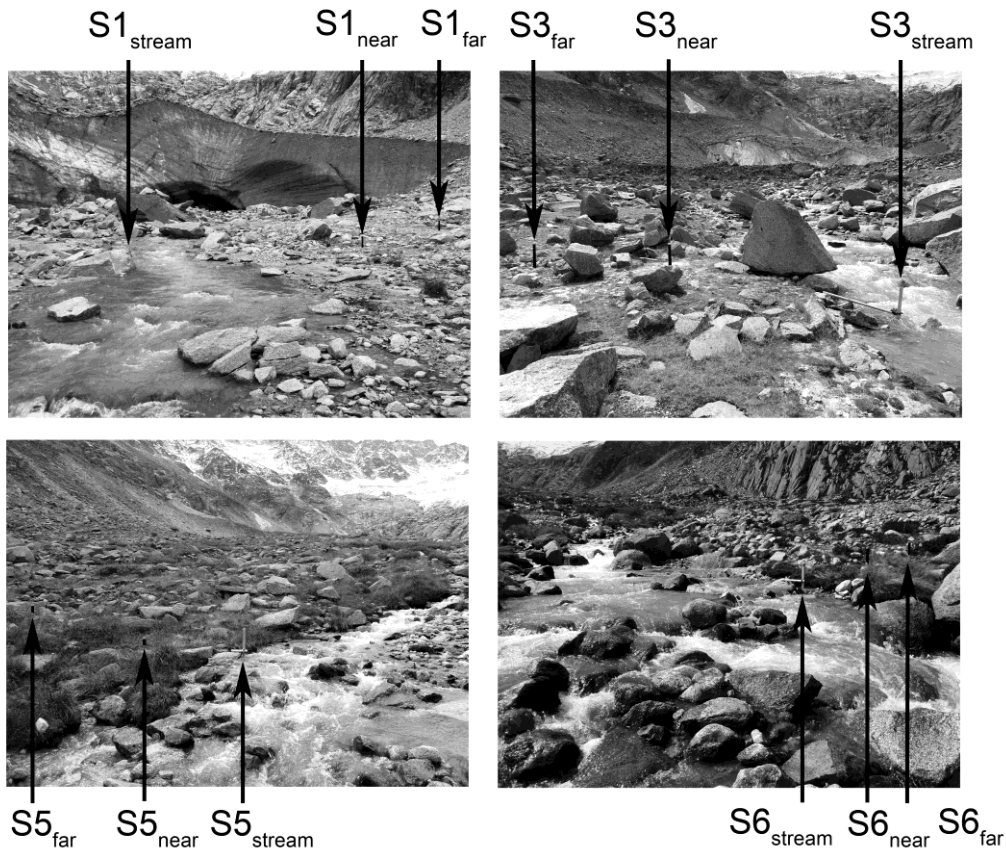


**Figure 4.2.** Photos (looking upstream) showing the four measurement transects with one stage recorder in the stream and two stage recorders in groundwater monitoring wells.

The sites were selected to represent different characteristics of the glacier forefield (Figure 4.2; Table 4.3): S1) nearly flat ground ( $\sim 4^\circ$ ) with a rather straight stream section of variable width, the shortest distance between stream and groundwater tubes was 5 m (near tube) and 10 m (far tube); S3) nearly flat ground ( $\sim 5^\circ$ ) with a meandering stream reach with highly variable cross-sections, the shortest distance between stream and groundwater tubes was 4 m (near tube) and 6 m (far tube); S5) steep slopes ( $\sim 13^\circ$ ) facing slightly toward the stream with a relatively straight stream section, the shortest distance between stream and groundwater tubes was 2 m (near tube) and 4 m (far tube); and S6) intermediate slopes ( $\sim 7^\circ$ ) and variable stream cross-section, the shortest distance between stream and groundwater tubes was 2 m (near tube) and 4 m (far tube).

Meteorological conditions were recorded at an automatic weather station situated on the glacier forefield (Figure 4.1). Hourly precipitation rates were measured using a tipping bucket rain gauge with a precision of 0.20 mm according to the manufacturer (ARG100, Campbell Scientific).

### 4.3 Observed water level fluctuations

During fair-weather periods, the recorded water levels showed clear daily fluctuations in the stream and groundwater stages during glacier melt (Figure 4.3). In contrast, rain events caused water levels to rise sharply with a fast recession both in the stream and the groundwater monitoring wells. The measured water levels indicated both losing (S3) and gaining stream reaches (S1, S5 and S6). However, at S5, which is the steepest location both parallel and perpendicular to the stream, diurnal groundwater fluctuations were small and rain hardly influenced the water stages. During tracer experiments at this location, we injected fluorescent dyes into the groundwater monitoring wells along this transect. Because of the steep down-valley gradient, these tracers were found downstream in small springs on the stream bank after a short time (after around 1 min for S5<sub>near</sub> and after around 20 min for S5<sub>far</sub>), indicating a gaining stream reach. Water levels in S5<sub>near</sub> are typically 20 cm below those in the adjacent stream channel, and exhibit very small diurnal fluctuations (<1cm in the well versus >5cm in the stream). From these observations, we infer that well S5<sub>near</sub> is largely isolated from the adjacent stream channel and its stage fluctuations. Although S5<sub>near</sub> drains rapidly to small springs on the stream bank roughly 1 m downstream of the transect (and roughly 3 cm below the well itself), the steep hydraulic gradient and fast groundwater flow apparently inhibit the propagation of stage fluctuations uphill from the springs to the well. Accordingly, we excluded data from this particular well in the following analysis.

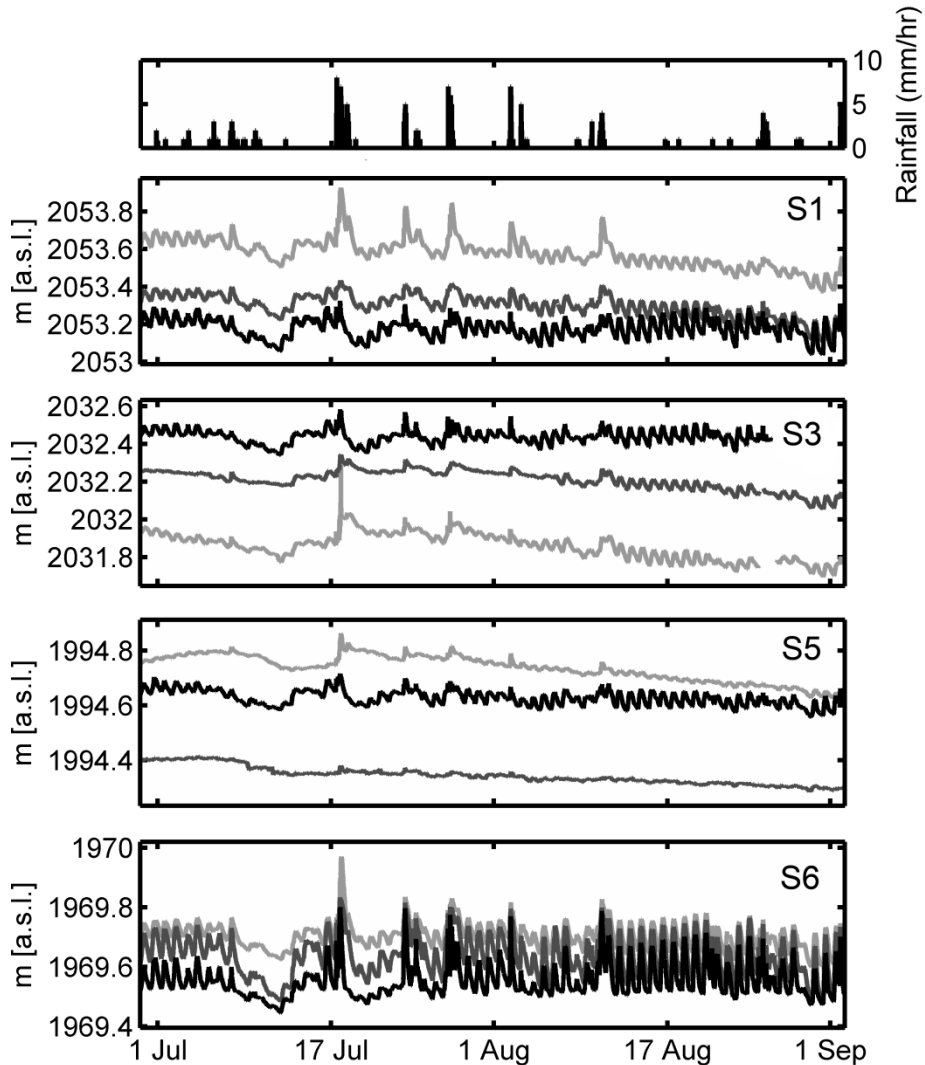


**Figure 4.3.** Water level fluctuations for two months in 2009. The stream level fluctuations (black lines) induce variations in groundwater stage both near (dark grey lines) and far (light grey lines) from the stream with similar properties as observed in tidally influenced regions.

To analyze the daily water level fluctuations, we selected three eight-day intervals with dry weather conditions. The accumulated precipitation, measured with the automatic weather station located on the forefield, was between 0 and 4 mm during these periods. We numbered the periods as follows:

- T<sub>1</sub> - 11 August 2009 to 19 August 2009
- T<sub>2</sub> - 22 September 2009 to 30 September 2009
- T<sub>3</sub> - 26 June 2010 to 4 July 2010

We first analyzed the relationship between the stream and groundwater level measurements from each sampling site. The time shift, determined by a cross-correlation analysis for the individual periods, showed that the groundwater fluctuations at all transects lagged behind the stream stage variations and that the time-lag increased with distance from the streams (Table 4.1). The high correlation coefficients showed that no large shape deformation of the propagating wave occurred between the stream and the groundwater measurements. This indicates that only the adjacent stream stage variations influenced the groundwater

## Analysis of groundwater level fluctuations

fluctuations, and that the component frequencies (Fourier modes) of the diurnal stage variations were equally damped over the short travel distance of the propagating wave. The amplitudes of the groundwater fluctuations were mostly damped compared to the stream level fluctuations, but not increasingly damped with increasing distance from the stream at all locations. In particular: at S1<sub>far</sub>, near the dead ice body, stage fluctuations were very large during the last monitoring period (T3), possibly due to local snowmelt; at another transect (S3), the groundwater fluctuations were larger in the far well than in the near-stream well; and in one monitoring well (S6<sub>near</sub>) the groundwater fluctuations were larger than the stream level variations. This suggests that the observed groundwater fluctuations may be driven by larger or smaller stream stage variations than measured by our stream level recorders.

**Table 4.1.** Ratio between amplitude of groundwater and stream level fluctuations ( $A_{ratio}$ ), and the time shift determined by cross-correlation analysis ( $\tau$ ) with the associated optimum correlation coefficient ( $r_{max}$ ). In most locations, the amplitudes were damped landward and the time-shift increased. Missing values are denoted with a dash.

Location	$A_{ratio}$			$\tau$ (min)			$r_{max}$		
	T <sub>1</sub>	T <sub>2</sub>	T <sub>3</sub>	T <sub>1</sub>	T <sub>2</sub>	T <sub>3</sub>	T <sub>1</sub>	T <sub>2</sub>	T <sub>3</sub>
S1 <sub>stream</sub> → S1 <sub>near</sub>	0.62	0.51	0.49	60	70	90	0.98	0.98	0.79
S1 <sub>stream</sub> → S1 <sub>far</sub>	0.46	0.55	1.88	130	120	130	0.97	0.97	0.90
S3 <sub>stream</sub> → S3 <sub>near</sub>	0.57	-	0.70	100	-	110	0.97	-	0.87
S3 <sub>stream</sub> → S3 <sub>far</sub>	0.82	0.50	0.72	160	220	140	0.94	0.90	0.81
S5 <sub>stream</sub> → S5 <sub>near</sub>	-	-	-	-	-	-	-	-	-
S5 <sub>stream</sub> → S5 <sub>far</sub>	0.24	0.38	0.47	90	50	90	0.87	0.93	0.76
S6 <sub>stream</sub> → S6 <sub>near</sub>	1.08	1.51	1.04	20	30	10	0.98	0.98	0.96
S6 <sub>stream</sub> → S6 <sub>far</sub>	0.66	0.93	0.61	40	40	30	0.97	0.98	0.95

T<sub>1</sub> - 11 Aug. 2009 to 19 Aug. 2009. T<sub>2</sub> - 22 Sep. 2009 to 30 Sep. 2009. T<sub>3</sub> - 26 Jun. 2010 to 4 Jul. 2010.

We then analyzed the relationship between the fluctuations in water level along the main stream channel between the four in-stream stage recorders (S1<sub>stream</sub>, S3<sub>stream</sub>, S5<sub>stream</sub> and S6<sub>stream</sub>). The time shift between the sampling sites, as determined by a cross-correlation analysis, was short, varying from 10 to 20 minutes from S1<sub>stream</sub> to S6<sub>stream</sub>. Note also that the observed stream level variations in the other channel draining the north-western part of the watershed were in phase with the measurements in the main channel. Although the stage variations at the four stream locations were almost exactly synchronized, their amplitudes varied by a factor of 2.3 to 3.1 (depending on the period examined) among the four sampling sites. This shows that streambed morphology, turbulence effects and the braiding of the streams have a strong impact on the amplitude of the diurnal water level fluctuations but not on their timing. The stream stages fluctuate nearly synchronously whereas the amplitudes vary greatly between the individual measurement locations.

## 4.4 Characterizing stream-groundwater interactions using estimates of residence times

The variations of groundwater levels in the riparian zone do not necessarily imply transport of water to or from the stream. Likewise, the hydraulic gradient measured perpendicular to the streams does not fully describe the groundwater flow direction, due to a significant down-valley gradient on the forefield. To estimate timescales of exchange between the stream and riparian groundwater, we measured the concentration of the radioactive noble gas radon ( $^{222}\text{Rn}$ , half-life 3.82 days) in the groundwater monitoring wells and the stream at two

## Chapter 4

occasions following dry weather periods. This measurement method has been used in many groundwater studies in lowland regions; see Hoehn and Vongunten (1989) and Vogt et al. (2010a) for a more detailed method description. Similar to these authors, we used a Rad7-radon detector (Durridge Co.) to measure  $^{222}\text{Rn}$  in 250 ml samples. From each sample, the radon concentration was measured four times, yielding the mean radon concentration and a standard deviation (Table 4.2).

**Table 4.2.**  $^{222}\text{Rn}$  concentrations (with standard deviation of four replicate measurements), measured on two different days following dry weather conditions. The high concentrations showed that no large mixing between groundwater and stream water occurs in spite of the large water level fluctuations in the stream and groundwater monitoring wells. The stream was sampled near site S3. Missing values are denoted with a dash.

Location	19 July 2010		6 September 2010	
	Concentration (Bq/l)	Standard deviation (Bq/l)	Concentration (Bq/l)	Standard deviation (Bq/l)
Stream	0.40	0.16	-	-
S1 <sub>near</sub>	49.5	2.2	94.2	3.2
S1 <sub>far</sub>	35.1	2.4	30.4	0.8
S3 <sub>near</sub>	8.5	1.8	11.5	2.0
S3 <sub>far</sub>	12.0	1.5	17.4	1.0
S5 <sub>near</sub>	47.2	1.5	56.8	5.0
S5 <sub>far</sub>	56.8	2.7	76.8	4.7
S6 <sub>near</sub>	66.0	8.8	97.3	5.6
S6 <sub>far</sub>	84.5	7.4	98.0	2.4

When nearly radon-free stream or melt water infiltrates into the aquifer, it gradually becomes enriched with radon, generated by the decay of radium present in the aquifer material. If no gas transfer occurs in the groundwater, the radon concentrations increase with time. After about four half-lives (~15 days), the radon concentrations in the groundwater reach a steady state as the decay rate comes into equilibrium with the production rate. With a known equilibrium concentration, measurements of the radon concentration along a groundwater flow path give an estimate of the time that passed since the water was in contact with the atmosphere (Hoehn and Vongunten, 1989). However, because all sampled groundwater wells are situated near the stream, it was not possible to determine the equilibrium concentration of radon. Therefore, we cannot determine the absolute radon age of the water, but we can nonetheless use the radon concentration as a relative travel time indicator.

The groundwater samples showed an increase in radon concentration with distance from the dead-ice body at three measurement locations (S1, S5 and S6). The highest radon concentrations (66.0 – 98.0 Bq/l) were measured in the most downstream sampling site (S6). This trend would seem to suggest either that the groundwater exchanges with the stream more slowly in the lower parts of the forefield than in the upper regions, or that water infiltrates in the upper parts of the forefield and travels downward. The hydraulic conductivities that we have measured at our sites imply relatively long time scales for down-valley groundwater transport (roughly 80 days to travel the distance of about 700 m from the dead-ice body to the most downstream transect). This estimate is calculated from the average down-valley gradient ( $7^\circ$ ), the average measured saturated hydraulic conductivity (21 m/day) and a specific yield (0.3) typical for sand and gravel aquifers (Carsel and Parrish, 1988; Loheide et al., 2005). Because radon concentrations in groundwater would reach equilibrium on timescales shorter than this, we assume that down-valley groundwater transport could only account for a fraction of the water reaching any of the transects. The lowest radon concentrations (8.5 – 17.4 Bq/l,

indicating relatively young groundwater) were measured at transect S3, where the groundwater levels were lower than the stream stage. The radon measurements and the hydraulic gradient are both consistent with infiltration of stream water into the aquifer at this sampling site.

At the gaining stream reaches (S1, S5 and S6), groundwater radon concentrations were markedly different from those in stream water (>30.4 Bq/l compared to 0.40 Bq/l of the stream water), even in the groundwater monitoring wells near the stream. Thus, we conclude that no large volume of water is flushed in and out between the riparian zone and the stream locally on a daily basis. In the particular case of well S5<sub>near</sub>, its radon concentrations are comparable to those in other groundwater wells (for example site S1) even though its water table is some 20 cm below the adjacent stream level, suggesting that it is hydraulically isolated from the adjacent stream channel, consistent with its small water-table fluctuations shown in Figure 4.3.

## 4.5 Modelling groundwater fluctuations

### *Theory of wave propagation*

In coastal regions, tide-induced sea level variations drive groundwater level fluctuations in adjacent aquifers. These fluctuations can be accurately modelled with a linear one-dimensional diffusion equation when the underlying impervious bed is horizontal (Montalto et al., 2007; Raubenheimer et al.; 1999 and Nielsen, 1990). In mountainous terrain, any groundwater fluctuations may be influenced by advective flow because of the sloping impervious bedrock. In these situations, the one-dimensional linear advection-diffusion equation may be more appropriate than the diffusion equation alone for describing wave propagation in the presence of downslope groundwater flow. For horizontal aquifers with simple boundary conditions, the two-dimensional problem of groundwater response to periodic loading can be solved analytically (Sun, 1997). In sloping terrain, a full two-dimensional modelling approach would increase the model complexity greatly, and would require data that are not available for our transects (for example, data describing the boundary conditions and bedrock topography). However, below we show that it is unlikely that groundwater flow parallel to the stream substantially influences the diurnal stage variations. We therefore believe that the one-dimensional advection-diffusion equation oriented perpendicular to the stream may appropriately represent the propagation of periodic stream level variations into the riparian zone.

### *Advection-diffusion model*

If the water table variations are small compared to the saturated aquifer thickness, the two-dimensional linear advection-diffusion equation can describe the variations in groundwater stage over a sloping base. Here we present a slightly rearranged equation given by Brutsaert (2005):

$$\frac{\partial h}{\partial t} = D \left( \frac{\partial^2 h}{\partial x^2} + \frac{\partial^2 h}{\partial y^2} \right) - v_x \frac{\partial h}{\partial x} - v_y \frac{\partial h}{\partial y} \quad (4.1)$$

## Chapter 4

where  $h$  is the hydraulic head (m),  $x$  is the distance normal from the stream (m),  $y$  is the distance parallel with the stream (m),  $t$  is the time (days),  $D$  is the hydraulic diffusivity ( $\text{m}^2/\text{day}$ ) and  $v_{x,y}$  is the direction-dependent velocity (m/day).

Fluctuations in stream level rapidly propagate downstream and pass by all the transects almost instantaneously. On the contrary, groundwater flow parallel to the stream is slow and the aquifer is highly dispersive (see discussion for more details). Therefore we expect that any fluctuation in the groundwater flow parallel to the stream dampens out over short distances and is unlikely to influence the groundwater measurements at the transects. We thus have a predominately one-dimensional wave propagation problem that drives the diurnal groundwater fluctuations in the monitoring wells and we may reduce the above equation to a one-dimensional advection-diffusion equation describing the wave propagation (Koussis et al., 1998):

$$\frac{\partial h}{\partial t} = D \frac{\partial^2 h}{\partial x^2} - v_x \frac{\partial h}{\partial x} \quad (4.2)$$

The hydraulic diffusivity and velocity are given by:

$$D = \frac{Kb}{S} \quad v_{x,y} = -\frac{K \sin(\theta_{x,y})}{S} \quad (4.3)$$

where  $K$  is the hydraulic conductivity (m/day),  $b$  is the saturated thickness of the aquifer (m),  $S$  is the specific yield (dimensionless) and  $\theta_{x,y}$  is the direction-dependent slope of the impervious bedrock (rad). Because equation (4.2) is linear, the propagation of groundwater fluctuations can be analysed independently of other hydrological long-term trends. We represent the stream stage fluctuations with a Fourier series:

$$h(0,t) = \sum_{n=1}^m A_n \sin(\omega_n t + \varphi_n) \quad (4.4)$$

where  $A_n$  is the amplitude (m),  $\omega_n$  is the angular frequency (rad/day) and  $\varphi_n$  is the phase angle (rad). We neglect the influence of the boundary on the opposite side of the stream (the mountain wall) because the distance between the stream and our groundwater measurements is small compared to the aquifer width. A solution for the advection-diffusion equation with this type of boundary condition (Dirichlet boundary condition on a semi-infinite domain) was presented by Logan and Zlotnik (1995) and used for tidally influenced regions by Su et al. (2003):

$$h(x,t) = \sum_{n=1}^m A_n \exp(-d_n x) \sin(\omega_n t - l_n x + \varphi_n) \quad (4.5)$$

where  $d_n$  determines the exponential damping of the propagating wave with distance from the stream:

$$d_n = \sqrt{\frac{\sqrt{\phi_n^2 + \psi^2} + \psi}{2}} - \frac{v_x}{2D} \quad (4.6)$$

and  $l_n$  determines the linear increase in phase shift of the propagating wave with distance from the stream:

$$l_n = \sqrt{\frac{\sqrt{\phi_n^2 + \psi^2} - \psi}{2}} \quad (4.7)$$

The damping and phase shift terms ( $d_n$  and  $l_n$ ) depend on the coefficients  $\phi_n$  and  $\psi$ , which in turn depend on the frequency, the hydraulic diffusivity and the advective flow velocity:

$$\phi_n = \frac{\omega_n}{D} \quad \text{and} \quad \psi = \frac{v_x^2}{4D^2} \quad (4.8)$$

### *Diffusion model*

With a horizontal aquifer base the velocity equals zero (see equation 4.3), and the groundwater fluctuations are described by the diffusion equation. In this case the solution simplifies to:

$$h(x, t) = \sum_{n=1}^m A_n \exp\left(-\sqrt{\frac{\omega_n}{2D}}x\right) \sin\left(\omega_n t - \sqrt{\frac{\omega_n}{2D}}x + \varphi_n\right) \quad (4.9)$$

### *Modelling procedure*

The groundwater fluctuations were simulated using the following procedure (see panels in Figure 4.4):

1. *Isolating diurnal water level fluctuations* – The records were detrended in order to better isolate diurnal water level fluctuations. Thus the linear trends of the dry weather records were removed from the time series (the same periods as analysed above).

2. *Determining model input* – We then approximated the stream stage fluctuations with a Fourier series of sine functions (see equation 4.4). The coefficients of the sine functions ( $A_n$ ,  $\omega_n$  and  $\varphi_n$ ) were extracted with a Fourier analysis and later used as model input (see step 3). For this analysis, we multiplied the detrended stream level records with a windowing function to make them periodic (Tukey window with alpha coefficient equal 0.125). The Fourier decomposition covered frequencies between 1/8 per day and 72 per day, given by the sampling frequency and the length of the data record.

3. *Modelling groundwater fluctuations* – We simulated the groundwater fluctuations with the models described above (equation 4.5 or 4.9) using the input determined in the previous step (the coefficients  $A_n$ ,  $\omega_n$  and  $\varphi_n$ ). The model parameters, for example hydraulic diffusivity, were determined by calibration (see details in the following sections). We used a non-linear optimization algorithm (Lagarias et al., 1998) to find the best match between the observed and simulated groundwater levels. The goodness-of-fit measures used for the calibration were only determined for the flat part of the windowing function, spanning seven days (the white region in the lowest panel of Figure 4.4).

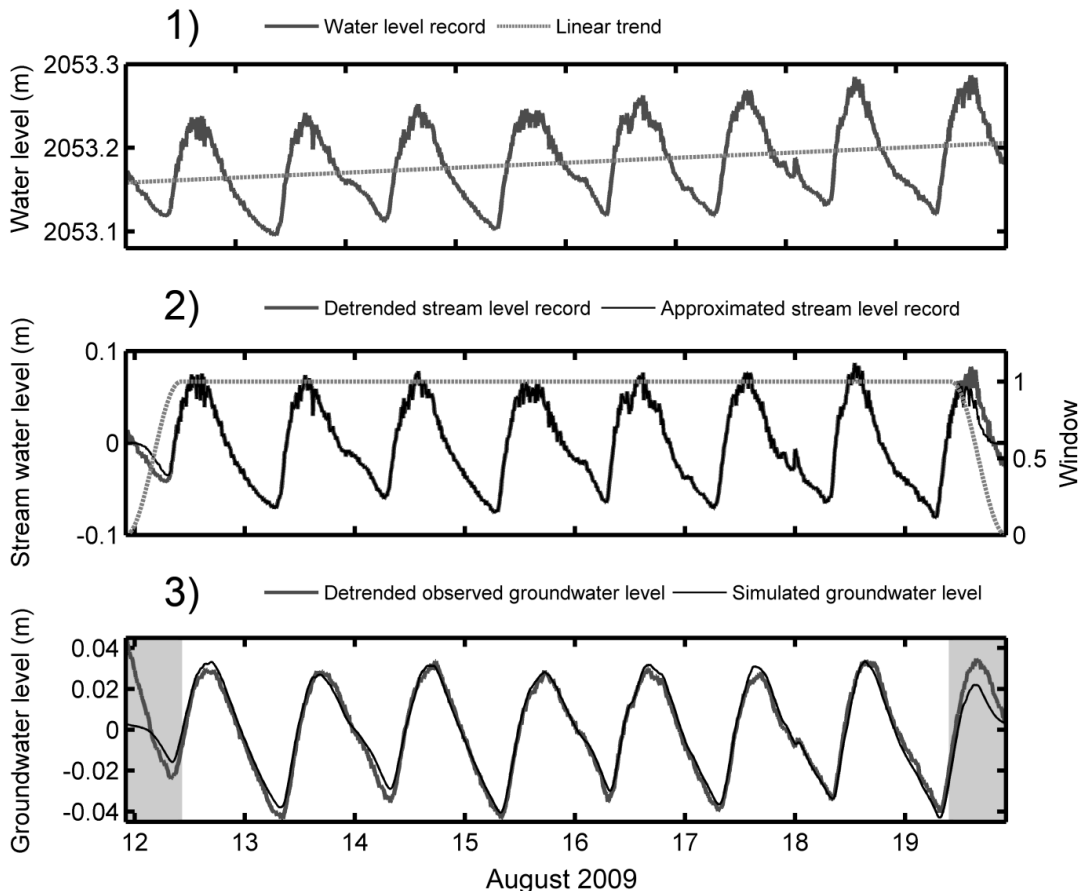


**Figure 4.4.** Illustration of the modelling procedure using data from site S1: (1) isolating diurnal water level fluctuations; (2) determining model input; and (3) modelling groundwater fluctuations. Note that the approximated stream level record depicted in the middle panel (2) matches the detrended stream level record very closely except at the beginning and at the end of the time series.

### ***Diffusion model calibration and results***

The diffusion model (equation 4.9) needs to be calibrated for the hydraulic diffusivity. We used two different calibration methods to define a range of hydraulic diffusivities and to test the diffusion model at each site for the monitoring wells both near and far from the stream:

*Calibration 1:* The stream stages fluctuated nearly simultaneously whereas their amplitudes varied between the locations. Therefore, in a first step, we used an objective function which reached its optimal value depending on the timing of the fluctuations and not depending on their amplitudes. Thus, we optimized the correlation coefficient between the simulated and observed groundwater time series to estimate hydraulic diffusivities. The correlation coefficient is insensitive to the amplitude of the time series and therefore the best-fit of the hydraulic diffusivity only depends on the shape and the timing of the signal. Because of the irregular topography and the variable stream cross-sections, the precise location of the hydraulic connection between stream and groundwater is uncertain. To take this uncertainty into account, we used a range of distances for which we calibrated the model (Table 4.3).

*Calibration 2:* The stream channels display large variations in width up- and downstream from the transects (Figure 4.2, Table 4.3). We expect that the amplitudes of the stream level fluctuations vary correspondingly up- and downstream from the stage recorders. Thus, the observed fluctuations in groundwater level may actually be driven by larger or smaller stream

## Analysis of groundwater level fluctuations

level variations than those that were measured by the stream stage recorders. To account for this amplitude uncertainty, we multiplied the observed stream stages by the ratio between the observed channel width at the stage recorder and a calibratable channel width. We assume that the amplitude of the water level fluctuations varied inversely proportional to the stream width. The calibrated channel width and hydraulic diffusivity were determined by minimizing the root mean squared error between the simulated and observed groundwater time series. If the calibrated channel width differed substantially from the maximum and minimum stream widths measured during the field survey (Table 4.3), the calibration is called into question and the resulting hydraulic diffusivities may not be reliable (due to, e.g., strong groundwater advection perpendicular to the stream). The root mean squared error was used as an objective function to reproduce both the amplitude and time-shift between the observed and simulated groundwater fluctuations. To account for the uncertainty in the distance of the hydraulic connection between stream and groundwater, we calibrated the model using the range of distances observed on-site (Table 4.3).

**Table 4.3.** Shortest and longest distances of the hydraulic connection between the stream and the groundwater monitoring wells estimated from field surveys. These distances cover a short reach around the stream stage recorder (roughly 10 to 20 m), representing a plausible upstream/downstream distance over which diurnal cycles in stream stage could excite fluctuations in the groundwater well levels. Within this stream reach, we also measured the minimum and maximum width of the streams.

Location	Minimum and maximum distance of hydraulic connection between stream and near groundwater well (m)	Minimum and maximum distance of hydraulic connection between stream and far groundwater well (m)	Minimum and maximum stream widths (m)	Stream width at stage recorder (m)
S1	5-10	10-15	3.5-8.5	3.6
S3	4-8	6-10	5.5-12.0	6.5
S5	2-5	4-10	4.5-7.5	4.8
S6	2-6	4-8	4.0-10.0	7.0

The one-dimensional diffusion model reproduced the observed groundwater stage variations accurately in most locations (Table 4.4). The correlation coefficients between the simulated and observed groundwater levels were high and similar to the results obtained with the cross-correlation analysis (compare with Table 4.1). The root mean squared errors were relatively low compared to the amplitude of the observed water level fluctuations (11 Aug – 19 Aug 2009: within 4 to 16% of the peak-to-peak amplitude; 22 Sep – 30 Sep 2009: within 4 to 15% of the peak-to-peak amplitude; 26 Jun – 4 Jul 2010: within 9 to 21% of the peak-to-peak amplitude). The model reproduced the observations more accurately in late summer and early autumn than in early summer. We suppose that melting snow patches affected the groundwater levels during early summer, such that the daily groundwater fluctuations were not solely driven by stream stage variations.

## Chapter 4

**Table 4.4.** Performance measures of the one-dimensional diffusion model based on the two calibration methods using the correlation coefficient and root mean squared error to indicate goodness-of-fit. Note that the goodness-of-fit measures do not vary with the distance of the hydraulic connection (see Table 4.3). Missing values are denoted by a dash.

Location	Calibration 1			Calibration 2		
	Correlation coefficient			Root mean squared error (mm)		
	T <sub>1</sub>	T <sub>1</sub>	T <sub>3</sub>	T <sub>1</sub>	T <sub>2</sub>	T <sub>3</sub>
<b>S1<sub>stream</sub> → S1<sub>near</sub></b>	0.99	0.99	0.88	3.8	2.5	9.3
<b>S1<sub>stream</sub> → S1<sub>far</sub></b>	0.99	0.99	0.95	3.3	2.5	19.5
<b>S3<sub>stream</sub> → S3<sub>near</sub></b>	0.99	-	0.88	3.1	-	7.5
<b>S3<sub>stream</sub> → S3<sub>far</sub></b>	0.96	0.91	0.82	8.4	7.3	10.5
<b>S5<sub>stream</sub> → S5<sub>near</sub></b>	-	-	-	-	-	-
<b>S5<sub>stream</sub> → S5<sub>far</sub></b>	0.87	0.93	0.78	2.4	2.3	3.0
<b>S6<sub>stream</sub> → S6<sub>near</sub></b>	0.99	0.97	0.95	9.8	11.2	13.9
<b>S6<sub>stream</sub> → S6<sub>far</sub></b>	0.98	0.98	0.95	7.6	6.0	7.4

T<sub>1</sub> - 11 Aug. 2009 to 19 Aug. 2009. T<sub>2</sub> - 22 Sep. 2009 to 30 Sep. 2009. T<sub>3</sub> - 26 Jun. 2010 to 4 Jul. 2010.

The hydraulic diffusivity varied more between the four sampling sites than between the three periods (Figure 4.5). The difference in hydraulic diffusivity between the periods may depend on changes in the hydraulic connection with stream level and variations in saturated thickness of the aquifer. The specific soil properties and aquifer depths influence the differences in the obtained hydraulic diffusivities between the locations. At each site, the hydraulic diffusivities for the near and far wells showed good consistency. The hydraulic diffusivities obtained by the two calibration procedures were identical (see vertical bars in Figure 4.5). This occurs because the simulated time-lags of the groundwater fluctuations are only influenced by the hydraulic diffusivity and not by the amplitudes of the stream stage variations, which depend on the calibrated channel width (see equation 4.9). Thus, when allowing the calibrated channel width to vary freely, the optimization algorithm finds the same value of hydraulic diffusivity for both calibration methods.

## Analysis of groundwater level fluctuations

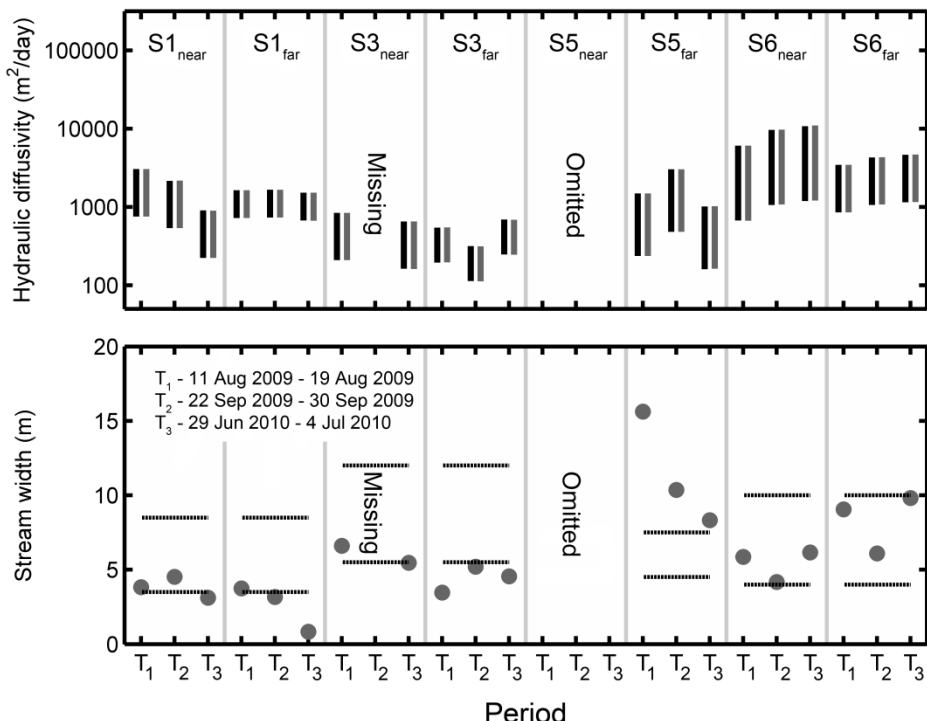


**Figure 4.5.** Best-fit values of the hydraulic diffusivity and calibrated channel width obtained by the two calibration procedures for the near and far wells (black – calibration 1; grey – calibration 2). The vertical bars show the effect on the optimal hydraulic diffusivities of the minimum and maximum distance of hydraulic connection (see Table 4.3). The calibrated channel widths (dots) do not vary with this distance. The horizontal lines indicate the maximum and minimum stream widths found upstream and downstream of the stream stage recorder (see Table 4.3).

The model results showed that the factor applied to the stream stages (reflecting the calibration of the channel width) varied with location and season (lower panel in Figure 4.5). The optimal value of the calibrated channel width primarily stayed within or close to the range of stream widths observed on-site. In some locations, large seasonal variations were found suggesting that the hydraulic connection may vary with time or that three-dimensional flow effects may affect the wave propagation. The smallest calibrated channel width (high stream stage multiplier) was observed for the uppermost location (S1<sub>far</sub>) in early summer (T3). Melting snow patches likely affected the groundwater fluctuations at this particular location. In two locations the calibrated channel width was consistently lower (S3<sub>far</sub>) or higher (S5<sub>far</sub>) than the measured range of stream widths. This indicates that the one-dimensional diffusion model did not fully describe the wave propagation or that the model input was not completely appropriate. Thus, the obtained hydraulic diffusivities in these two locations may not be reliable. However, at one of these sites (S3), the hydraulic diffusivities estimated from the two groundwater wells are consistent with one another. Note also that the calibrated channel widths did not vary with the distance of the hydraulic connection. This occurs because the time-lag of the simulated groundwater fluctuations are only influenced by the hydraulic diffusivity and not by the amplitude of the input signal (see equation 4.9). Thus, when increasing this distance, an increase in the hydraulic diffusivity is necessary in order to match the time-lag between simulated and observed groundwater fluctuations; the ratio  $x/\sqrt{2D}$  in equation (4.9) stays constant. Then the coefficient determining the amplitude damping does not vary with distance and the calibrated channel width stays constant for the best match between the simulated and observed groundwater fluctuations.

### **Advection-diffusion model calibration and results**

In this section we examine how groundwater advection may influence the estimate of hydraulic diffusivity. We tested the advection-diffusion model for the steepest location (S5) where tracer experiments showed that groundwater flows fast towards the stream but slightly downstream of the site. We found velocities up to  $\sim 250$  m/day determined by the first arrival in springs on the stream bank of a fluorescent dye injected into the S5<sub>far</sub> groundwater monitoring well (for a description of the tracer experiments see section “Observed water level fluctuations”). We determined the root mean squared error between simulated and observed groundwater fluctuations for a range of velocities and hydraulic diffusivities. At the remaining locations, which are much flatter, we neglected the influence of advection because similar tracer experiments did not provide evidence of fast groundwater flow. Again, note that we did not model the groundwater records at site S5<sub>near</sub> because it does not display any significant stage fluctuations.

The shape of the response surface showed that the method cannot constrain the hydraulic diffusivity and velocity simultaneously (Figure 4.6). The advection-diffusion model reproduced the observations with lower root mean squared errors (between 13 and 54% lower depending on period) and higher correlation coefficients (between 5 and 34% higher depending on period) compared to the diffusion model (velocity equal to zero). The optimal velocities varied between -29 and -184 m/day and were directed toward the stream, consistent with the dye tracer observations. The calibration of the advection-diffusion model gave hydraulic diffusivity estimates between 123 and 1823 m<sup>2</sup>/day, a factor of roughly  $\sim 2$  to  $\sim 4$  higher than those obtained by the diffusion model. Thus, we expect that the diffusion model may underestimate the hydraulic diffusivities in the presence of advection directed towards the stream.

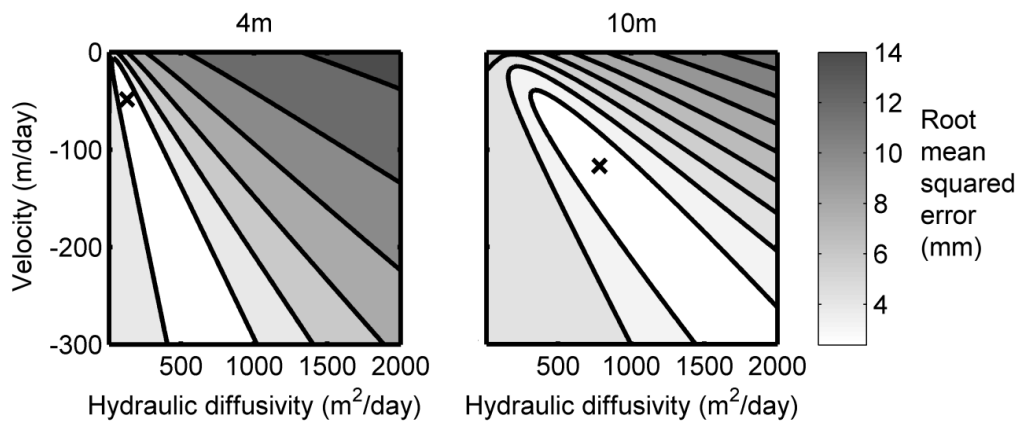


**Figure 4.6.** Response surfaces showing the root mean squared errors (mm) between the simulated and observed groundwater fluctuations simulated for site S5<sub>far</sub> (11 August 2009 – 19 August 2009). The two panels show the shortest (left) and the longest (right) distance of the hydraulic connection between the stream and the groundwater monitoring well (see Table 4.3). The crosses mark the position of the lowest root mean squared error.

## 4.6 Discussion

In spite of the heterogeneous soils, the one-dimensional models reproduced the observed groundwater fluctuations accurately (Figure 4.7). The separation between the stream and the groundwater monitoring wells appears to be large enough that the glacial till can be approximated by a homogenous medium. This is encouraging, as the model depicts spatially averaged soil properties with only one parameter in spite of the heterogeneous material with large cobbles and stones. Between the groundwater monitoring wells at each transect, the hydraulic conductivity varied by a factor of ~13 or less, whereas the hydraulic diffusivity varied by a factor of ~3 or less. The larger variability in measured hydraulic conductivities indicates that our approach for estimating hydraulic diffusivities integrates over a larger volume than the slug tests do. Typically, glacial tills show large variability in hydraulic conductivity, and this variability decreases with increasing sample volume (Monhanty, 1994). Therefore, combining our approach with measurements of depth to the bedrock is potentially useful when determining average hydraulic conductivities for larger heterogeneous areas.

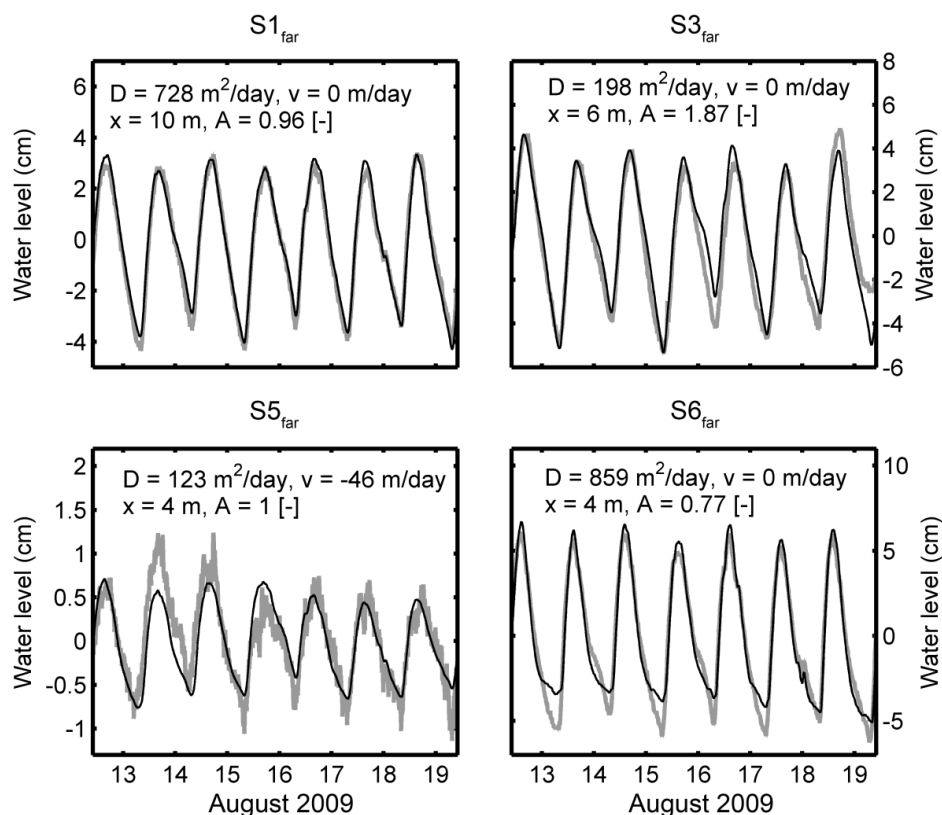


**Figure 4.7.** Measured and simulated groundwater fluctuations (grey and black curves, respectively) for the farthest groundwater wells at the four transects (11 August 2009 – 19 August 2009). The model, integrating the heterogeneous soil properties into one parameter, captures the groundwater fluctuations accurately. Note that the y-axis differs between the panels. The numbers presented in the figure correspond to the shortest distance of the hydraulic connection displayed in Table 4.3.

We recognize that the one-dimensional model applied in this study represents a simplification of the complex groundwater flow around each transect. However, we do not expect that a disturbance in groundwater table height occurring far up- or downstream will greatly influence the measurements in the monitoring wells adjacent to the streams. First, groundwater advection parallel to the stream is slow, i.e. below 20 m/day for the flatter sites S1, S3 and S6. These velocities were estimated using the highest measured hydraulic

## Chapter 4

conductivity (45 m/day) and the observed terrain slope (varying between 3° and 7° parallel to the stream). Therefore, any disturbance in groundwater stage should not be advected far over time-scales at which stream stage fluctuations propagate to the monitoring wells (Table 4.1). More important, disturbances in groundwater stage disperse over short distances. Given the diffusivities we have estimated, diurnal groundwater fluctuations should be damped to approximately one third of their original amplitude over distances of approximately 20 m or less. In this calculation we used the average hydraulic diffusivity obtained for the far monitoring wells (Figure 4.5, vertical bars). The length scales over which groundwater fluctuations dampen are short relative to the length of the stream reaches, but still long enough to allow stream fluctuations to propagate to the monitoring wells. Therefore we may assume a one-dimensional wave propagation problem. In spite of groundwater flow parallel to the stream, the stages in the monitoring wells primarily respond to the diurnal stream level fluctuations and not to groundwater variations occurring far up- or downstream of the transects.

The linear advection-diffusion model relies on the assumption of small water table fluctuations compared to the saturated thickness of the aquifer. We estimated the aquifer depth using the obtained hydraulic diffusivities (see values in Figure 4.7) with the relationship  $D = K_b/S$  (see equation 4.3). Specific yields ( $S$ ) typical for sand and gravel aquifers vary around 0.30 (Carsel and Parrish, 1988; Loheide et al. 2005). Using the highest observed value for the hydraulic conductivity ( $K$ ), we calculated minimum aquifer depths of ~0.8-1.3 m at two locations (S3 and S5) and ~4.9-5.7 m at the remaining sites (S1 and S6). The ratio between the driving stream amplitude and the estimated depth to the bedrock was found to vary between 0.01 and 0.04, which is lower than found in other studies where the small amplitude theory was shown to be valid (Cartwright et al., 2004). We thus expect that the model assumption of small water table fluctuations holds.

While the simplicity of the presented models is appealing, it is also the main limitation of the approach discussed here. The stream-groundwater interactions in such complex terrain cannot be fully described as a one-dimensional wave propagation phenomenon. The amplitudes of the stream fluctuations vary significantly over short distances. This is why the stream stage input had to be multiplied with a factor (see calibration 2), allowing for calibration within a reasonable range of stream stage amplitudes. However, omitting the amplitude information and working with the timing and shape of the groundwater fluctuations instead may provide more reliable estimates of hydraulic diffusivities. To improve the models, we recommend further studies focusing on groundwater fluctuations and flow patterns observed over smaller areas on proglacial fields using arrays of groundwater monitoring wells located in the riparian zone. Delineating the bedrock topography before installing the wells may provide useful information about where to optimally position the transects. By using this approach combined with measurements of hydraulic conductivity obtained through slug tests, the estimated hydraulic diffusivities may also be validated.

In our study site, the radon concentration measurements showed that the diurnal water level fluctuations did not result in large local mixing between stream water and groundwater. This is contrary to the findings presented by Loheide and Lundquist (2009), who showed that snowmelt-induced stream stage fluctuations caused a large volume of water to be pumped in and out of a riparian meadow aquifer, in a relatively flat landscape compared to our more steeply-sloping proglacial valley. Our results suggest that for certain slopes and diffusivities the hydraulic gradients do not switch direction with the diurnal stream stage fluctuations, as may occur in flatter and more homogeneous aquifers.

## 4.7 Conclusions

In this study, we measured diurnal fluctuations in stream stage and riparian groundwater levels in the Damma glacier forefield in central Switzerland. Groundwater levels in the riparian zone lagged behind the stream stage fluctuations. In spite of the large water level variations, elevated radon concentrations in groundwater wells located just a few meters from the stream showed that riparian groundwater was not rapidly mixing with stream water. Diurnal fluctuations in groundwater levels were sometimes damped and always time-lagged relative to those in the stream. The observed time-lag and damping of the groundwater fluctuations varied between the four measurements transects, highlighting the heterogeneity of the forefield. Despite variations between the sites, the diurnal groundwater fluctuations showed many similarities with those observed in tidally influenced coastal regions, where analytical models based on the diffusion equation accurately describe the wave propagation.

To describe the groundwater fluctuations, we used a diffusion model which has so far mostly been applied in coastal regions. In spite of the visibly heterogeneous soil, irregular topography and variable stream cross sections, the measured groundwater fluctuations were accurately modelled in most locations using reasonable parameter values. It is promising that a standard diffusion model, derived from the groundwater flow equations, with just one calibration parameter depicting the soil properties (the hydraulic diffusivity) captures the observed groundwater level fluctuations. Therefore, modelling techniques developed for tidal regions may find application in riparian settings such as glacier forefields where the stream stages fluctuate strongly.

Within this study site situated on a glacier forefield, groundwater flows downhill following the sloping impervious bedrock. In the steepest measurement location, where groundwater flows rapidly towards the stream, the diffusion model did not reproduce the observed groundwater fluctuations with reasonable parameter values. With the advection-diffusion model, the groundwater fluctuations were reproduced without manipulating the model input. However, the model calibration could not constrain the hydraulic diffusivity and advection velocity simultaneously. More measurements and improved models are needed to better constrain diffusivity estimates in steeply sloping terrain.

The measured stream levels fluctuated almost synchronously along the sampled length of the streams, whereas the amplitudes of the stage height variations differed greatly between the measurement sites. Therefore, determining hydraulic diffusivities by a calibration sensitive to only the shape and timing of the diurnal fluctuations seems to provide more reliable estimates than using the amplitude information of the signal in the calibration. As the results of this study suggests, the combination of monitoring wells along transects with diffusion modelling has large potential to yield spatially averaged hydraulic properties of highly heterogeneous soils, where single point measurement methods may fail. Combined with additional measurements (for example methods delineating the bedrock boundary), the approach presented here may also yield estimates of additional aquifer properties such as the hydraulic conductivity.

### Acknowledgments

Financial support for this study was provided by the BigLink project of Competence Center for Environment and Sustainability (CCES) of the ETH Domain. Masaki Hayashi and Henning Löwe deserve gratitude for giving much helpful advice. We also thank the students and staff who helped during the field work. The recommendations given by three anonymous reviewers improved the manuscript greatly.

# **Chapter 5**

## **5 The energy balance and temperature dynamics of a proglacial stream, and their implications for spatially integrated hydraulic geometry and riparian aquifer transmissivity**

Jan Magnusson and Tobias Jonas

*WSL Institute for Snow and Avalanche Research SLF, Flüelastrasse 11, CH-7260 Davos Dorf, Switzerland*

James Kirchner

*Swiss Federal Institute for Forest, Snow, and Landscape Research (WSL), CH-8903 Birmensdorf, Switzerland*

*Department of Environmental Sciences, Swiss Federal Institute of Technology (ETH), CH-8092 Zürich, Switzerland*

Manuscript Submitted to Water Resources Research.

### **ABSTRACT**

Proglacial fields typically have complex topography and heterogeneous sediments, resulting in highly variable flow and temperature regimes in surface runoff and groundwater. Using data from the Damma glacier forefield (Switzerland), we examined how longitudinal stream temperature changes can be used to infer reach-averaged hydrological and thermal processes in proglacial riparian zones. A simple energy balance showed that radiative forcing and frictional warming largely explained the observed temperature patterns in three stream reaches, with groundwater inflow dominating the energy balance in a fourth reach. Daytime stream warming depends on channel width, and here we show that stream temperature measurements can be used to infer reach-averaged hydraulic geometry relationships between stream width and discharge, which are difficult to obtain by other methods in braided gravel-bed streams. We further show that stream temperatures can be combined with near-stream groundwater levels and temperatures to infer groundwater inflow rates and hydraulic transmissivities in the riparian zone, although with considerable uncertainty. Our results illustrate how proglacial stream temperatures can yield spatially integrated information about hydrological and thermal processes in glacial forefields, where extreme spatial heterogeneity makes conventional methods difficult to apply.

## 5.1 Introduction

Temperatures influence many biological, physical and chemical variables in streams, including chemical reaction rates (Gooseff et al., 2005), distributions and growth rates of aquatic organisms (Caissie, 2006), water quality variables such as dissolved oxygen (Webb et al., 2008), and the viscosity of water itself, which influences streambed infiltration rates in 'losing' reaches (Constanz, 1998). Therefore, it is important to understand the factors regulating stream temperatures and to anticipate how temperature dynamics may respond to environmental changes. In this study, we use stream temperatures and meteorological observations to investigate the factors controlling temperature dynamics along individual reaches in a braided proglacial stream.

Proglacial stream temperatures typically display a fast response to meteorological forcing, with large increases in temperature over short distances downstream (Brown and Hannah, 2008; Uehlinger et al., 2003). These temperature increases can result both from heat fluxes at the stream surface and from inflow of groundwater (Brown et al., 2006; Cadbury et al., 2008), and depend on the width and depth of the channel as well as the flow velocity of the water (Leach and Moore, 2011; Chikita et al., 2010). As a result, one can likely use observations of longitudinal variations in stream temperature to infer for instance stream width variations as a function of discharge and the mixing of surface and groundwater across proglacial fields. In other words, water temperatures can be treated as a tracer of hydrological processes such as stream-groundwater interactions (Anderson, 2005).

In many studies, interactions between surface water and groundwater have been inferred from temperature measurements in the stream or streambed (e.g. O'Driscoll and DeWalle, 2006; Westhof et al., 2007; Vogt et al. 2010b). These methods may yield spatially integrated stream-groundwater exchange rates along whole reaches (Becker et al., 2004). Proglacial fields are characterized by highly heterogeneous soils and stream channels, and consequently one may expect that stream-groundwater exchange will be highly localized. Thus spatially integrated measurements, such as those provided by temperature measurements at the reach scale, may be particularly useful in these settings. Conventional methods such as differential discharge measurements (Ruehl et al., 2006) may not be suitable in complex, often braided, proglacial channels. Similarly, measuring temperature profiles in the streambed (Stonestrom and Blasch, 2003) may be impractical because it is very hard to install the sensors in the stony sediments.

In addition to serving as a tracer for quantifying surface-groundwater interactions, stream temperature variations may also help in characterizing stream properties such as channel width. On proglacial fields, for example, the average stream width along a reach may be very difficult to measure manually, because channel cross sections may vary greatly over short distances (Ashmore and Sauks, 2006). Since channel geometry exerts a first-order influence on the energy balance of a stream, however, it may be possible to infer reach-averaged stream width from diurnal temperature dynamics, as we show below. For the above-mentioned reasons, we analyzed what patterns in stream temperatures do reveal about the energy balance and the flow and mixing of water across the glacier forefield.

In this study, we use temporal and spatial patterns of stream temperature and discharge in the Damma glacier forefield in the central Swiss Alps to draw inferences about (a) the energy balance of the stream, (b) variations of stream width as a function of discharge in the complex braided channel, and (c) surface/groundwater interactions. We present an energy balance model describing the temperature increase downstream along the forefield. With the model,

we identify the dominant thermal and hydrological processes influencing the longitudinal temperature increase along four different stream reaches. For an individual reach that is largely heated through the stream surface, we use diurnal temperature dynamics to derive the basic hydraulic geometry relationships describing the stream width as function of discharge. Along another stream reach, we find a strong correlation between the hydraulic gradient in the riparian zone and the observed downstream temperature increase, consistent with gradient-driven groundwater inflows to the channel.

## 5.2 Field site and data

The Damma glacier basin in the central Swiss Alps ( $N46^{\circ}38.177' E08^{\circ}27.677'$ ) covers an area of about  $12 \text{ km}^2$  (Figure 5.1). The glacier forefield in the valley is bounded laterally by two large moraines and a debris-covered dead ice body. Both moraines were created at the end of the Little Ice Age (~1850), and the dead-ice body is now separated from the glacier, which has retreated further up the valley headwall. The forefield itself covers an area of about half a square kilometer and spans an elevation range of 1950 to 2050 m a.s.l. The hydrological regime of the study area is dominated by runoff from the seasonal snow cover and the glacier (Magnusson et al., 2011).

Water flows to the glacier forefield from two separate regions of the watershed (Figure 5.1). From the area in the south-west of Figure 5.1, water flows to the proglacial field from both the glacier and the dead-ice body. Melt water coming from the glacier first flows underneath the dead ice body before emerging as a single stream channel on the proglacial field. From the area in the north-west of Figure 5.1, the water reaching the forefield mainly originates from the glacier and flows across the 1850 moraine before joining the stream from the south-west in the middle of the forefield. The channels are braided, particularly above and around their confluence, and are characterized by highly variable geometries with large stones and rocks. The entire forefield is well above the treeline, and no large vegetation shades the streams. The granite bedrock is covered by debris and glacial till of unknown depth. The soils are mainly composed of cobbles and sand with some silt and minor amounts of clay.

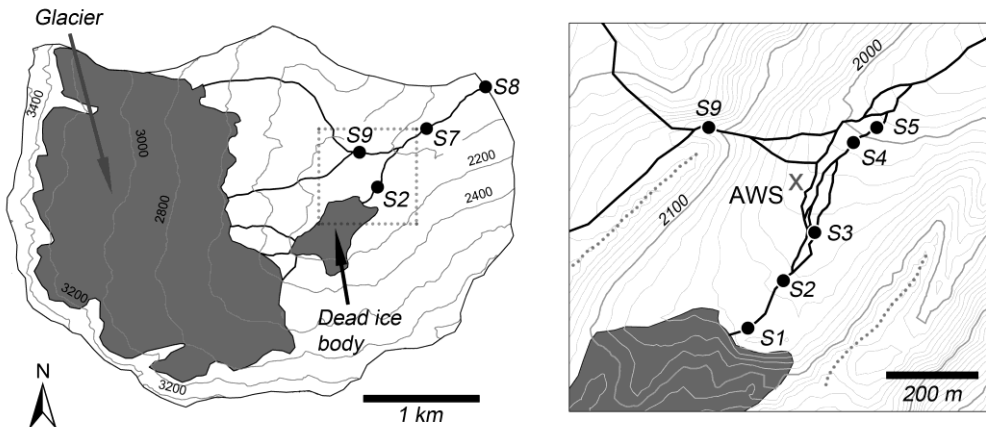


**Figure 5.1.** The Damma glacier watershed (left panel) and its proglacial field (right panel) in central Switzerland. The glacier forefield is bounded by a dead ice body and two large moraines from the Little Ice Age (grey dotted lines in the right panel). The temperature measurement sites (S1, S2, S3, S4, S5, S8 and S9) are located along the stream emerging from the dead ice body and the stream draining the north-western part of the catchment. At three of the sites, groundwater stage and temperature were measured in monitoring well transects perpendicular to the stream (sites S1, S3 and S5). The three discharge gauging sites are located such that they measure the water flowing in from the north and south (sites S9 and S2, respectively) and out of the forefield (site S7). The automatic weather station (AWS) is situated in the middle of the proglacial field.

Over one field season, from 27 June to 8 October 2009, we recorded thermal, hydrological and meteorological variables across the proglacial field. We measured stream temperature at seven locations (S1, S2, S3, S4, S5, S8 and S9) using standalone sensors, some of which measured both water level and temperature (Hobo U20 Water Level Logger, with 2-minute sampling interval) and others of which measured temperature alone (Hobo Pro v2 Temp Logger, with 5-minute sampling interval). The measurements were averaged to hourly values. At three of the stream monitoring locations, we also recorded groundwater levels and temperatures in two fully-screened monitoring wells (site S1, S3 and S5), situated along transects perpendicular to the stream channel. The distance between the stream and the near-stream monitoring wells varied from roughly 2 to 5 m; the distances from the streams to the farther wells varied from approximately 4 to 10 m. The distances separating each pair of wells ranged from about 2 to 5 m. For more details about the groundwater monitoring, see Magnusson et al. (In review). The site names given here are consistent with another study of the proglacial field (Magnusson et al., In review, presented in Chapter 4), and as no measurements were used from site S6 this location was omitted in Figure 5.1.

We cross-calibrated the temperature sensors against one another by placing them together in a stirred laboratory water bath, and slowly varying the temperature over the entire range observed in the streams (1–10 °C). All of the sensors agreed within a range of  $\pm 0.11$  °C in these common bath experiments (exceeding the manufacturer's specifications of 0.20 and 0.37 °C for the two sensor types). We corrected for observed constant offsets between the sensor readings; the largest correction was 0.10 °C. Otherwise, no visible systematic deviations were detected between the temperature readings from the different probes over the entire temperature range.

We continuously recorded discharge at three locations, to capture surface water flows into and out of the forefield: (a) at the stream draining the north-western regions of the watershed (site S9), (b) at the stream close to the dead ice body draining the south-western part of the catchment (site S2), and (c) downstream from the confluence of the streams, at a point that

captures the complete catchment runoff (site S7). Stream stage was measured at these locations using the combined water level and temperature loggers described above (Hobo U20 Water Level Logger with 2-minute sampling interval). The measured stream water levels were converted to runoffs using a stage-discharge rating curve measured by dilution gauging. The root mean squared error between the dilution gauging measurements and the discharges obtained by the rating curve varied between  $0.06 \text{ m}^3/\text{s}$  and  $0.14 \text{ m}^3/\text{s}$  depending on location. In the analysis that follows, we used hourly averaged discharge values.

We monitored meteorological conditions at an automatic weather station situated in the middle of the glacier forefield (Figure 5.1). The station recorded air temperature, relative humidity, wind speed, precipitation and solar radiation (hourly values averaged from 5-minute sampling). During the study period, meteorological conditions were relatively warm and moist; the average air temperature was approximately  $10^\circ\text{C}$  and the relative humidity was roughly 75 %. During this period, precipitation fell as rain in the forefield, but occasionally fell as snow at higher altitudes. The precipitation gauge recorded approximately 360 mm of rainfall over the study period, and during 48 % of the days rainfall totalled more than 1 mm. In spite of the rather moist climate, many days were very sunny, and nearly half of the days (53 %) during the monitoring period had at least one hour with hourly average solar radiation exceeding  $700 \text{ W/m}^2$ . The distance from the weather station to any point on the forefield is 350 m or less, so we believe that meteorological conditions recorded at the station are representative for the streams in the forefield. Terrain analysis also showed that the streams on the proglacial field received sunlight simultaneously.

### 5.3 Observed thermal and hydrological conditions across the proglacial field

The observed stream temperatures displayed large variations across the glacier forefield (Figure 5.2, upper panel). Low temperatures, varying between  $0.7$  and  $4.2^\circ\text{C}$ , were recorded downstream of the dead ice body (site S1) during the monitoring period. In spite of the short distance between the measurement location and the dead ice body, measured temperatures were well above the melting point and displayed small diurnal fluctuations. This indicates that much of the water reaching this location was warmed as it crossed the rock face below the glacier, before passing underneath the dead ice body (see also Figure 5.1). Markedly higher temperatures (Figure 5.2, upper panel), varying between  $0.1$  and  $11.4^\circ\text{C}$ , were observed in the northern tributary stream as it crossed the northern large moraine (site S9). The glacier melt water reaching this location had already travelled between 1 and 2 km across an open rock face (Figure 5.1), allowing significant warming from solar radiation and, at night, conduction of heat from the rock (Brown, 1969). Temperatures recorded downstream of the confluence (at site S8) were intermediate between temperatures at the two upstream observations (site S1 and S9), ranging from  $1.5$  to  $9.2^\circ\text{C}$  during the monitoring period. The peak-to-peak amplitudes in the diurnal temperature fluctuations at site S8 were also intermediate between the amplitudes of the two upstream measurements. The large temporal and spatial variability in stream temperatures observed at the Damma forefield is typical for other proglacial fields as well (Brown and Hannah, 2008; Uehlinger et al., 2003).

The observed stream temperatures at the site below the confluence (site S8) could not be explained by simply mixing the water passing the two upstream measurement locations. Combining the daily average measurements of discharge and stream temperature from the two upstream sites (temperatures measured at sites S9 and S1, discharges measured at site S9 and S2) yields a calculated stream temperature below the confluence as shown by the dashed line

in Figure 5.2 (middle panel). The measured daily average stream temperature below the confluence (black line, middle panel, Figure 5.2) is approximately 1.5 °C higher than the calculated value. This difference can be attributed to warming of the stream by surface heat fluxes, frictional warming or groundwater inflows. (The travel time from the both upstream sites to the downstream site is less than one hour, so we did not account for the time lag between the measurements.)

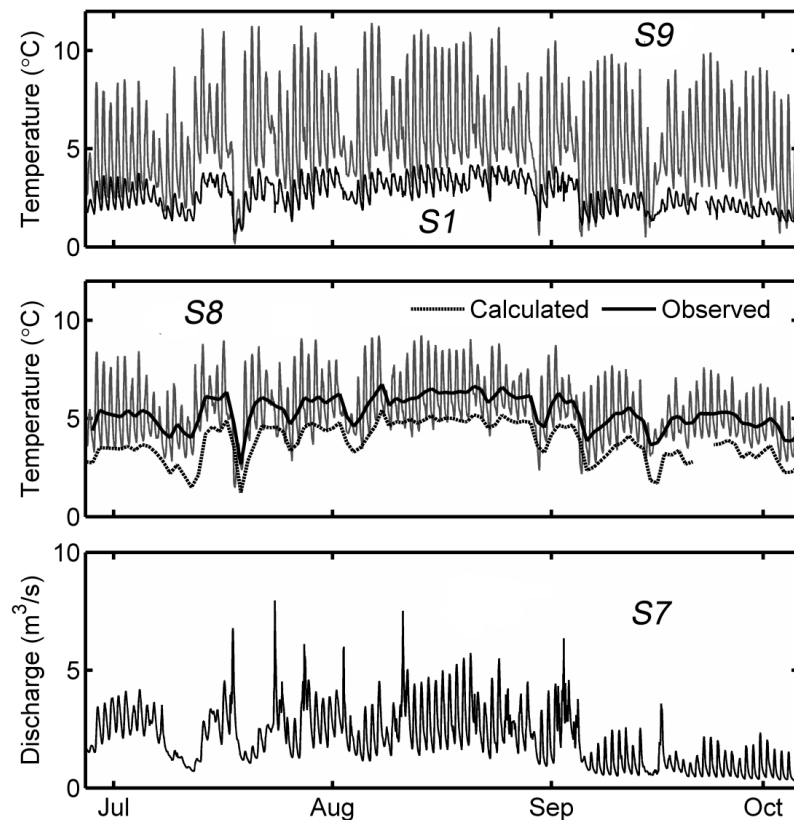


**Figure 5.2.** The observed hourly stream temperatures (sites S1, S8 and S9) and discharges (site S7) show large diurnal and seasonal variations. The middle panel shows that the stream temperatures calculated by mixing the two main streams flowing into the forefield (dashed line) are systematically lower than the observed stream temperatures of the water leaving the forefield (black line). For clarity, daily averaged values are shown for these calculated and measured temperatures.

Groundwater inflows often influence longitudinal stream temperature patterns (Westhoff et al., 2007). At our study site, Figure 5.3 shows that the sum of the discharges measured at the two upstream locations nearly equalled the discharges observed at the downstream site (coefficient of determination  $r^2 = 0.98$ , slope of regression line through origin = 0.96, root mean squared error =  $0.15 \text{ m}^3/\text{s}$ ). The discrepancy between the discharge measurements presented above was slightly smaller than the uncertainty in the measurements themselves. This mass balance calculation shows that if stream-groundwater interactions play an important role across the forefield, any gains and losses of stream water must approximately balance as the stream flows between the upstream (sites S2 and S9) and downstream (site S7) discharge measurement sites. On proglacial fields, surface water can often infiltrate into the riparian zone along the streams, and return back to the channels further downstream (Malard et al., 2002), potentially having absorbed additional heat from the riparian subsurface.

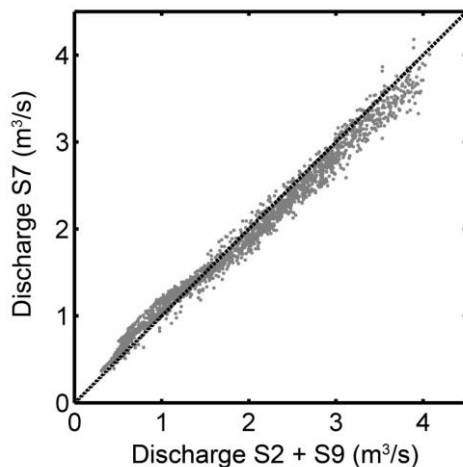


**Figure 5.3.** Stream discharge measured at the downstream gauging station (site S7), compared to the sum of measured discharges on the two main tributaries (sites S2 and S9) including the one-to-one line. The close agreement indicates that no large net gains or losses of groundwater occurred along the braided streams on the proglacial field.

#### 5.4 Temperature increase observed over individual stream reaches

By analysing the temperature increase along stream channels, we gain more information about the processes influencing the stream heating than by studying single temperature measurements. Therefore, we begin by comparing three temperature measurements delineating two individual stream reaches (S2 to S4 and S4 to S5; Figure 5.4, upper panel). These two reaches were selected because they display visually different diurnal patterns of temperature increases. Later on, we analyse all the reaches delineated by our temperature measurements along the channel originating from the dead ice body.

Figure 5.4 (middle panel) shows that the temperature increase over the longer reach (S2 to S4) is larger, particularly during daytime, than over the shorter reach (S4 to S5). Along the longer reach, the temperature increase responded strongly to solar radiation ( $r^2 = 0.92$ ) and less to air temperature variations ( $r^2 = 0.56$ ). The stream temperatures reacted quickly to changes in meteorological conditions, and did not show any long-term memory of past variations in either solar radiation or air temperature. This is not paradoxical because cold melt water continually flushes the system quickly, with the result that residence times are much shorter than one solar heating cycle. The shorter reach, on the other hand, displayed weaker correlations with solar radiation ( $r^2 = 0.60$ ) and air temperature ( $r^2 = 0.38$ ) than the longer reach did. The correlations above were determined using a cross-correlation analysis that shifted the signals in time until the strongest correlations were achieved. The differences in the correlation coefficients between the reaches show that the two time series describing the temperature increase differ in shape, which is also visually obvious in Figure 5.4. This shape difference indicates that different processes control the temperature increases along the two stream reaches. The strong correlation between the temperature increase and shortwave radiation along the longer reach suggests that direct solar heating is an important process warming the stream. The night-time temperature increase along the shorter reach (S4 to S5) nearly equals that of the longer reach (S2 to S4), despite a much smaller change in altitude and thus a much smaller contribution from frictional warming (see below), suggesting a substantial influence of groundwater inflow over the shorter reach. This inference is consistent with the results of tracer tests, in which dye tracers injected into the groundwater

monitoring wells at site S5 were detected in small springs on the nearby stream bank after a short time (< 20 min).

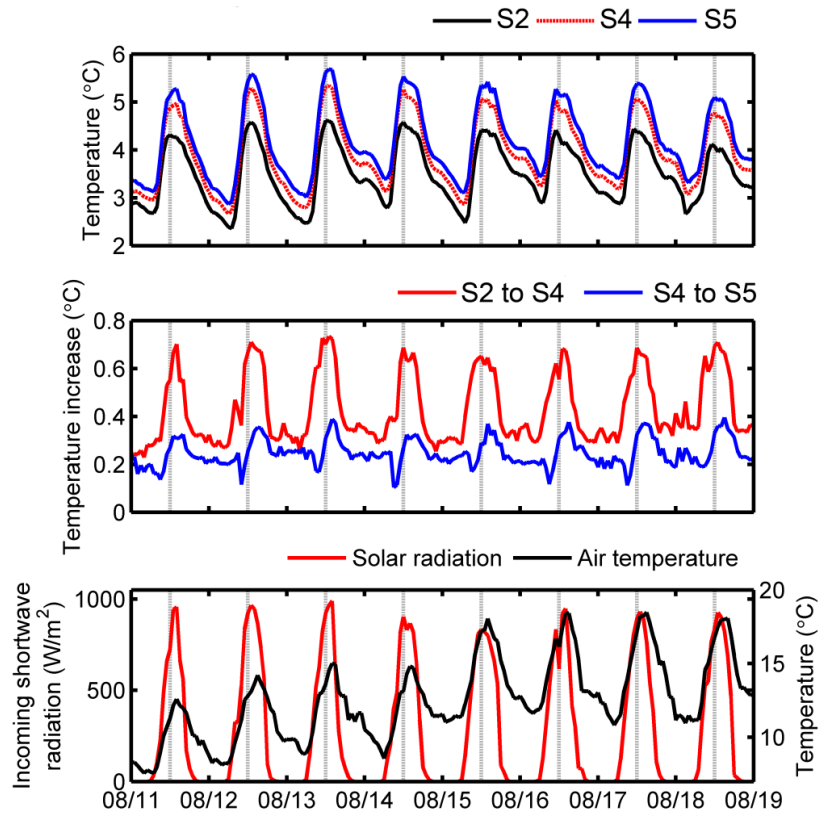


**Figure 5.4.** Measured stream temperature at three locations (top panel), and the temperature increase over two individual reaches (middle panel), compared to meteorological conditions observed at the forefield (bottom panel). The temperature increases over the two stream reaches showed different behaviour: the temperature change over the upstream reach (S2 to S4, middle panel, in red) showed a clear response to solar radiation whereas the downstream reach (S4 to S5, middle panel, in blue) displayed a weak response to variations in both air temperature and solar radiation.

## 5.5 Processes influencing stream temperature warming: Theory

The observed downstream temperature increases described above can be interpreted more quantitatively in terms of the energy balance of the stream. Here we present a simple energy balance equation that can be used to identify the dominant processes controlling the heat balance of the individual stream reaches between our measurement sites. This energy balance equation allows us to interpret the measured temperature time series in terms of stream characteristics such as channel width and the mixing of different water sources along the studied stream sections.

The downstream temperature change  $\Delta T$  ( $^{\circ}\text{C}$ ) over a stream reach of length  $L$  ( $\text{m}$ ) and average width  $w$  ( $\text{m}$ ) can be described by the following equation:

$$\underbrace{\Delta T(t)}_{\text{Temperature change}} = \underbrace{\frac{Q(t)w(t)}{q(t)c\rho} \frac{L}{c\rho}}_{\text{Surface heat transfer}} + \underbrace{\frac{g\Delta z}{c}}_{\text{Frictional heating}} + \underbrace{\Delta T_G(t) \frac{q_G(t)}{q(t)}}_{\text{Groundwater discharge}} \quad (5.1)$$

Here  $Q$  ( $\text{W m}^{-2}$ ) is the heat flux across the stream surface,  $c$  ( $\text{J kg}^{-1} \text{K}^{-1}$ ) is the specific heat capacity of water,  $\rho$  ( $\text{kg m}^{-3}$ ) is the density of water,  $\Delta z$  ( $\text{m}$ ) is the change in altitude between

## Analysis of stream temperatures

the up- and downstream end of the reach,  $g$  ( $m s^{-2}$ ) is the gravitational acceleration,  $\Delta T_G$  ( $^{\circ}C$ ) is the difference between groundwater and stream water temperature,  $q$  ( $m^3 s^{-1}$ ) is stream discharge and  $q_G$  ( $m^3 s^{-1}$ ) is the groundwater discharge. The first term of equation (5.1) can also be written in the more intuitive form  $(Q A \tau) / (V c \rho)$ , where  $A$  and  $V$  are the surface area and volume of the stream reach and  $\tau = V/q$  is the mean residence time of water in the reach.

Equation (5.1) predicts how temperature will change along each stream reach as a result of (a) heat transfer across the stream surface, (b) frictional heating due to dissipation of gravitational potential energy, and (c) groundwater inflow. Surface heat exchange warms or cools the stream at a rate that is proportional to the heat flux, the length of the stream and the average width of the stream, and inversely proportional to the discharge. The second term of equation (5.1) assumes that the available potential gravitational energy completely dissipates into heat, and the third term assumes that groundwater inflows are small compared to the stream discharge.

In this study, we consider the following four components of surface heat exchange:

$$Q = LE + H + SW_{net} + LW_{net} \quad (5.2)$$

where  $LE$  ( $W m^{-2}$ ) is latent heat flux,  $H$  ( $W m^{-2}$ ) is sensible heat flux,  $SW_{net}$  ( $W m^{-2}$ ) is net shortwave radiation and  $LW_{net}$  ( $W m^{-2}$ ) is net longwave radiation.

*Latent heat flux.* The turbulent heat fluxes were calculated following Leach and Moore (2010). We estimated the latent heat flux using the parameterization below:

$$LE = 285.9 (0.132 + 0.143u)(e_a - e_w) \quad (5.3)$$

where  $u$  ( $m s^{-1}$ ) is the wind speed,  $e_a$  ( $kPa$ ) is the vapour pressure of air and  $e_w$  ( $kPa$ ) is the vapour pressure directly above the stream surface. The latter was calculated by combining the saturation pressure function (Stull, 2000) and the measured water temperature. The vapour pressure of air was determined by multiplying the measured relative humidity with the results obtained from the saturation pressure function using measured air temperature as input.

*Sensible heat flux.* We estimated the sensible heat flux by scaling the calculated latent heat flux with the Bowen ratio  $\beta$ :

$$H = \beta LE \quad (5.4)$$

where  $\beta$  is given by:

$$\beta = 0.66 (p/1000) [(T_w - T_a)/(e_w - e_a)] \quad (5.5)$$

and  $p$  ( $kPa$ ) is the air pressure,  $T_w$  ( $^{\circ}C$ ) is the stream water temperature and  $T_a$  ( $^{\circ}C$ ) is the air temperature. Air pressure was set constant to 80.3 kPa.

*Shortwave radiation.* The net shortwave radiation  $SW_{net}$  was calculated with the water albedo  $\alpha$  (dimensionless) and the measured incoming shortwave radiation  $SW_{in}$  ( $W m^{-2}$ ):

$$SW_{net} = (1 - \alpha)SW_{in} \quad (5.6)$$

The water albedo was set constant to 0.05 (Leach and Moore, 2010).

*Longwave radiation.* The net longwave radiation  $LW_{net}$  was determined using parameterizations. The incident atmospheric radiation was calculated by combining the clear-sky algorithm of Dilley and O'Brien (1998) with the cloud-correction algorithm of Unsworth and Monteith (1975). For the parameterizations, we used measurements of air temperature, relative humidity and incoming shortwave radiation as input. We estimated the cloud cover by comparing the measured solar radiation with the clear-sky radiation following Campbell (1985). This combination of parameterizations was shown to give reliable predictions of incoming long-wave radiation for our study site (Magnusson et al., 2011). The outgoing longwave radiation was determined from the measured stream temperature using the Stefan-Boltzmann radiation law. The emissivity of water was set constant to 0.95 (Leach and Moore, 2010).

## 5.6 Processes influencing stream temperature warming: Identifying dominant processes

The stream energy balance equation (equation 5.1) shows that surface heat flux per unit discharge influences the longitudinal temperature increase along a reach. In the case of the long stream reach (S2 to S4) which shows a strong response to meteorological forcing, we find a clear relationship between the observed temperature increase and the surface heat flux divided by discharge (Figure 5.5). One particularly interesting event occurs in the beginning of September, when stream discharge suddenly decreases abruptly after a snowfall on the glacier (which raised the glacier's surface albedo and lowered its melt rate). Following this snowfall, the longitudinal warming along this reach displayed much larger diurnal fluctuations than before. Surface heat fluxes were similar before and after the snowfall event, but discharge dropped from roughly  $1 - 4 \text{ m}^3/\text{s}$  to roughly  $0.5 - 1 \text{ m}^3/\text{s}$ . The lower discharge resulted in a high ratio between daytime surface heat fluxes and stream flow. From equation (5.1), we can infer that sudden increase in stream warming occurs because the flow rate  $q(t)$  decreases more than the stream surface area, which is given by the (variable) stream width  $w(t)$  times the (fixed) reach length  $L$ .

## Analysis of stream temperatures

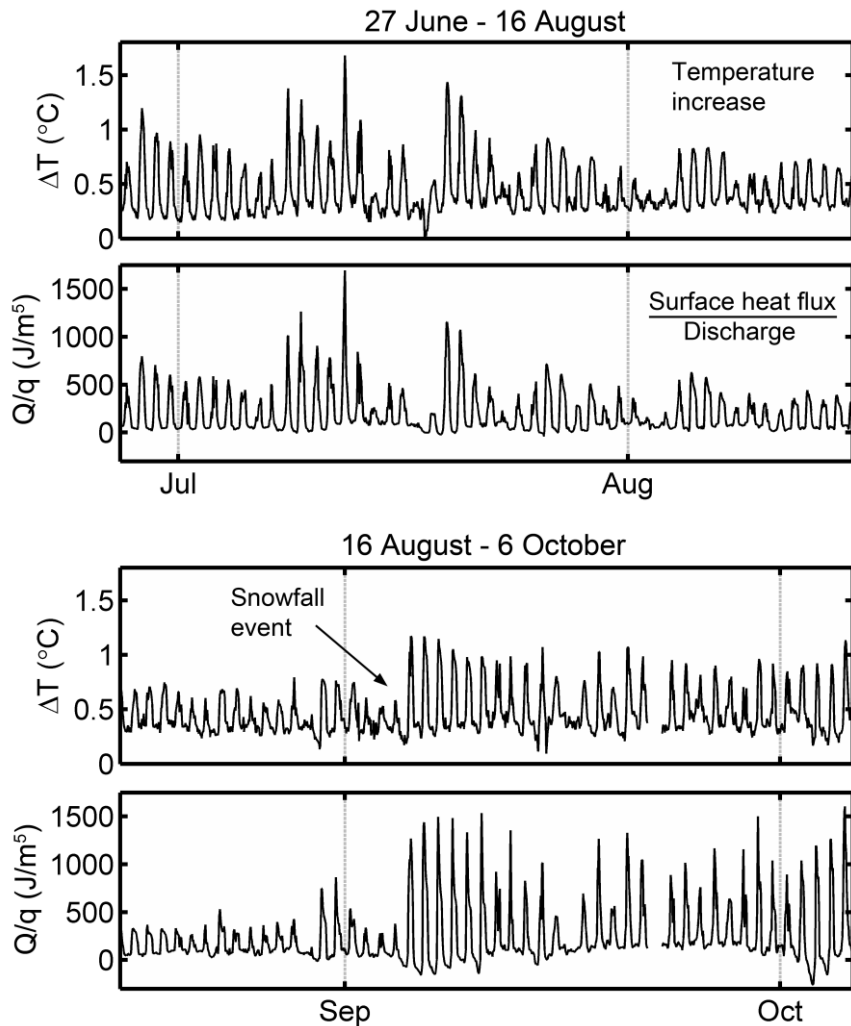


**Figure 5.5.** The observed stream temperature increase ( $\Delta T$ ) shows a strong relationship with the surface heat fluxes per unit discharge ( $Q/q$ ) for the reach stretching from site S2 to S4. In the beginning of September, the discharge decreased abruptly but the surface heat fluxes remained high (large  $Q/q$  ratio). Due to the lower volume of water in the stream, the diurnal temperature rise was much larger than before.

With the energy balance equation described above, we analysed whether the heat transfer across the stream surface, frictional warming or groundwater inflow dominated the longitudinal temperature increase observed over the four stream reaches (site S1 to S2, S2 to S3, S3 to S4, and S4 to S5). To assess the importance of surface heat transfer, we plotted the observed downstream change in stream temperature ( $\Delta T$  on the vertical axis of Figure 5.6) as a function of the calculated heat flux across the stream surface divided by discharge ( $Q/q$  on the horizontal axis of Figure 5.6). The regression line through the points can be interpreted by using a slightly rearranged version of the temperature model presented above (see equation 5.1):

$$\underbrace{\Delta T(t)}_{y\text{-axis}} = \underbrace{\frac{Lw(t)}{cp} \frac{Q(t)}{q(t)}}_{\text{Slope } x\text{-axis}} + \underbrace{\frac{g\Delta z}{c}}_{\text{Intercept}} + \underbrace{\Delta T_G(t) \frac{q_G(t)}{q(t)}}_{\text{Error term}} \quad (5.7)$$

The slope of the regression line describes the relationship between the average stream width, the stream length, the specific heat of water and the density of water ( $Lw/cp$ ). The slope is not constant because the stream width varies as a function of discharge. For this reason, we

plotted three discharge intervals in Figure 5.6. The steepening of the slope with increasing discharge reflects an increase in channel width at higher discharges. The intercepts of the regression lines in Figure 5.6 indicate the influence of frictional warming ( $g\Delta z/c$ ). In Figure 5.6, we treat the influence of groundwater inflows on the longitudinal stream temperature increase as an error term. Groundwater inflows would likely disturb the linear relationship between the temperature increase ( $\Delta T$ ) and the heat transfer across the stream surface divided by discharge ( $Q/q$ ). Then the intercept of the regression line may also no longer equal the contribution by frictional warming ( $g\Delta z/c$ ). The method does not provide any information about groundwater discharge if the groundwater temperature is too close to the stream temperature.

We first illustrate the method using the long stream reach stretching from S2 to S4, where we suspect that the temperature increase largely depends on the heating across the stream surface (Figure 5.6, Table 5.1). The surface heat fluxes divided by discharge ( $Q/q$ ) explained 88-91 percent of the variance in the temperature increase ( $\Delta T$ ) in Figure 5.6, indicating that heat fluxes across the stream surface dominate the temperature warming over this long reach. As mentioned above, the slopes of the regression lines differed between the discharge ranges because the stream width is a function of discharge. The observed intercept, varying between 0.21 and 0.27 °C, exceeded the calculated frictional warming of 0.10 °C. This discrepancy may indicate uncertainties in the calculated surface heat fluxes, measurement errors, or the influence of groundwater inflow.

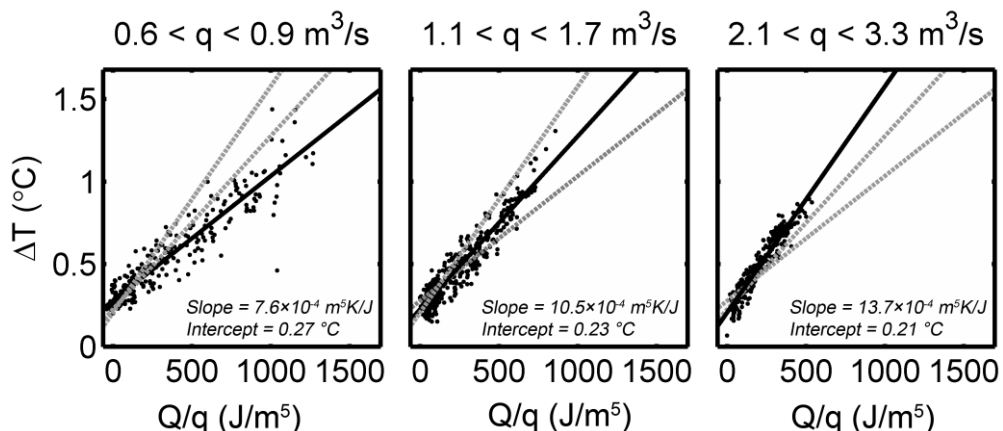


**Figure 5.6.** Observed temperature increases over the long reach stretching from S2 to S4, showing linear relationships with surface heat fluxes per unit discharge, in three ranges of discharge. The slope of this relationship increases with discharge, reflecting the increase in stream width (and thus surface area) with increasing discharge. The regression line for each discharge range is shown in black; the lines for the other two discharge ranges are shown as grey dashed lines for comparison.

Using the method shown in Figure 5.6, we also analyzed the longitudinal temperature increase observed along four shorter stream reaches (Table 5.1). The measurements over the three upstream reaches (S1 to S2; S2 to S3; S3 to S4) displayed similar characteristics as obtained in the analysis for the long stream reach (S2 to S4) which encompasses two of those shorter reaches. In most cases, the observed longitudinal temperature increase correlated strongly with the surface heat flux divided by discharge, and the slope of the regression line always became steeper as discharge increased. The intercept approximately matched or slightly exceeded the calculated frictional warming. Thus, the surface heat fluxes also seem to dominate the temperature warming over these three smaller reaches (S1 to S2; S2 to S3; S3 to S4), of which two cover the long stream section (S2 to S4) analyzed above. The difference

## Analysis of stream temperatures

between the intercept of the regression line and the calculated frictional warming may again indicate uncertainties within the calculated surface heat fluxes, measurement errors, or the influence of stream-groundwater exchange.

In contrast, the longitudinal temperature increase observed over a very short reach (S4 to S5, 60 m in length) behaved differently from those observed over the upstream sections. The  $r^2$  between the temperature increase and the surface heat flux divided by discharge was very low, ranging between 0.00 and 0.09, and the intercepts of the regression lines varied between 0.22 and 0.26 °C, greatly exceeding the calculated frictional warming of 0.02 °C. This relatively large temperature increase, combined with the weak response to radiative forcing, suggests that another process, likely groundwater inflow, dominates the temperature increase across this short reach.

**Table 5.1.** Linear relationships between the longitudinal temperature increase and the heat transfer across the stream surface per unit discharge, bounded within defined discharge intervals (see Figure 5.6), for individual stream reaches (see Figure 5.1). High  $r^2$  values and small differences between the intercept of the regression line and the calculated frictional warming indicate reaches where stream warming is primarily controlled by surface heat fluxes rather than groundwater inflows. Uncertainties are reported as  $\pm 1$  standard error.

Stream reach	Discharge interval ( $m^3/s$ )	$r^2$	Slope of regression line ( $m^5 K/J$ )	Intercept of regression line (°C)	Calculated frictional warming (°C)	Length of stream reach (m)
S2 to S4	0.6-0.9	0.88	$7.6 \pm 0.2 \times 10^{-4}$	$0.27 \pm 0.01$	0.10	330
	1.1-1.7	0.90	$10.5 \pm 0.2 \times 10^{-4}$	$0.23 \pm 0.00$		
	2.1-3.3	0.91	$13.7 \pm 0.3 \times 10^{-4}$	$0.21 \pm 0.01$		
S1 to S2	0.6-0.9	0.67	$2.9 \pm 0.1 \times 10^{-4}$	$-0.01 \pm 0.01$	0.02	130
	1.1-1.7	0.75	$4.7 \pm 0.1 \times 10^{-4}$	$-0.02 \pm 0.00$		
	2.1-3.3	0.82	$10.3 \pm 0.3 \times 10^{-4}$	$0.01 \pm 0.01$		
S2 to S3	0.6-0.9	0.79	$3.6 \pm 0.1 \times 10^{-4}$	$0.16 \pm 0.01$	0.03	130
	1.1-1.7	0.63	$4.8 \pm 0.2 \times 10^{-4}$	$0.10 \pm 0.00$		
	2.1-3.3	0.64	$6.3 \pm 0.3 \times 10^{-4}$	$0.05 \pm 0.01$		
S3 to S4	0.6-0.9	0.86	$3.9 \pm 0.1 \times 10^{-4}$	$0.11 \pm 0.01$	0.07	200
	1.1-1.7	0.88	$5.7 \pm 0.1 \times 10^{-4}$	$0.13 \pm 0.00$		
	2.1-3.3	0.81	$7.4 \pm 0.2 \times 10^{-4}$	$0.16 \pm 0.01$		
S4 to S5	0.6-0.9	0.03	$-3.7 \pm 1.3 \times 10^{-6}$	$0.26 \pm 0.01$	0.02	60
	1.1-1.7	0.00	$1.9 \pm 1.5 \times 10^{-5}$	$0.22 \pm 0.00$		
	2.1-3.3	0.09	$17.4 \pm 0.4 \times 10^{-5}$	$0.25 \pm 0.01$		

## 5.7 Inferring hydraulic geometry relationships from stream temperature measurements

The steam energy balance (equation 5.1) indicates that the longitudinal temperature increase over a stream reach depends on stream width. Thus, observations of stream warming along a reach represent indirect measurements of stream width, which may be helpful in estimating reach-averaged hydraulic geometry relationships in irregular channels such as ours. The three basic hydraulic geometry relationships express width, depth, and velocity as power functions of discharge (Leopold and Maddock, 1953; Park, 1977):

$$\text{Width} = aq^b \quad (5.8)$$

$$\text{Depth} = cq^f \quad (5.9)$$

$$\text{Velocity} = kq^m \quad (5.10)$$

The hydraulic geometry of channels is conventionally determined by direct measurements across a range of flows. However, such measurements, particularly measurements of stream width, can be problematic in highly irregular channels such as proglacial streams. These are typically braided streams, and they also often display cascading flow because of the steep down-valley gradient and the large relative roughness of the channel bed. As a result, cross-sections of these channels are often highly variable over short distances, making it difficult to infer average hydraulic geometry relationships over a channel reach.

We can estimate the relationship between stream width and discharge over the long reach stretching from S2 to S4, using the energy balance equation (equation 5.7) described in the preceding section. By rewriting equation 5.7, we obtain an expression for the stream width

$$w(t) = \frac{q(t)c\rho}{Q(t)L} \left( \Delta T(t) - \frac{g\Delta z}{c} - \Delta T_r(t) \right) \quad (5.11)$$

in which all terms except the channel width  $w(t)$  and a so-called residual temperature increase  $\Delta T_r$ , can be directly measured or calculated (note that here,  $c$  is the specific heat of water rather than the hydraulic geometry constant in equation (5.9)). The residual temperature increase may arise due to groundwater inflow (compare with equation 5.7), but other factors, including measurement errors, may also influence the observed temperature increase. We estimated the residual heating by (a) determining the intercept of the regression lines between  $Q/q$  and  $\Delta T$  for discharges within decile ranges (i.e. the lowest 10% of flows, the next 10% and so forth) as in the preceding section, (b) subtracting the contribution of frictional warming from those intercepts and (c) fitting a parametric function through those points as a function of discharge ( $\Delta T_r = 0.24 \times q^{-0.29} - 0.09$ ). We assumed that this parametric function described the residual temperature increase (Figure 5.7). In addition, we restricted our calculations using equation (5.11) to periods when the calculated net surface heat flux  $Q(t)$  exceeded 700 W/m<sup>2</sup>, so that shortwave radiation dominates the energy balance, and the fractional uncertainty in  $Q(t)$  is relatively small.

## Analysis of stream temperatures

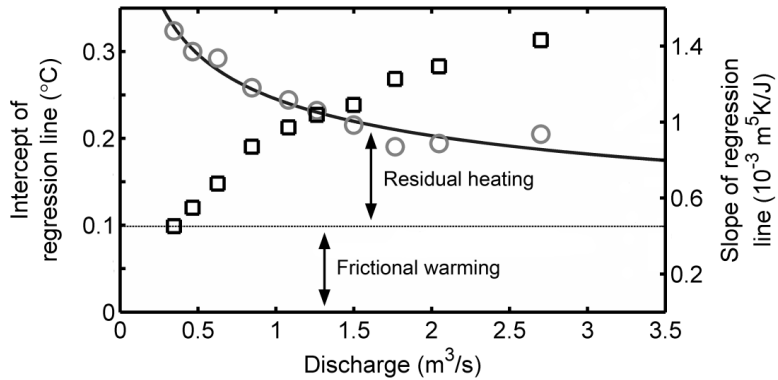


**Figure 5.7.** Slopes and intercepts (black squares and grey circles, respectively) of regression relationships between longitudinal temperature increases from S2 to S4 ( $\Delta T$ ) and surface heating per unit discharge ( $Q/q$ ) for a series of discharge bins. The slopes of the regression lines (black squares) become steeper with increasing discharge, reflecting an increase in stream width. The regression intercepts (grey circles, with fitted black curve) indicate the increase in stream temperature with no net surface heating. They decline with increasing discharge, but always exceed the calculated frictional warming.

In Figure 5.8, the resulting estimates of stream width are shown as a function of discharge, together with the fitted hydraulic geometry relationship  $w = 11.7 \pm 0.2 q^{0.46 \pm 0.02}$  (uncertainties reported as  $\pm 1$  standard error). The individual values of calculated stream width are somewhat uncertain (the RMSE around the fitted curve is 1.7 m). Nonetheless there is a clear relationship between discharge and calculated stream width, which approximately follows the power-law form observed in many streams (see discussion at the end of this section).

As stream width increases with increasing discharge (Figure 5.8), the slope of the relationship between longitudinal warming ( $\Delta T$ ) and surface heat flux per unit discharge ( $Q/q$ ) becomes steeper as well (Figure 5.7). From equation 5.7, one can infer the average stream width in a narrow range of discharge from the slope of relationship between  $\Delta T$  and  $Q/q$ , denoted  $s_{heat}$  below:

$$w = s_{heat} \frac{c\rho}{L} \quad (5.12)$$

For the stream reach stretching from site S2 to S4, we calculated regression slopes between  $\Delta T$  and  $Q/q$  for 10 discharge bins, corresponding to the lowest 10% of flows, the next 10% and so forth (Figure 5.7). Stream widths inferred from these slopes using equation (5.12), shown as black squares in Figure 5.8, are consistent with the hydraulic geometry relationship inferred from individual values of  $\Delta T$  and  $Q/q$  using equation (5.11), shown as the grey dots and solid line in Figure 5.8. Thus, both methods imply similar stream widths and similar hydraulic geometry relationships between stream width and discharge.

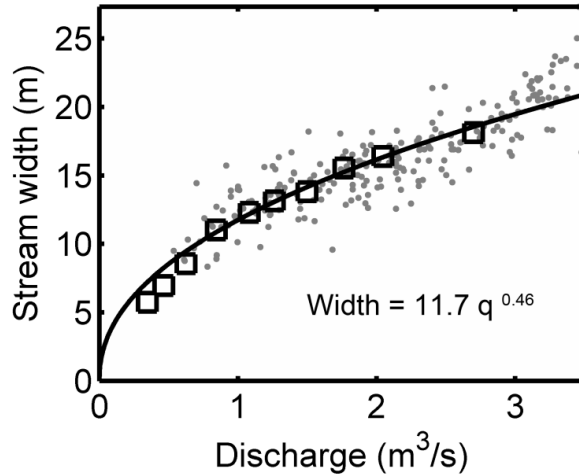


**Figure 5.8.** Relationship between stream width and discharge determined with the energy balance model (equation 5.11) for the stream reach stretching from site S2 to S4 (grey dots and solid line). Black squares show stream widths inferred from the slope of the relationship between  $\Delta T$  and  $Q/q$  for discrete ranges of discharge (see equation 5.12 and Figure 5.7).

Next, we measured the flow velocity as a function of discharge using travel-time measurements of fluorescent dye tracers. The flow velocity was determined from the centroid of the tracer concentration curve. Most of our velocity measurements were taken over a 90-m reach surrounding site S2 (open circles, Figure 5.9). We also made several velocity measurements over the 700-m reach from site S2 to S7 (solid circles, Figure 5.9). From the fitted velocity relationship  $v = 0.46 \pm 0.01 q^{0.29 \pm 0.04}$  ( $\pm 1$  standard error), combined with the width relationship  $w = 11.7 \pm 0.2 q^{0.46 \pm 0.02}$ , we calculate the relationship between average depth and discharge across the study reach as  $d = 0.19 \pm 0.01 q^{0.25 \pm 0.05}$  (with standard errors estimated by Gaussian error propagation). In Figure 5.10, we compare this reach-averaged depth-discharge relationship with observed stream stage at the two locations along the study reach where stream level was measured (sites S2 and S3). As Figure 5.10 shows, stage variations observed at the two sites are consistent with the inferred hydraulic geometry relationship. The numerical values differ (note the different scales on the left and right axes), which should be expected for at least three reasons: (a) average depth over an entire reach will generally differ from average depth at any cross-section, (b) average depth at any cross-section will be less than total depth, and will increase more slowly as a function of discharge (because the channel is not rectangular), and (c) there will be a constant offset between total depth and stream stage (because stream stage is measured relative to an arbitrary datum rather than the thalweg elevation).

## Analysis of stream temperatures

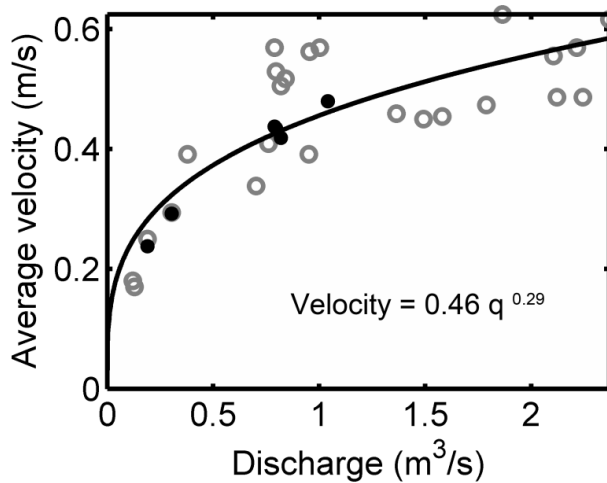


**Figure 5.9.** Stream flow velocities measured using dye tracers, with fitted power-law hydraulic geometry relationship. Velocities measured over 90-m reach surrounding site S2 (open circles) have greater variability than those measured over the entire reach from site S2 to site S7 (solid circles).

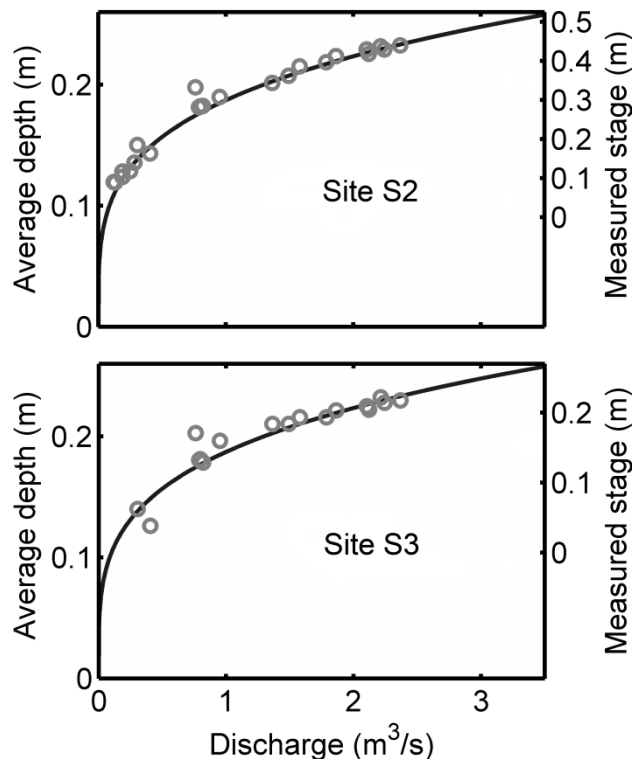


**Figure 5.10.** Predicted hydraulic geometry relationship between reach-averaged stream depth and discharge (black curve), compared to stage measurements at two sites along the studied reach (gray points).

The exponents obtained for the three hydraulic geometry relationships are comparable with observations made elsewhere. The fitted width exponent is towards the upper end of the range usually observed in natural channels (Park, 1977). However, high width exponents are typical for shallow gravel-bed streams, as noted by Smith and Pavelsky (2008), who found a similar exponent ( $b = 0.48 \pm 10\%$ ) in a remote sensing study of a braided channel in Siberia. In another study, Chikita et al. (2010) reported a slightly lower value than ours ( $b = 0.42$ ) for a glacial forefield stream in Alaska. To our knowledge, the highest obtained width exponent ( $b = 1.05$ ) was reported by Ashmore and Sauks (2006) for a proglacial braided stream in

## Chapter 5

British Columbia. Our velocity exponent ( $m = 0.29$ ) falls well within the range of values summarized by Park (1977). Our depth exponent ( $f = 0.25$ ) is slightly lower than the majority of observations reported by Park (1977), but is higher than the depth exponent reported by Chikita et al. (2010) for their proglacial stream ( $f = 0.17$ ). These studies, based on direct measurements, suggest that the exponents derived here may be realistic. Our results indicate that the studied stream reach accommodates discharge mostly through widening rather than large changes in depth and flow velocity.

Our analysis above shows that stream channel geometry has a direct and quantifiable effect on thermal relations in proglacial streams. Stream width has a strong enough effect on stream temperature dynamics (particularly when radiative heat fluxes are large) that the method outlined here can be used to derive reasonable estimates of the relationship between stream width and discharge. Of course, direct measurements of stream width would be preferable to the indirect estimates obtained from stream temperature dynamics. However, measuring stream widths can be very difficult in shallow, irregular, highly braided channels like ours, which lack well-defined banks. Furthermore, our method gives estimates of average effective widths over long stream reaches; such estimates are difficult to obtain by most other methods.

### 5.8 Processes influencing stream warming: Analysing the stream energy balance

In this section, we analyze the physical processes influencing the stream temperatures at the study site in more detail. With the ongoing glacier retreat, a good understanding of such physical processes is important, because stream temperatures in these environments are sensitive to changes in climate and runoff regimes, along with changing distances between the streams and the glaciers themselves (Chikita et al, 2010, Webb et al, 2008). In the following analysis, we investigate the temperature increase observed over the long stream reach stretching from S2 to S4, which shows a strong response to meteorological forcing (Table 5.1 and Figure 5.4). Along this reach, the temperature increases almost proportionally with the surface heat fluxes within defined ranges of discharge (Figure 5.11, right panel). On the other hand, stream warming is inversely related to discharge within narrow ranges of surface heat fluxes (Figure 5.11, left panel). This observation is consistent with previous results from alpine streams showing that longitudinal increases in stream temperature often are inversely related to discharge (Constantz, 1998). In the case of proglacial streams, however, one might not expect an inverse relationship between discharge and longitudinal warming, because rates of glacial melt (and therefore discharge) are highest precisely when air temperatures and solar fluxes (and therefore rates of heat transfer at the air-stream interface) are also highest. Our results show that along with surface heat fluxes, stream morphology and discharge variations influence the heating of proglacial streams on the Damma glacier forefield.

## Analysis of stream temperatures

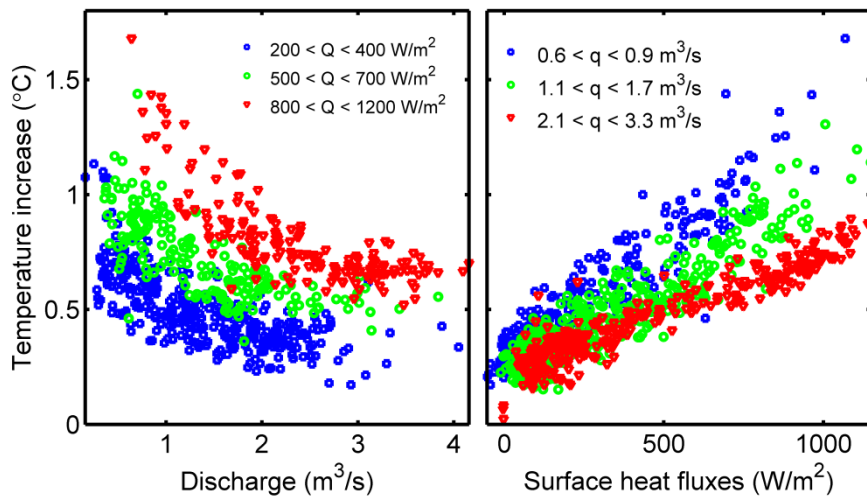


**Figure 5.11.** Longitudinal stream warming (here, for the 330 m reach from S2 to S4) shows a strong positive relationship with the surface heat fluxes, but an inverse relationship with stream discharge. Left panel shows stream warming as a function of discharge for three distinct ranges of surface heat flux. Right panel shows stream warming as a function of surface heat flux for three distinct ranges of discharge.

On average over the monitoring period, all of the energy balance components were positive, making the stream water warmer (Table 5.2). Shortwave radiation contributed most to the average stream energy balance. The residual heating, given by the parametric function obtained above ( $\Delta T_r = 0.24 \times q^{-0.29} - 0.09$ ), was the second largest term in the energy balance during daytime, and the largest term at night. Thus, if we assume that the residual heating arises due to groundwater advection or hyporheic exchange, we find that such processes play an important role in the heating along this stream reach. Frictional warming increases the stream temperature along the reach by about 0.10 °C independent of time and discharge (see equation 5.1), and therefore contributes significantly to the stream energy balance. During the monitoring period, air temperatures exceeded stream temperatures about 98% of the time, implying positive sensible heat fluxes. These large temperature differences, combined with high relative humidity, also resulted in positive latent heat fluxes during both daytime and nighttime (that is, more water vapour condensed onto the stream surface than evaporated from it). The higher air than stream temperatures furthermore is an indication of a net positive longwave radiation flux to the stream, which also our results suggest (although small). The relative importance of different energy balance components shifts with time of day, however (Table 5.2).

## Chapter 5

**Table 5.2.** The calculated contribution of different heat sources to the temperature increase between S2 and S4, averaged over the monitoring period for all measurements, and those made during daytime and nighttime only. Here, daytime was defined as hours with positive solar radiation, and nighttime as hours without sunlight. On average over the monitoring period, solar radiation together with frictional warming and the residual heating component (see text) dominated the energy balance. Note also that the average heat fluxes always were positive, even the nighttime averages.

Energy balance component	Time of day	Heat flux (W/m <sup>2</sup> )	Temperature increase (°C)	Fraction of heating (%)
<i>Shortwave radiation</i>	Whole day	198	0.16	35
<i>Longwave radiation</i>	Whole day	4	0.00	0
<i>Sensible heat</i>	Whole day	52	0.05	10
<i>Latent heat</i>	Whole day	18	0.01	3
<i>Frictional warming</i>	Whole day	114	0.10	21
<i>Residual heating</i>	Whole day	154	0.15	31
<i>Shortwave radiation</i>	Daytime	319	0.26	45
<i>Longwave radiation</i>	Daytime	5	0.00	1
<i>Sensible heat</i>	Daytime	55	0.04	8
<i>Latent heat</i>	Daytime	19	0.01	2
<i>Frictional warming</i>	Daytime	122	0.10	18
<i>Residual heating</i>	Daytime	156	0.14	26
<i>Shortwave radiation</i>	Nighttime	0	0.00	0
<i>Longwave radiation</i>	Nighttime	1	0.00	0
<i>Sensible heat</i>	Nighttime	47	0.05	15
<i>Latent heat</i>	Nighttime	16	0.01	4
<i>Frictional warming</i>	Nighttime	101	0.10	31
<i>Residual heating</i>	Nighttime	152	0.16	50

Stream temperature predictions are of interest in many applications, so the question arises how well the energy balance model reproduces the observed temperature increase (equation 5.1). Therefore, we simulated the hourly longitudinal stream temperature change from S2 to S4 by (a) using the stream energy balance equation (equation 5.1) to describe the temperature increase along the stream channel, (b) replacing the groundwater inflow term in that equation with the parametric function ( $\Delta T_r = 0.24 \times q^{-0.29} - 0.09$ ) that describes the residual heating, and (c) applying the hydraulic geometry relationship derived above, which describes the average stream width as a function of discharge presented above ( $w = 11.7 q^{0.46}$ ). The low error ( $RMSE = 0.08$  °C) and strong correlation ( $r^2 = 0.87$ ) between the simulated and observed temperature increases (see Figure 5.12) closely matched the model performance reported in a previous study of proglacial stream temperatures (Chikita et al., 2010).

## Analysis of stream temperatures

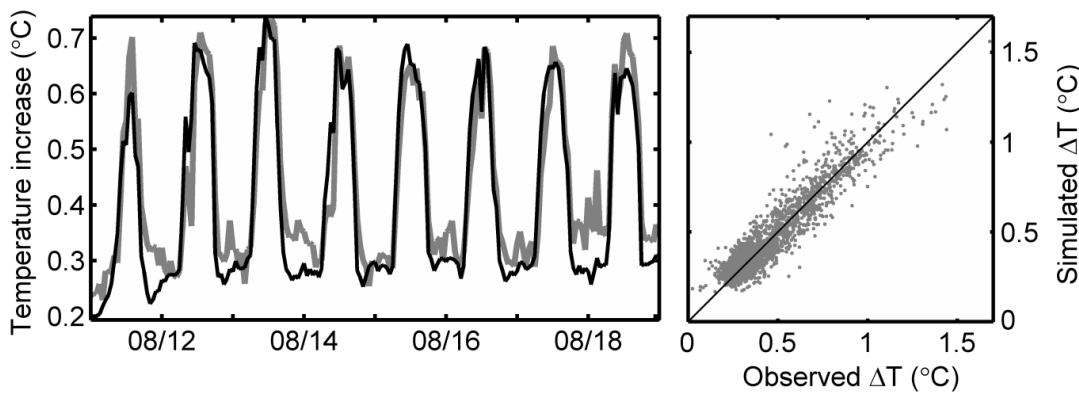


**Figure 5.12.** Temperature increase predicted from surface heat transfer, frictional warming, and residual heating (equation 5.1, black line), compared to observed warming between S2 and S4 (grey line). Left panel shows predicted and observed time series for a fair-weather period in August. Right panel compares hourly predicted and observed values for the entire monitoring period (late June through early October).

In the remaining section, we discuss different uncertainties that may influence our analysis using the energy-balance equation. We are confident in our estimates of net shortwave radiation flux to the water surface; solar flux is measured nearby at the weather station on the forefield, and the albedo of water varies only slightly between different studies (Leach and Moore, 2010; Chikita et al., 2010). We are also confident in our estimates of frictional warming, because they depend only on the elevation difference along the reach (which can be measured precisely), and on the assumption that the available gravitational potential energy is completely dissipated to heat (which is accurate because the change in kinetic energy of the flow is trivial by comparison). The calculated incoming longwave radiation reproduced measurements made at a weather station located 2.6 km north-east of the forefield and at an altitude of 2586 m with low errors (mean bias of -8 W/m<sup>2</sup> and root mean squared error of 28 W/m<sup>2</sup>). The calculated turbulent heat fluxes are more uncertain, mainly because the parameters in the equations were determined under conditions different from those prevailing at our study site (see Leach and More 2010; Webb and Zhang, 1997). However, at our alpine study site solar radiation dominates the surface heat fluxes, with low contributions from turbulent heat fluxes.

The conductive heat flux through the streambed is negligible in gravel-bedded streams, so we did not include it in the energy-balance equation (Brown, 1969). In addition, convection typically transports much more heat than conduction through the hyporheic zone (Malard et al., 2001). Thus, we think that energy transfer at the streambed interface is probably dominated by heat inputs from groundwater discharge. Some studies suggest that hyporheic flow may store and release heat through the same interface and influence the stream temperature dynamics (Alexander and Caissie, 2003; Evans and Petts, 1997). We did not investigate hyporheic heat transport, however, because it was very difficult to install sensors in the streambed sediments.

## 5.9 Inferring information about surface-groundwater interactions from stream temperature measurements

If the longitudinal stream temperature increase depends on groundwater inflow, we can infer rates of groundwater discharge and aquifer properties from stream and groundwater temperature data, along with measurements of hydraulic head and stream discharge. Anderson (2005) has summarized solutions to the so-called "inverse problem" of inferring groundwater flow or hydraulic conductivity from signals in water temperature and head data. In our situation, if the heating across the stream surface and frictional warming is small, the observed temperature increase primarily depends on groundwater discharge. Then the warming along a stream reach will be predicted by the following mixing model (compare with equation 5.1):

$$\Delta T(t) \cong \Delta T_G(t) \frac{q_G(t)}{q(t)} \quad (5.13)$$

where  $\Delta T$  ( $^{\circ}\text{C}$ ) is the longitudinal stream temperature increase,  $\Delta T_G$  ( $^{\circ}\text{C}$ ) is the difference between the groundwater and stream water temperature,  $q_G$  ( $\text{m}^3 \text{s}^{-1}$ ) is the groundwater discharge and  $q$  ( $\text{m}^3 \text{s}^{-1}$ ) is the stream flow.

In an idealized situation, with a straight stream reach alongside a homogeneous aquifer, the groundwater discharge from the riparian zone increases proportionally with the hydraulic gradient. Thus, Darcy's law may be used to describe the groundwater discharge as:

$$q_G = k d_a L \frac{\Delta h(t)}{\Delta l} \quad (5.14)$$

where  $k$  ( $\text{m s}^{-1}$ ) is the hydraulic conductivity,  $d_a$  ( $\text{m}$ ) is the aquifer depth,  $L$  ( $\text{m}$ ) is the aquifer width and  $\Delta l$  ( $\text{m}$ ) is the distance between the stream and groundwater monitoring well. Darcy's law implies that groundwater inflow increases proportionally with the hydraulic gradient, the hydraulic conductivity, the length of the stream channel and the saturated aquifer thickness. We assume that the bedrock is horizontal perpendicular to stream. We also assume that groundwater only discharges from the one side of the stream, where the ground surface slopes steeply toward the channel. This assumption reflects the site characteristics along the short test reach stretching from S4 to S5. If instead groundwater discharged equally from both sides of the stream, L would be replaced by 2L in equation (5.14).

At the short (60 m) test reach between S4 and S5, we measured groundwater levels, temperatures, and gradients using two monitoring wells, located along a transect perpendicular to the stream (2 m and 4 m from the channel) at site S5. In the following analysis, we used the groundwater levels measured far from the stream (about 4 m away from the stream) and the temperature measurements recorded in the monitoring well near to the stream (about 2 m away from the stream).

To observe the effects of groundwater inflows on stream temperature dynamics, it is necessary to minimize the influence of frictional warming and air-stream heat fluxes. Therefore we only analyzed the longitudinal temperature change observed during nighttime, between 21:00 and 06:00, when we assume that groundwater inflow dominated the heat budget. Furthermore, we subtracted the calculated contribution of frictional warming from the observed temperature increase over the short test reach (S4 to S5) and the neighbouring upstream reach (S3 to S4). As discussed above, the observed temperature increase between S3

## Analysis of stream temperatures

and S4 is well correlated with surface heat fluxes, with a relatively small regression intercept that is largely explained by frictional warming (see Table 5.1). We therefore used the temperature increase between S3 and S4 (corrected for frictional warming) as a measure of surface heat fluxes. We estimated the influence of surface heat fluxes using the temperature gradient observed over the upstream section (S3 to S4), multiplied by the length of the downstream section (S4 to S5). For every time-step, we subtracted this product from the observed longitudinal stream temperature change over the groundwater-influenced reach (S4 to S5). In the following, we use values of the corrected temperature increase averaged for the nighttime period between 21:00 and 06:00. On average over the monitoring period, the resulting correction factor of 0.02 °C was much smaller than the observed average temperature increase of 0.20 °C.

The temperature increase along the reach stretching from site S4 to S5 (corrected for frictional heating and surface heat fluxes as described above) correlated well with the head difference between the groundwater level and stream level (Figure 5.13). The remaining variables, which we think may influence the warming of the water, did not show a strong correlation with the increase in stream temperature. In particular, the stream temperature increase correlated very weakly with both the stream discharge and the difference between the stream and groundwater temperature. These weak correlations may arise because both stream and groundwater temperatures vary over relatively narrow ranges (Figure 5.13), or because the change in temperature in the short reach from S4 to S5 is rather small.

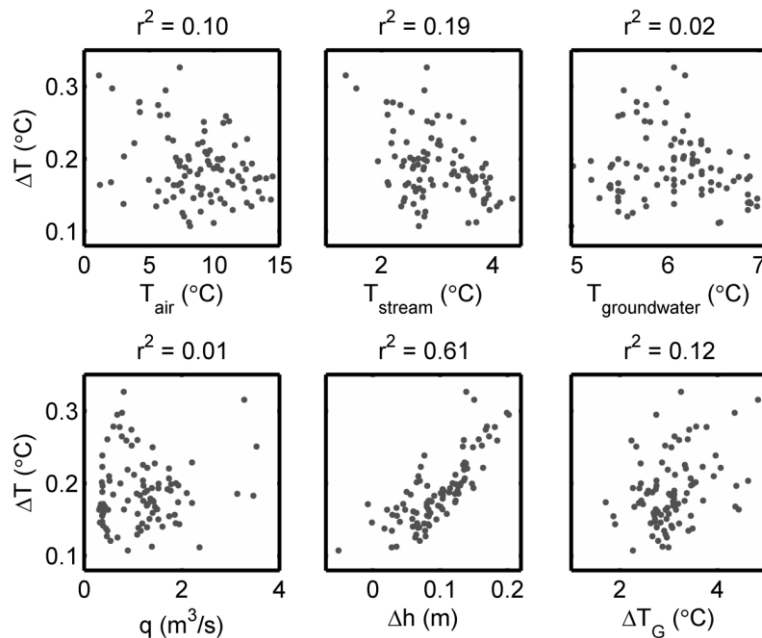


**Figure 5.13.** Temperature increase from S4 to S5, corrected for surface heating and frictional warming (see text), compared to several variables that could influence stream warming: air, stream, and groundwater temperatures ( $T_{air}$ ,  $T_{stream}$ , and  $T_{groundwater}$ , respectively), stream discharge ( $q$ ), head difference between the stream and a groundwater well 4 m from the channel ( $\Delta h$ ), and temperature difference between the stream and groundwater ( $\Delta T_G$ ). The observed temperature increase shows a clear relationship to the stream-groundwater head difference, but no strong correlation to the other variables. The figures show nighttime averaged values (21:00–06:00).

In the idealized model situation described above, we may model the longitudinal stream temperature increase by combining the mixing equation with Darcy's law (equation 5.13 and 5.14):

$$\underbrace{\Delta T(t)}_{y\text{-axis}} \simeq \frac{k d_a L}{\underbrace{\Delta l}_{\text{Slope}}} \frac{\Delta h(t) \Delta T_G(t)}{\underbrace{q(t)}_{x\text{-axis}}} \quad (5.15)$$

In Figure 5.14, we plot the longitudinal temperature increase ( $\Delta T$ , on the vertical axis) against the combination of the time-dependent variables that govern the observed stream temperature warming according to equation 5.15 ( $\Delta T_G \Delta h / q$ , on the horizontal axis). The slope of the regression line through the points gives information about the hydraulic transmissivity ( $k d_a$ ) because we know the stream length ( $L$ ) and the distance between the groundwater monitoring well and the stream channel ( $\Delta l$ ). With a regression slope of  $0.10 \pm 0.02 \text{ m}^2/\text{s}$  ( $\pm 1$  standard error) obtained from Figure 5.14, we calculate a hydraulic transmissivity of  $6.7 \pm 1.0 \times 10^{-3} \text{ m}^2/\text{s}$  ( $\pm 1$  standard error) for this particular reach. However, the regression line intercept is above zero, suggesting that the hydraulic gradients and temperature differences measured at our particular groundwater well transect may not be representative for the whole study reach.

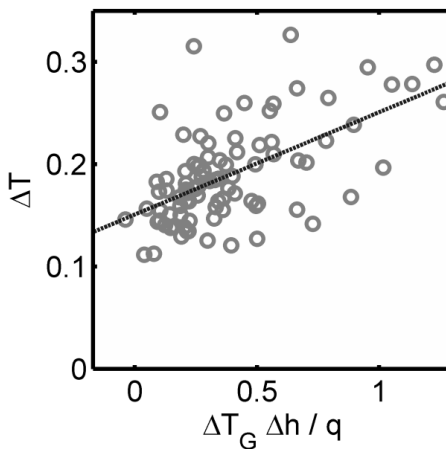


**Figure 5.14.** Temperature increase from S4 to S5, corrected for surface heating and frictional warming (see text), as a function of the product of the stream-groundwater temperature and head differences ( $\Delta T_G$  and  $\Delta h$ , respectively), divided by discharge ( $q$ ). Line shown is fitted by linear regression. The figure shows nightime averaged values (21:00 to 06:00).

We can also calculate the hydraulic transmissivity with another approach, directly from the uncorrected hourly measurements of stream temperature, discharge and meteorological variables. We combined the energy balance equation of the stream with Darcy's law (equation 5.1 and 5.14), and rearranged the result into the following form:

$$\underbrace{\Delta T(t)}_y = \underbrace{\frac{L}{c\rho} \frac{w(t)Q(t)}{q(t)}}_{k_1} + \underbrace{\frac{k d_a L}{\Delta l} \frac{\Delta h(t) \Delta T_G(t)}{q(t)}}_{k_2} + \underbrace{\frac{g \Delta z}{c}}_{k_3} \quad (5.16)$$

By regressing the response variable ( $\Delta T$ ) on the two explanatory variables ( $wQ/q$  and  $\Delta h \Delta T_G / q$ ), we estimated the two coefficients ( $k_1$  and  $k_2$ ) and the intercept ( $k_3$ ) by multiple regression. Here we used the width-discharge relationship  $w = 11.7 q^{0.46}$ , the discharges measured at site S2 and the same groundwater measurements that we used above. The regression analysis produces estimates of the three constants:  $k_1 = 5.6 \pm 0.6 \times 10^{-6} \text{ Km}^4/\text{J}$ ,  $k_2 = 2.4 \pm 0.6 \times 10^{-2} \text{ m}^2/\text{s}$  and  $k_3 = 0.22 \pm 0.00 \text{ }^\circ\text{C}$  ( $\pm 1$  standard error). The model produces an intercept that is much larger than the expected contribution by frictional warming. However, the regression estimate for  $k_1$  yields an inferred stream length  $L = 23 \text{ m}$  which is in the right order of magnitude (the real-world value is 60 m). Furthermore, the regression estimate for  $k_2$

## Analysis of stream temperatures

yields an inferred hydraulic transmissivity  $kd_a$  of  $1.6 \pm 0.4 \times 10^{-3} \text{ m}^2/\text{s}$ , which is similar to the estimate obtained earlier from Figure 5.14 and equation 5.15. Thus, both methods yield similar results for the hydraulic transmissivity, which we consider as an encouraging result, given the difficulties in using conventional methods to estimate the hydraulic properties of the heterogeneous sediments typically found on glacier forefields.

In a previous study, we estimated the hydraulic diffusivity between the stream and our monitoring wells using diurnal groundwater level fluctuations (Magnusson et al., In review). We simulated water level fluctuations propagating from the stream into the riparian zone using a diffusion model, and the calibration procedure yielded hydraulic diffusivities between  $1.3 \times 10^{-3}$  and  $1.2 \times 10^{-1} \text{ m}^2/\text{s}$  for four sites across the forefield (including sites S1, S3 and S5). Because hydraulic transmissivity equals hydraulic diffusivity times the specific yield of the aquifer material, we can convert this diffusivity estimate into an equivalent transmissivity. Specific yields for sand and gravel, the sediments found at our field site, are typically about 0.30 (Carsel and Parrish, 1988; Loheide et al., 2005). With this specific yield, our diffusivity estimates imply hydraulic transmissivities ranging between  $4.0 \times 10^{-4}$  and  $3.8 \times 10^{-2} \text{ m}^2/\text{s}$  for the four sites on the forefield. Both of the hydraulic transmissivity estimates derived above from temperature fluctuations ( $6.7 \pm 1.0 \times 10^{-3} \text{ m}^2/\text{s}$  and  $1.6 \pm 0.4 \times 10^{-3} \text{ m}^2/\text{s}$ ) are within the range of values given by the diffusion model. Note that the diffusion model may not yield reliable estimates of hydraulic diffusivity when strong downhill groundwater flow influences the propagation of groundwater level fluctuations (which seems to be the case for site S5). Therefore, we compared our results derived from temperature fluctuations with the range of hydraulic transmissivities given by the diffusion model for all sites (see Magnusson et al. (In review) for details).

The mixing model (equation 5.13) allows us to estimate a time series of groundwater inflow as a fraction of stream discharge (Figure 5.15). This method may be particularly useful for spatially integrated estimates of groundwater discharge from heterogeneous aquifers (Becker et al., 2004). The results indicate that the relative contribution of groundwater inflow to stream discharge over this reach was higher during summer than early autumn (Figure 5.15). The declining trend in the fraction groundwater inflow ( $q_G/q$ ) corresponds to a similar trend in groundwater level and in the head difference between the groundwater and the stream. The seasonally decreasing head difference is a result of a general downward trend in the observed riparian zone groundwater level, rather than variations in stream level. However, the heterogeneous sediments and complex topography of the field site lead to highly complex stream and groundwater flow patterns (Magnusson et al., In review). Therefore, any inferences drawn from local measurements of head gradients (e.g., Figures 12-14) should be treated with caution. More work is needed to explore the spatial heterogeneity of groundwater levels in complex mountainous sites like the Damma glacier forefield.

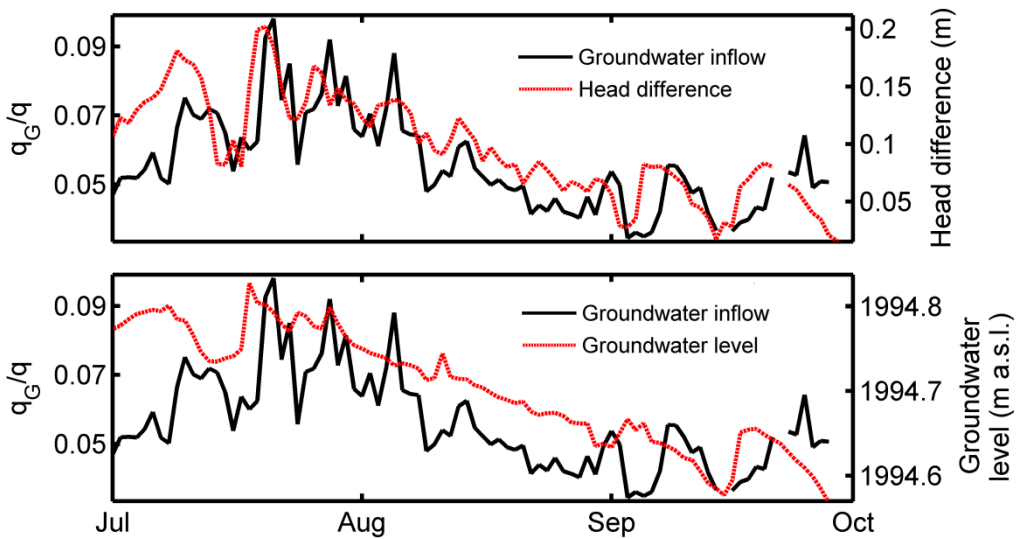


**Figure 5.15.** The calculated fraction of groundwater inflow in stream discharge ( $q_G/q$ ) over the reach from site S4 to S5 declines during the season, and follows the downward trend in groundwater levels in the nearby riparian zone. Groundwater levels were measured 4 m from the stream at site S5. The figure shows nighttime averaged values (21:00 to 06:00).

## 5.10 Summary and conclusions

In this study, we measured time series of stream and groundwater temperature, along with groundwater level and discharge, across the Damma glacier forefield in the central Swiss Alps. The seasonal and diurnal patterns observed at the Damma forefield are similar to those observed in other glacierized catchments (Uehlinger et al., 2003; Brown and Hannah, 2008). Our results show that radiative forcing influenced the stream temperatures strongly over short distances downstream along the forefield, and groundwater inflow also appears to affect the observed stream temperatures.

By using a simple energy balance equation to interpret the observed longitudinal stream temperature increases, we identified several processes dominating the stream's heat budget. Over three adjacent reaches, the analysis suggested that the heat fluxes across the stream surface and frictional warming largely explained the observed longitudinal increase in stream temperature. Over a fourth stream reach, however, neither surface heat fluxes nor frictional warming could explain the observed downstream temperature increase, leaving groundwater inflow as the most plausible dominant source of stream warming.

Where downstream temperature increases were strongly correlated with radiative forcing, we used the stream energy balance to estimate stream width as a function of discharge. The resulting estimates of stream width were consistent with hydraulic geometry relationships derived by direct measurements in other proglacial streams. Our estimated hydraulic geometry relationships imply that the Damma proglacial stream responds to discharge variations primarily by changing its width, with smaller variations in depth and flow velocity.

The observed stream warming along another reach showed a weak response to meteorological forcing, but still a relatively large temperature increase, most likely due to groundwater inflow. By analysing the nighttime temperature increase along that reach, we found a strong relationship between the hydraulic gradient in the riparian zone and the observed longitudinal stream temperature increase. With a simple mixing equation, we estimated a time series of

## Analysis of stream temperatures

groundwater inflow as a fraction of discharge; this time series correlated well with groundwater levels in the riparian zone. We also used the correlation between the observed stream warming and the stream-groundwater head difference to estimate the hydraulic transmissivity of the aquifer sediments. The substantial uncertainties in this estimate mean that it should be treated only as a proof-of-concept demonstration that this approach may have promise for inferring the hydraulic properties of heterogeneous sediments in mountainous terrain. Such heterogeneous environments present severe challenges to conventional methods for estimating hydraulic properties, motivating the search for alternative methods such as the one outlined here.

Our results illustrate how detailed studies of proglacial stream temperatures can yield valuable spatially integrated information about hydrological and thermal processes along entire stream reaches. In this study, we used inexpensive sensors that are easily deployable in remote areas such as our study site. However, our results also indicate the potential value of higher-resolution studies of temperature dynamics and heat fluxes in proglacial streams, for example using a distributed temperature sensing system in combination with direct measurements of the energy balance components over the stream surface.

### Acknowledgements

Financial support for this study was provided by the BigLink project of the Competence Center for Environment and Sustainability (CCES) of the ETH Domain. We thank the many students and staff, particularly B. Fritschi, K. Steiner and F. Herzog, who helped greatly with the fieldwork.



# Chapter 6

## 6 Conclusions and outlook

This work investigates the hydrological response of a glacier forefield to meteorological forcing on diurnal, seasonal and decadal time scales. The main conclusions and some suggestions for further research are summarized below.

The two different hydrological simulations, by an energy balance model and a temperature index model, provided similar estimates of the temporal variations in water sources (snow melt, ice melt and rain) contributing to discharge (Section 2.7). The seasonally varying contributions of the different water sources, as given by the hydrological models, seem to partially explain the temporal variations of the stream chemistry in the watershed (Hindshaw et al., 2011). The fraction of snow and ice melt contributing to discharge are likely accurate because (a) the models capture the seasonal decline of snow on the glacier reasonably and (b) the models reproduce the total observed runoff accurately (Section 2.6 and 2.7). It was also shown that the energy balance model captured the observed discharge better during spring than the temperature index model, whereas the latter showed a better match against the observed runoff during glacier ablation. This comparison study therefore also suggests that the glacier component of the energy balance model and the snow component of the temperature index model can be improved.

In spite of the rather large distance between the meteorological stations used as input for the two hydrological models, most local weather observations in or near the study site were well reproduced (Section 2.4 to 2.6). This was achieved by using efficient extrapolation schemes for the meteorological variables and carefully selected input data stations. Both the extrapolated air temperature and shortwave radiation agreed rather well with the local observations, which is encouraging because they are likely the two most important input variables for models simulating snow and ice melt. On the other hand, the extrapolated precipitation rates and wind speeds were less representative of the local observations, particularly if compared on an hourly basis. However, the analysis suggests that the extrapolations schemes capture the daily averaged wind speeds and precipitation rates decently (Section 2.4 to 2.5). The simple extrapolation schemes tested in this study may have wide application, and should be further developed and validated in more regions.

The two melt models showed different sensitivity to the distribution of solid precipitation (influencing the simulated snow patterns) in the watershed. The energy balance model only yielded accurate discharge predictions when the snow distribution was correctly modelled (Section 2.7). The simulation results were also sensitive to the parameterization of turbulent heat fluxes. More work is needed to improve simulations of the sensible and latent heat fluxes on glaciers, particularly when the input data is measured outside of the glacier boundary layer. However, note that shortwave radiation typically controls the energy-balance of alpine glaciers (Sicart et al., 2008) and a correctly modelled surface albedo, influenced by the snow distribution on the glacier, is likely more important than capturing the turbulent heat fluxes precisely. The fact that the results are sensitive to variations in input data quality suggests that a simulation using the physically based model can be rejected in the case of inappropriate input data.

## Chapter 6

The runoff simulations by the temperature index model were rather insensitive to the distribution of solid precipitation in the watershed (Section 2.7). The calibration of this model compensated for an inaccurate snow distribution. For short-term forecasts, the model may still provide accurate results but the question arises whether a parametric model with wrongly constrained parameters gives reliable long-term forecasts. Thus, it would be valuable to study how different parameter sets, obtained by calibrating a parametric melt model using several input data sets of different quality, influence the results of long-term simulations such as climate change assessments.

Before the above mentioned study was conducted, the sensitivity of the snow cover persistence to climate change was investigated. Simpler methods were used to distribute the forcing data to the watershed and no local stations in/near the basin were available for evaluating the quality of the input data. Nevertheless, the study suggests that (a) the snow season reduces by between two and three months, and (b) that the maximum snow water equivalent averaged over the watershed decreases by nearly one third (Section 3.4). The results refer to a reference period (1981-2007) and a projection period (2071-2100). Currently, but not as a part of this thesis, a climate change study incorporating the results given above (Chapter 2) is being conducted for the study basin.

Much is known about melt modelling of snow and glacier ice, and about conceptual runoff simulations in alpine watersheds. In contrast, groundwater dynamics are sparsely studied in high alpine regions, in particular in such complex field sites as the Damma glacier forefield. It is difficult to obtain groundwater measurements in such regions, and one has to rely on naturally occurring signals (e.g. water level fluctuations) rather than those artificially generated (e.g. pumping tests). Apart from such practical problems, the main difficulty lies in the large spatial heterogeneity of the field site, such that many measurements are highly local and not representative of any average characteristics. Therefore, in addition to direct measurements, a number of methods were assessed that allow spatially averaged properties such as bulk hydraulic properties to be indirectly inferred.

Diurnal stream level fluctuations driven by glacier melt propagated into the groundwater of the riparian zone (Section 4.3) and could be measured in monitoring wells 10 m away from the stream channels. The fluctuations in the groundwater level could be reproduced with a diffusion model forced by the diurnal stream level fluctuations for most locations. The model calibration yielded an estimate of the hydraulic diffusivity reflecting spatial variations in soil properties and aquifer thickness. The analysis of propagating groundwater level fluctuations can be valuable; the hydraulic properties of the sediments and the thickness of the saturated zone along the whole distance between the stream and groundwater monitoring location influences the dampening and velocity of the propagating wave. Thus, the estimated hydraulic diffusivities represent a large sample of the heterogeneous sediments covering the bedrock. However, to strengthen confidence in the hydraulic diffusivities obtained by the diffusion model, they should also be tested against estimates given by other methods.

As argued in Section 4.6, it seems more promising to infer the hydraulic diffusivity from the timing of the observed groundwater level fluctuations, rather than using the amplitude information. However, it is still not clear why the amplitudes of the groundwater level fluctuations vary so much spatially. One likely reason is that the amplitudes of the stream level fluctuations vary spatially near the monitoring wells (as indicated in Section 4.5), but local heterogeneity of the sediments may also influence the amplitude of the groundwater fluctuations. It is also not known, particularly in steep and complex terrain, along what path

## Conclusions and outlook

the groundwater wave propagates from the stream to the monitoring wells (why the hydraulic diffusivities were calculated for a range of distances as outlined in Section 4.5). Thus, measurements using an array of groundwater monitoring wells would be useful in order to learn more about (a) how the groundwater wave propagates, particularly in sloping terrain, and (b) to constrain the estimated hydraulic diffusivities better.

Radon concentration measurements of the stream and groundwater showed that no large amount of water was moved back and forth between the stream and the riparian zone on diurnal time scales (Section 4.4). However, little is known about how groundwater moves through the complete glacier forefield. It would be possible to estimate the water travel time if the equilibrium concentration of radon for the particular aquifer could be determined. Measurements of groundwater travel times across the proglacial field would likely solve many questions related to the subsurface water flows through the entire forefield. Therefore, groundwater travel time measurements would be very interesting, particularly in combination with measurements of the aquifer geometry.

Measurements of longitudinal stream temperature variations were useful as an integrative measurement of thermal and hydrological processes along entire reaches (Chapter 5). By analyzing the observed temperature increase with an energy balance equation, several processes influencing the stream warming were identified. Apart from radiative forcing and frictional warming, variations in the width of the stream influenced the temperature increase considerably. The stream width had a strong enough effect, that a reasonable estimate of the relationship between channel width and discharge could be calculated using the observed stream warming. Thus, longitudinal variations in stream temperature are useful as an integrative measurement of thermal and hydrological processes.

The discharge measurements showed that no large net exchange rates between the stream and groundwater occurred along the braided streams on the proglacial field (Section 5.3). Along one short reach, the observed stream warming indicated that groundwater inflow was a plausible explanation for the temperature increase (Section 5.6 and 5.9). This explanation does not contradict the results from the discharge measurements; the estimated contribution by possible groundwater inflows was low along the small reach in the braided stream system. However, much is still unknown about local stream-groundwater interactions along the braided channels, and methods based on stream temperature measurements may prove useful for studying such processes. Further measurements are needed to test the temperature methods, particularly in combination with spatially distributed measurements of groundwater head and temperature in the riparian zone and the streambed.

The objective of this thesis was to learn more about hydrological processes occurring across a glacier forefield. I hope that this work has given some valuable insights into those processes, helping in further studies of such field sites.



## 7 References

- Alexander MD, Caissie D. 2003. Variability and comparison of hyporheic water temperatures and seepage fluxes in a small Atlantic salmon stream. *Ground Water*, 41(1): 72-82.
- Anderson MP. 2005. Heat as a ground water tracer. *Ground Water*, 43(6): 951-968.
- Anderson SP. 2007. Biogeochemistry of glacial landscape systems, Annual Review of Earth and Planetary Sciences. *Annual Review of Earth and Planetary Sciences*, pp. 375-399.
- Ashmore P, Sauks E. 2006. Prediction of discharge from water surface width in a braided river with implications for at-a-station hydraulic geometry. *Water Resources Research*, 42(3), W03406.
- Barnett TP, Adam JC, Lettenmaier DP. 2005. Potential impacts of a warming climate on water availability in snow-dominated regions. *Nature*, 438(7066): 303-309.
- Bavay M, Lehning M, Jonas T, Loewe H. 2009. Simulations of future snow cover and discharge in Alpine headwater catchments. *Hydrological Processes*, 23(1): 95-108.
- Becker MW, Georgian T, Ambrose H, Siniscalchi J, Fredrick K. 2004. Estimating flow and flux of ground water discharge using water temperature and velocity. *Journal of Hydrology*, 296(1-4): 221-233.
- Beniston M. 1997. Variations of snow depth and duration in the Swiss Alps over the last 50 years: links to changes in large-scale climatic forcings. *Clim. Change*, 36, 281-300.
- Beniston M, Keller F, Goyette S. 2003a. Snow pack in the Swiss Alps under changing climatic conditions: an empirical approach for climate impacts studies. *Theor. Appl. Climatol.* 74, 19-31.
- Beniston M, Keller F, Koffi B, Goyette S. 2003b. Estimates of snow accumulation and volume in the Swiss Alps under changing climatic conditions. *Theor. Appl. Climatol.* 76, 125-140.
- Bernasconi SM, Biglink Project M. 2008. Weathering, soil formation and initial ecosystem evolution on a glacier forefield: a case study from the Damma Glacier, Switzerland. *Mineralogical Magazine*, 72(1): 19-22.
- Beven K. 2009. Environmental Modelling; An Uncertain Future? Routledge: London and New York.
- Boulton G, Zatsepin S. 2006. Hydraulic impacts of glacier advance over a sediment bed. *Journal of glaciology*, 52:497-527
- Bouwer H, Rice RC. 1976. Slug test for determining hydraulic conductivity of unconfined aquifers with completely or partially penetrating wells. *Water Resources Research*, 12:423-428.

## Chapter 7

- Bradley RS, Vuille M, Diaz HF, Vergara W. 2006. Threats to water supplies in the tropical Andes. *Science*, 312(5781): 1755-1756.
- Brown GW. 1969. Predicting temperatures of small streams. *Water Resources Research*, 5(1): 68-75.
- Brown LE, Hannah DM, Milner AM. 2006. Hydroclimatological influences on water column and streambed thermal dynamics in an alpine river system. *Journal of Hydrology*, 325(1-4): 1-20.
- Brown LE, Hannah DM. 2008. Spatial heterogeneity of water temperature across an alpine river basin. *Hydrological Processes*, 22(7): 954-967.
- Brutsaert W. 2005. Hydrology: An Introduction. 605 pp., Cambridge Univ. Press, U.K.
- Buck AL. 1981. New equations for computing vapor-pressure and enhancement factor. *Journal of Applied Meteorology*, 20(12): 1527-1532.
- Bultot F, Gellens D, Schadler B, Spreafico M. 1994. Effects of climate-change on snow accumulation and melting in the Broye catchment (Switzerland). *Clim. Change* 28, 339-363.
- Butler JJ. 1997. The Design, Performance, and Analysis of Slug Tests. Lewis Pub; 252.
- Cadbury SL, Hannah DM, Milner AM, Pearson CP, Brown LE. 2008. Stream temperature dynamics within a New Zealand glacierized river basin. *River Research and Applications*, 24(1): 68-89.
- Caissie D. 2006. The thermal regime of rivers: a review. *Freshwater Biology*, 51(8): 1389-1406.
- Campbell GS. 1985. Soil Physics with BASIC: Transport Models for Soil-Plant Systems, Elsevier: New York.
- Carsel RF, Parrish RS. 1988. Developing joint probability-distributions of soil-water retention characteristics. *Water Resources Research*, 24:755-769.
- Cartwright N, Nielsen P, Li L. 2004. Experimental observations of watertable waves in an unconfined aquifer with a sloping boundary. *Advances in Water Resources*, 27:991-1004.
- Chikita KA, Kaminaga R, Kudo I, Wada T, Kim Y. 2010. Parameters determining water temperature of a proglacial stream: The Phelan Creek and the Gulkana Glacier, Alaska. *River Research and Applications*, 26(8): 995-1004.
- Christensen JH. 2005. Prediction of Regional scenarios and Uncertainties for Defining European Climate change risks and Effects. PRUDENCE final report. Copenhagen. Denmark.
- Christensen JH, Carter TR, Rummukainen M, Amanatidis G. 2007. Evaluating the performance and utility of regional climate models: the PRUDENCE project. *Clim. Change*, 81, 1-6.

## References

- Clow DW, Schrott L, Webb R, Campbell DH, Torizzo A, Dornblaser M. 2003. Ground Water Occurrence and Contributions to Streamflow in an Alpine Catchment, Colorado Front Range. *Ground Water*, 41(7): 937-950.
- Constantz J. 1998. Interaction between stream temperature, streamflow, and groundwater exchanges in Alpine streams. *Water Resources Research*, 34(7): 1609-1615.
- Dadic R, Corripio JG, Burlando P. 2008. Mass-balance estimates for Haut Glacier d'Arolla, Switzerland, from 2000 to 2006 using DEMs and distributed mass-balance modeling. *Annals of Glaciology*, 49(2): 22-26.
- Dankers R, Christensen OB. 2005. Climate change impact on snow coverage, evaporation and river discharge in the subarctic Tana Basin, Northern Fennoscandia. *Clim. Change*, 69, 367-392.
- Deque M, Jones RG, Wild M, Giorgi F, Christensen JH, Hassell DC, Vidale PL, Rockel B, Jacob D, Kjellstrom E, de Castro M, Kucharski F, van den Hurk B. 2005. Global high resolution versus Limited Area Model climate change projections over Europe: quantifying confidence level from PRUDENCE results. *Clim. Dyn.* 25, 653-670.
- Deque M, Rowell DP, Luthi D, Giorgi F, Christensen JH, Rockel B, Jacob D, Kjellstrom E, de Castro M, van den Hurk B. 2007. An intercomparison of regional climate simulations for Europe: assessing uncertainties in model projections. *Clim. Change*, 81, 53-70.
- Dilley AC, O'Brien DM. 1998. Estimating downward clear sky long-wave irradiance at the surface from screen temperature and precipitable water. *Quarterly Journal of the Royal Meteorological Society*, 124(549): 1391-1401.
- Egli L, Jonas T, Meister R. 2009. Comparison of different automatic methods for estimating snow water equivalent. *Cold Regions Science and Technology*, 57(2-3): 107-115.
- Etchevers P, Golaz C, Habets F, Noilhan J. 2002. Impact of a climate change on the Rhone river catchment hydrology. *J. Geophys. Res. Atmos.* 107(D16), 4293.
- Etchevers P, Martin E, Brown R, Fierz C, Lejeune Y, Bazile E, Boone A, Dai Y, Essery R, Fernandez A, Gusev Y, Jordan R, Koren V, Kowalczyk E, Nasonova NO, Pyles RD, Schlosser A, Shmakin AB, Smirnova TG, Strasser U, Verseghy D, Yamazaki T, Yang ZL. 2004. Validation of the energy budget of an alpine snowpack simulated by several snow models (SnowMIP project). *Annals of Glaciology*, 38, 150-158.
- Evans EC, Petts GE. 1997. Hyporheic temperature patterns within riffles. *Hydrological Sciences Journal-Journal Des Sciences Hydrologiques*, 42(2): 199-213.
- Fairchild II, Killawee JA, Sharp MJ, Spiro B, Hubbard B, Lorrain RD, Tison JL. 1999. Solute generation and transfer from a chemically reactive alpine glacial-proglacial system. *Earth Surface Processes and Landforms*, 24(13): 1189-1211.
- Farinotti D, Huss M, Bauder A, Funk M. 2009. An estimate of the glacier ice volume in the Swiss Alps. *Global and Planetary Change*, 68(3): 225-231.

## Chapter 7

Farinotti D, Magnusson J, Huss M, Bauder A. 2010. Snow accumulation distribution inferred from time-lapse photography. *Hydrological Processes*, 24: 2087-2097.

Fierz C, Riber P, Adams EE, Curran AR, Fohn PMB, Lehning M, Pluss C. 2003. Evaluation of snow-surface energy balance models in alpine terrain. *Journal of Hydrology*, 282, 76-94.

Flerchinger GN, Xaio W, Marks D, Sauer TJ, Yu Q. 2009. Comparison of algorithms for incoming atmospheric long-wave radiation. *Water Resources Research*, 45: ARTN W03423.

Gellens D, Barbeau K, Schadler B, Roulin E, Aschwanden H, Gellens-Meulenberghs F. 2000. Snow cover modelling as a tool for climate change assessment in a Swiss Alpine catchment. *Nordic Hydrology*, 31, 73-88.

Giesler R, Hogberg M, Hogberg P. 1998. Soil chemistry and plants in Fennoscandian boreal forest as exemplified by a local gradient. *Ecology*, 79(1): 119-137.

Giorgi F, Bi X, Pal JS. 2004. Mean, interannual variability and trends in a regional climate change experiment over Europe. I. Present-day climate (1961-1990). *Clim. Dyn.* 22, 733-756.

Gooseff MN, Strzepek K, Chapra SC. 2005. Modeling the potential effects of climate change on water temperature downstream of a shallow reservoir, Lower Madison River, MT. *Climatic Change*, 68(3): 331-353.

Gurnall AM, Edwards PJ, Petts GE, Ward JV. 1999. A conceptual model for alpine proglacial river channel evolution under changing climate conditions. *Catena*, 38: 223-242.

Ha KJ, Shin SH, Mahrt L. 2009. Spatial variation of the regional wind field with land-sea contrasts and complex topography. *Journal of Applied Meteorology and Climatology*, 48(9): 1929-1939.

Haemmerli A, Waldhuber S, Miniaci C, Zeyer J, Bunge M. 2007. Local expansion and selection of soil bacteria in a glacier forefield. *European Journal of Soil Sciences*, 58(6): 1437-1445.

Hannah DM, Brown LE, Milner AM, Gurnell AM, McGregor GR, Petts GE, Smith BPG, Snook DL. 2007. Integrating climate-hydrology-ecology for alpine river systems. *Aquatic Conservation-Marine and Freshwater Ecosystems*, 17(6): 636-656.

Hantel M, Hirtl-Wielke LM. 2007. Sensitivity of alpine snow cover to European temperature. *Int. J. Climatol.* 27, 1265-1275.

Helbig N, Loewe H, Lehning M. 2009. Radiosity approach for the shortwave surface radiation balance in complex terrain. *Journal of the Atmospheric Sciences*, 66(9): 2900-2912.

Helbig N, Loewe H, Mayer B, Lehning M. 2010. Explicit validation of a surface shortwave radiation balance model over snow-covered complex terrain. *Journal of Geophysical Research-Atmospheres*, 115: D18113.

Hindshaw RS, Tipper ET, Reynolds BC, Lemarchand E, Wiederhold JG, Magnusson J, Bernasconi S, Kretzschmar R, Bourdon B. 2011. Hydrological control of stream water

## References

- chemistry in a glacial catchment (Damma Glacier, Switzerland). *Chemical Geology*, 285:215-230.
- Hinton MJ, Schiff SL, English MC. 1993. Physical-properties governing groundwater-flow in a glacial till catchment. *Journal of Hydrology*, 142(1-4): 229-249.
- Hirashima H, Nishimura K, Yamaguchi S, Sato A, Lehning M. 2008. Avalanche forecasting in a heavy snowfall area using the snowpack model. *Cold Regions Science and Technology*, 51, 191-203.
- Hock R. 1999. A distributed temperature-index ice- and snowmelt model including potential direct solar radiation. *Journal of Glaciology*, 45(149): 101-111.
- Hock R. 2003. Temperature index melt modelling in mountain areas. *Journal of Hydrology*, 282(1-4): 104-115.
- Hock R, Holmgren B. 2005. A distributed surface energy-balance model for complex topography and its application to Storglaciaren, Sweden. *Journal of Glaciology*, 51(172): 25-36.
- Hodson AJ, Gurnell AM, Washington R, Clark MJ, Hagen JO. 1998. Meteorological and runoff time-series characteristics in a small, high-Arctic glaciated basin, Svalbard. *Hydrological Processes*, 12(3): 509-526.
- Hoehn E, Vongunten HR. 1989. Radon in groundwater - A tool to assess infiltration from surface waters to aquifers. *Water Resources Research*, 25:1795-1803.
- Horton P, Schaeefli B, Mezghani A, Hingray B, Musy A. 2006. Assessment of climate-change impacts on alpine discharge regimes with climate model uncertainty. *Hydrological Processes*, 20, 2091-2109.
- Hosaka M, Nohara D, Kitoh A. 2005. Changes in snow cover and snow water equivalent due to global warming simulated by a 20 km-mesh global atmospheric model. *SOLA 1*, 93-96.
- Huss M, Bauder A, Funk M, Hock R. 2008a. Determination of the seasonal mass balance of four Alpine glaciers since 1865. *Journal of Geophysical Research-Earth Surface*, 113(F1): ARTN F01015.
- Huss M, Farinotti D, Bauder A, Funk M. 2008b. Modelling runoff from highly glacierized alpine catchment basins in a changing climate. *Hydrological Processes*, 22: 3888-3902.
- IPCC, 2007. Climate Change 2007 - The Physical Science Basis. Cambridge University Press, Cambridge.
- Jackson THR. 1994. A spatially distributed snowmelt-driven hydrological model applied to Upper Sheep Creek. PhD thesis, Utah State University, Logan, Utah.
- Jasper K, Calanca P, Gyalistras D, Fuhrer J. 2004. Differential impacts of climate change on the hydrology of two alpine river basins. *Clim. Res.* 26, 113-129.

## Chapter 7

- Jobard S, Dzikowski M. 2006. Evolution of glacial flow and drainage during the ablation season. *Journal of Hydrology*, 330(3-4): 663-671.
- Jonas T, Marty C, Magnusson J. 2009. Estimating the snow water equivalent from snow depth measurements in the Swiss Alps. *Journal of Hydrology*, 378(1-2): 161-167.
- Keller F, Goyette S, Beniston M. 2005. Sensitivity analysis of snow cover to climate change scenarios and their impact on plant habitats in alpine terrain. *Clim. Change* 72, 299-319.
- Klok EJ, Jasper K, Roelofsma KP, Gurtz J, Badoux A. 2001. Distributed hydrological modelling of a heavily glaciated Alpine river basin. *Hydrological Sciences Journal-Journal des Sciences Hydrologiques*, 46(4): 553-570.
- Koboltschnig GR, Schoener W, Zappa M, Kroisleitner C, Holzmann H. 2008. Runoff modelling of the glacierized Alpine Upper Salzach basin (Austria): multi-criteria result validation. *Hydrological Processes*, 22: 3950-3964.
- Kormann C. 2009. Untersuchung des Wasserhaushaltes und der Abflussdynamik eines Gletschervorfeldes. Master's thesis, TU Dresden.
- Koussis AD, Smith ME, Akylas E, Tombrou M. 1998. Groundwater drainage flow in a soil layer resting on an inclined leaky bed. *Water Resources Research*, 34:2879-2887.
- Lagarias JC, Reeds JA, Wright MH, Wright PE. 1998. Convergence properties of the Nelder-Mead simplex method in low dimensions. *SIAM Journal on Optimization*, 9(1): 112-147.
- Laternser M, Schneebeli M. 2003. Long-term snow climate trends of the Swiss Alps (1931-99). *Int. J. Climatol.* 23, 733-750.
- Laternser M. 2002. Snow and avalanche climatology of Switzerland. PhD thesis, ETH Zürich, dissertation No. 18230.
- Leach JA, Moore RD. 2010. Above-stream microclimate and stream surface energy exchanges in a wildfire-disturbed riparian zone. *Hydrological Processes*, 24(17): 2369-2381.
- Leach JA, Moore RD. 2011. Stream temperature dynamics in two hydrogeomorphically distinct reaches. *Hydrological Processes*, 25(5): 679-690.
- Lehning M, Bartelt P, Brown B, Fierz C, Satyawali P. 2002a. A physical SNOWPACK model for the Swiss avalanche warning Part II: Snow microstructure. *Cold Regions Science and Technology*, 35, 147-167.
- Lehning M, Bartelt P, Brown B, Fierz C. 2002b. A physical SNOWPACK model for the Swiss avalanche warning. Part III: meteorological forcing, thin layer formation and evaluation. *Cold Regions Science and Technology*, 35(3): 169-184.
- Lehning M, Volksch I, Gustafsson D, Nguyen TA, Stahli M, Zappa M. 2006. ALPINE3D: a detailed model of mountain surface processes and its application to snow hydrology. *Hydrological Processes*, 20, 2111-2128.

## References

- Lehning M, Fierz C. 2008. Assessment of snow transport in avalanche terrain. *Cold Regions Science and Technology*, 51: 240-252.
- Lehning M, Loewe H, Ryser M, Raderschall N. 2008. Inhomogeneous precipitation distribution and snow transport in steep terrain. *Water Resources Research*, 44(7): W07404.
- Leopold LB, Maddock T. 1953. The hydraulic geometry of stream channels and some physiographic implications. U.S. Geol. Surv. Prof. Pap. 252, 56 pp.
- Liston GE, Elder K. 2006a. A distributed snow-evolution modeling system (SnowModel). *Journal of Hydrometeorology*, 7(6): 1259-1276.
- Liston GE, Elder K. 2006b. A meteorological distribution system for high-resolution terrestrial modeling (MicroMet). *Journal of Hydrometeorology*, 7(2): 217-234.
- Logan JD, Zlotnik V. 1995. The convection-diffusion equation with periodic boundary-conditions. *Applied Mathematics Letters*, 8:55-61.
- Loheide II SP, Butler JJ, Gorelick SM. 2005. Estimation of groundwater consumption by phreatophytes using diurnal water table fluctuations: A saturated-unsaturated flow assessment. *Water Resources Research*, 41:14.
- Loheide II SP, Lundquist JD. 2009. Snowmelt-induced diel fluxes through the hyporheic zone. *Water Resources Research*, 45, W07404.
- Lopez-Moreno JI, Goyette S, Beniston M, Alvera B. 2008. Sensitivity of the snow energy balance to climatic changes: prediction of snowpack in the Pyrenees in the 21<sup>st</sup> century. *Clim. Res.* 36, 203-217.
- Magnusson J, Farinotti D, Jonas T, Bavay M. 2011. Quantitative evaluation of different hydrological modelling approaches in a partly glacierized Swiss watershed. *Hydrological Processes*, 25(13): 2071-2084.
- Magnusson J, Kobierska F, Huxol S, Jonas T, Kirchner JW. In review. Melt water driven stream and groundwater stage fluctuations on a glacier forefield (Damma gletscher, Switzerland). *Hydrological Processes*.
- Magnusson J, Jonas T, Kirchner JW. Submitted. The energy balance and temperature dynamics of a proglacial stream, and their implications for spatially integrated hydraulic geometry and riparian aquifer transmissivity. *Water Resources Research*.
- Malard F, Tockner K, Ward JV. 2000. Physico-chemical heterogeneity in a glacial riverscape. *Landscape Ecology*, 15(8): 679-695.
- Malard F, Mangin A, Uehlinger U, Ward JV. 2001. Thermal heterogeneity in the hyporheic zone of a glacial floodplain. *Canadian Journal of Fisheries and Aquatic Sciences*, 58(7): 1319-1335.
- Malard F, Tockner K, Dole-Olivier MJ, Ward JV. 2002. A landscape perspective of surface-subsurface hydrological exchanges in river corridors. *Freshwater Biology*, 47(4): 621-640.

## Chapter 7

Martin E, Lejeune Y. 1998. Turbulent fluxes above the snow surface. *Annals of Glaciology*, 26: 179-183.

Marty C, Philipona R, Frohlich C, Ohmura A. 2002. Altitude dependence of surface radiation fluxes and cloud forcing in the Alps: results from the alpine surface radiation budget network. *Theoretical and Applied Climatology*, 72(3-4): 137-155.

Marty C. 2008. Regime shift of snow days in Switzerland. *Geophys. Res. Lett.* 35, L12501.

Michlmayr G, Lehning M, Koboltschnig G, Holzmann H, Zappa M, Mott R, Schoener W. 2008. Application of the Alpine3D model for glacier mass balance and glacier runoff studies at Goldbergkees, Austria. *Hydrological Processes*, 22: 3941-3949.

Middelkoop H, Daamen K, Gellens D, Grabs W, Kwadijk JCJ, Lang H, Parmet B, Schadler B, Schulla J, Wilke K. 2001. Impact of climate change on hydrological regimes and water resources management in the Rhine basin. *Clim. Change* 49, 105-128.

Mohanty BP, Kanwar RS, Everts CJ. 1994. Comparison of saturated hydraulic conductivity measurement methods for a glacial-till soil. *Soil science society of American Journal*, 58: 672-677.

Montalto FA, Parlange JY, Steenhuis TS. 2007. A simple model for predicting water table fluctuations in a tidal marsh. *Water Resources Research*, 43:22.

Mott R, Faure F, Lehning M, Loewe H, Hynek B, Michlmayr G, Prokop A, Schoener W. 2008. Simulation of seasonal snow-cover distribution for glacierized sites on Sonnblick, Austria, with Alpine 3D model. *Annals of Glaciology*, 49: 155-160.

Nakicenovic N, Gruebler A, McDonalds A. 1998. Global Energy Perspectives. Cambridge University Press, Cambridge.

Nielsen P. 1990. Tidal dynamics of the water-table in beaches. *Water Resources Research*, 26:2127-2134.

O'Driscoll MA, DeWalle DR. 2006. Stream-air temperature relations to classify stream-ground water interactions in a karst setting, central Pennsylvania, USA. *Journal of Hydrology*, 329(1-2), 140-153.

Obleitner F, Lehning M. 2004. Measurement and simulation of snow and superimposed ice at the Kongsvegen glacier, Svalbard (Spitzbergen). *J. Geophys. Res.* 109, D04106.

Oerlemans J, Grisogono B. 2002. Glacier winds and parameterisation of the related surface heat fluxes. Tellus Series A-Dynamic Meteorology and Oceanography 54(5): 440-452. Climate Conference 2001, Utrecht, Netherlands, August, 2001.

Park CC. 1977. World-wide variations in hydraulic geometry exponents of stream channels - analysis and some observations. *Journal of Hydrology*, 33(1-2): 133-146.

Paterson WSB. 1994. The Physics of Glaciers, 3rd edn, Pergamon: Oxford.

## References

- Peck EL, Brown MJ. 1962. An approach to the development of isohyetal maps for mountainous areas. *Journal of Geophysical Research*, 67: 681-694.
- Pirazzini R, Nardino M, Orsini A, Calzolari F, Georgiadis T, Levizzani V. 2000. Parameterization of the downward longwave radiation from clear and clouded skies at Ny Alesund (Svalbard), IRS 2000. In: Smith, W. L. & Timofeyev, Y. M. A. (eds) Current Problems in Atmospheric Radiation. Deepack Publishing, Hampton, Virginia, pp. 559-562.
- Raisanen J. 2008. Warmer climate: less or more snow? *Clim. Dyn.* 30, 307-319.
- Rasmus S, Raisanen J, Lehning M. 2004. Estimating snow conditions in Finland in the late 21<sup>st</sup> century using the SNOWPACK model with regional climate scenario data as input. *Annals of Glaciology*, 38, 238-244.
- Raubenheimer B, Guza RT, Elgar S. 1999. Tidal water table fluctuations in a sandy ocean beach. *Water Resources Research*, 35:2313-2320.
- Roy JW, Hayashi M. 2009. Multiple, distinct groundwater flow systems of a single moraine-talus feature in an alpine watershed. *Journal of Hydrology*, 373(1-2): 139-150.
- Ruehl C, Fisher AT, Hatch C, Los Huertos M, Stemler G, Shennan C. 2006. Differential gauging and tracer tests resolve seepage fluxes in a strongly-losing stream. *Journal of Hydrology*, 330(1-2): 235-248.
- Ryan BC. 1977. Mathematical-model for diagnosis and prediction of surface winds in mountainous terrain. *Journal of Applied Meteorology*, 16(6): 571-584.
- Schaefli B, Hingray B, Musy A. 2007. Climate change and hydropower production in the Swiss Alps: quantification of potential impacts and related modelling uncertainties. *Hydrology and Earth System Sciences*, 11(3): 1191-1205.
- Schaefli B, Hingray B, Niggli M, Musy A. 2005. A conceptual glaciohydrological model for high mountainous catchments. *Hydrology and Earth System Sciences*, 9: 95-109.
- Scherrer SC, Appenzeller C, Laternser M. 2004. Trends in Swiss Alpine snow days: the role of local- and large-scale climate variability. *Geophys. Res. Lett.* 31, L13215.
- Scherrer SC, Appenzeller C. 2006. Swiss Alpine snow pack variability: major patterns and links to local climate and largescale flow. *Clim. Res.* 32, 187-199.
- Schwarb C, Frei C, Schaer C, Daly M. 2001. Mean annual and seasonal precipitation throughout the European Alps 1971-1990. Hydrological Atlas of Switzerland. Plates 2.6, 2.7, Technical Report.
- Schwarz AMJ, Green TGA, Seppelt RD. 1992. Terrestrial vegetation at Canada Glacier, Southern Victoria Land, Antarctica. *Polar Biology*, 12(3-4): 397-404.

## Chapter 7

Shabalova MV, van Deursen WPA, Buishand TA. 2003. Assessing future discharge of the river Rhine using regional climate model integrations and a hydrological model. *Clim. Res.* 23, 233-246.

Shepard D. 1968. A two-dimensional interpolation function for irregularly-spaced data. In: Proceedings of the 1968 ACM National Conference, pp. 517-524.

Sicart JE, Hock R, Six D. 2008. Glacier melt, air temperature, and energy balance in different climates: The Bolivian Tropics, the French Alps, and northern Sweden, *J. Geophys. Res.* 113, D24113.

Smith LC, Pavelsky TM. 2008. Estimation of river discharge, propagation speed, and hydraulic geometry from space: Lena River, Siberia. *Water Resources Research*, 44(3), W03427.

Stahl K, Moore RD, Shea JM, Hutchinson D, Cannon AJ. 2008. Coupled modelling of glacier and streamflow response to future climate scenarios. *Water Resources Research*, 44(2), W02422.

Stearns C, Weidner G. 1993. Sensible and latent heat flux estimates in Antarctica. *Antarctic Research Series*, 61: 109-138.

Stoessel F, Guala M, Fierz C, Manes C, Lehning M. 2010. Micrometeorological and morphological observations of surface hoar dynamics on a mountain snow cover. *Water Resources Research*, 46: W04511.

Stonestrom DA, Blasch KW. 2003. Determining temperature and thermal properties for heat-based studies of surface-water ground-water interactions. In Heat as a Tool for Studying the Movement of Ground Water Near Streams, ed. D.A. Stonestrom and J. Constantz, 73-80. USGS Circular 1260. Reston, Virginia: USGS.

Stull R.B. 2000. Meteorology for Scientists and Engineers. Brooks/Cole: Pacific Grove.

Su NH, Liu FW, Anh V. 2003. Tides as phase-modulated waves inducing periodic groundwater flow in coastal aquifers overlaying a sloping impervious base. *Environmental Modelling & Software*, 18:937-942.

Sun HB. 1997. A two-dimensional analytical solution of groundwater response to tidal loading in an estuary. *Water Resources Research*, 33:1429-1435.

Swift DA, Nienow PW, Hoey TB, Mair DWF. 2005. Seasonal evolution of runoff from Haut Glacier d'Arolla, Switzerland and implications for glacial geomorphic processes. *Journal of Hydrology*, 309, 133-148.

Thorne R, Woo MK. 2006. Efficacy of a hydrologic model in simulating discharge from a large mountainous catchment. *Journal of Hydrology*, 330(1-2): 301-312.

Uehlinger U, Malard F, Ward JV. 2003. Thermal patterns in the surface waters of a glacial river corridor (Val Roseg, Switzerland). *Freshwater Biology*, 48(2): 284-300.

## References

- Unsworth MH, Monteith JL. 1975. Long-wave radiation at ground. 1. Angular-distribution of incoming radiation. *Quarterly Journal of the Royal Meteorological Society*, 101(427): 13-24.
- Verbunt M, Gurtz J, Jasper K, Lang H, Warmerdam P, Zappa M. 2003. The hydrological role of snow and glaciers in alpine river basins and their distributed modeling. *Journal of Hydrology*, 282(1-4): 36-55.
- Vogt T, Hoehn E, Schneider P, Freund A, Schirmer M, Cirpka OA. 2010a. Fluctuations of Electrical Conductivity as a Natural Tracer for Bank Filtration in a Losing Stream. *Advances in Water Resources*, 33: 1296-1308.
- Vogt T, Schneider P, Hahn-Woernle L, Cirpka OA. 2010b. Estimation of seepage rates in a losing stream by means of fiber-optic high-resolution vertical temperature profiling. *Journal of Hydrology*, 380(1-2): 154-164.
- Warburton J. 1992. Observations of bed-load transport and channel bed changes in a proglacial mountain stream. *Arctic and Alpine Research*, 24(3): 195-203.
- Ward JV, Malard F, Tockner K, Uehlinger U. 1999. Influence of ground water on surface water conditions in a glacial flood plain of the Swiss Alps. *Hydrological Processes*, 13(3): 277-293.
- Webb BW, Zhang Y. 1997. Spatial and seasonal variability in the components of the river heat budget. *Hydrological Processes*, 11(1): 79-101.
- Webb BW, Hannah DM, Moore RD, Brown LE, Nobilis F. 2008. Recent advances in stream and river temperature research. *Hydrological Processes*, 22(7): 902-918.
- Westhoff MC, Savenije HHG, Luxemburg WMJ, Stelling GS, van de Giesen NC, Selker JS. 2007. A distributed stream temperature model using high resolution temperature observations. *Hydrology and Earth System Sciences*, 11: 1469-1480.
- White AF, Brantley SL. 2003. The effect of time on the weathering of silicate minerals: why do weathering rates differ in the laboratory and field. *Chemical Geology*, 202(3-4): 479-506.
- Wielke LM, Haimberger L, Hantel M. 2004. Snow cover duration in Switzerland compared to Austria. *Meteorologische Zeitschrift*, 13, 13-17.
- Winstral A, Marks D. 2002. Simulating wind fields and snow redistribution using terrain-based parameters to model snow accumulation and melt over a semi-arid mountain catchment. *Hydrological Processes*, 16: 3585-3603.
- Winstral A, Marks D, Gurney R. 2009. An efficient method for distributing wind speeds over heterogeneous terrain. *Hydrological Processes*, 23(17): 2526-2535.
- Zappa M, Pos F, Strasser U, Warmerdam P, Gurtz J. 2003. Seasonal water balance of an Alpine catchment as evaluated by different methods for spatially distributed snowmelt modelling. *Nordic Hydrology*, 34(3): 179-202.

## Chapter 7

Zappa M, Song ZH, Baumgartner MF, Gurtz J, Schaedler B. 2005. The Changjiang flood forecasting assistance project. Proceedings of the International Conference on Headwater Control VI: Hydrology, Ecology and Water Resources in Headwaters, Bergen, Norway.

Zemp M, Haeberli W, Hoelzle M, Paul F. 2006. Alpine glaciers to disappear within decades? *Geophys. Res. Lett.* 33, L13504.

## 8 Acknowledgements

Sometimes when walking around on the glacier forefield with its many braided streams, a phrase my dad once in a while says came into my mind: ‘Många bäcker små bildar till slut en å’. The phrase says that many small streams eventually become a river. I think this small phrase also translates to all the work we do; with the help from others we get further than when working alone.

First, I sincerely want to thank both of my supervisors, Tobias Jonas and James Kirchner. They helped me greatly during the years, and their enthusiasm and interest in the work we did was very encouraging. I also liked many moments with both of them, for instance the difficulty in keeping up with Tobias pace in field when he, a little bit like a curious child, was searching for the perfect spot for some measurement. I also really enjoyed the meetings with James. It could often happen that he suddenly slammed his hand hard against the table when realizing something interesting about a measurement result. I really enjoyed such moments, and of course all the help they gave me during the years!

Manfred Stähli and Stefano Bernasconi deserve much gratitude. They initiated the BigLink-project and contributed with many valuable ideas during the years. Many project members also helped in different ways for the studies presented in this thesis. For the snow and glacier related studies, I foremost want to thank Daniel Farinotti and Andreas Bauder, and their colleagues for helping out in field. For the remaining studies, in particular Hans Göransson, Ruth Hindshaw and Rienk Smittenberg gave a helping hand. I also wish to thank Jan Seibert for agreeing to co-examine this thesis.

Bruno Fritschi and Karl Steiner prepared and installed many of the instruments in field. They deserve special gratitude for going to the field site whenever needed, in spite of very unpleasant conditions once in a while. The mechanical workshop in Davos also made a significant contribution by assembling the weather stations: thanks Franz Herzog, Andreas Moser, Andreas Tröger, Christian Simeon and Silvio Burger among others. In the valley of the Göschenenalp, foremost Cornelia Stoimenova-Mattli at the local hostel and Bernhard Mattli at the Kraftwerk Göschenen were always greatly supportive .

Many colleagues and friends helped me much over the years. It all started with David Gustafsson, who helped me take the step from an undergrad student to the doctoral studies in Switzerland. Masaki Hayashi showed a great interest in the work we did on the forefield, and contributed with some important ideas. Stephan Huxol kindly measured the age of the groundwater during a couple of field trips for us. Henning Löwe helped to solve many physics problems, and always took time to discuss one problem or the other. Michael Lehning, Mathias Bavay and Ignacio López-Moreno contributed with much experience to the snow studies. Manuel Nitsche, Nena Griessinger, Arne Bergau, and many others helped out during the field trips. I am also very grateful to my both office mates and fellow doctoral students, Luca Egli and Florian Kobierska, who encouraged and supported me all the time.

Last but not least, I do not know how to thank my parents and my brother enough with words. En stor kram och ett stort tack till er, jag tycker om er så mycket så mycket! Along with my family, I also wish to thank all my friends for all the fun activities in the mountains, or elsewhere. Finally, thank you very much Christine!

## 9 Curriculum vitae

### Jan Olof Magnusson

born February 1, 1980 in Lidköping, Sweden

#### Education

- 1999-2006 M.Sc. in Aquatic and Environmental Engineering. Uppsala University
- 2003-2004 Exchange student (Erasmus) at the University of Innsbruck, Austria
- 2007 Scientific internship at the WSL Institute for Snow and Avalanche Research SLF (Davos, Switzerland)
- Since 2007 PhD-student at the WSL Institute for Snow and Avalanche Research SLF (Davos, Switzerland) and the Swiss Federal Institute of Technology (ETH), Zürich

#### Publications

Jonas T, Marty C, Magnusson J. 2009. Estimating the snow water equivalent from snow depth measurements in the Swiss Alps. *Journal of Hydrology*. 378(1–2): 161–167.

Magnusson J, Jonas T, Lopez-Moreno I, Lehning M. 2010. Snow cover response to climate change in a high alpine and half-glacierized basin in Switzerland. *Hydrology Research*. 41:230–240.

Farinotti D, Magnusson J, Huss M, Bauder A. 2010. Snow accumulation distribution inferred from time-lapse photography. *Hydrological Processes*. 24: 2087–2097.

Magnusson J, Farinotti D, Jonas T, Bavay M. 2011. Quantitative evaluation of different hydrological modeling approaches in a partly glacierized Swiss watershed. *Hydrological Processes*. *Hydrological Processes*. 25(13): 2071–2084.

Hindshaw RS, Tipper ET, Reynolds BC, Lemarchand E, Wiederhold JG, Magnusson J, Bernasconi S, Kretzschmar R, Bourdon B. 2011. Hydrological control of stream water chemistry in a glacial catchment (Damma Glacier, Switzerland). *Chemical Geology*. 285:215–230.